Agenzia nazionale per le nuove tecnologie,
l'energia e lo sviluppo economico sostenibile

MINISTERO DELLO SVILUPPO ECONOMICO

Ricerca di Sistema elettrico

Sviluppo e validazione di un approccio e di modelli per le analisi di sicurezza di reattori veloci di IV generazione

A. Del Nevo, I. Di Piazza, C. Parisi, E. Martelli, P. Balestra, G. Caruso, A. Naviglio

Report RdS/PAR2014/195

SVILUPPO E VALIDAZIONE DI UN APPROCCIO E DI MODELLI PER LE ANALISI DI SICUREZZA DI REATTORI VELOCI DI IV GENERAZIONE

A. Del Nevo, I. Di Piazza, C. Parisi - ENEA, E. Martelli, P. Balestra, F. Giannetti, G. Caruso, A. Naviglio - CIRTEN: CERSE-UNIROMA1

Settembre 2015

Report Ricerca di Sistema Elettrico
Accordo di Programma Ministero dello Sviluppo Economico - ENEA
Piano Annuale di Realizzazione 2014
Area: Produzione di energia elettrica e protezione dell'ambiente
Progetto: Sviluppo competenze scientifiche nel campo della sicurezza nucleare e collaborazione ai programmi internazionali per il nucleare di IV Generazione
Linea: Collaborazione nei programmi internazionali per il nucleare di IV Generazione
Obiettivo: Progettazione di sistema e analisi di sicurezza
Responsabile del Progetto: Mariano Tarantino, ENEA

Il presente documento descrive le attività di ricerca svolte all'interno dell'Accordo di collaborazione Sviluppo competenze scientifiche nel campo della sicurezza nucleare e collaborazione ai programmi internazionali per il nucleare di IV Generazione

Responsabile scientifico ENEA: Mariano Tarantino, ENEA

Responsabile scientifico CIRTEN: Giuseppe Forasassi, CIRTEN

Ricerca Sistema Elettrico	Sigla di identificazione	Distrib.	Pag.	di
	ADPFISS – LP2 – 088	L	1	90

Titolo

Sviluppo e validazione di un approccio e di modelli per le analisi di sicurezza di reattori veloci di IV generazione

[Development and validation of an approach and numerical models for safety analysis of FBR]

Descrittori

Tipologia del documento: Rapporto Tecnico

Collocazione contrattuale: Accordo di programma ENEA-MSE su sicurezza nucleare e Reattori di IV generazione

Argomenti trattati: Reattori Nucleari Veloci, Termoidraulica dei reattori nucleari Sicurezza nucleare, Analisi incidentale

Sommario

Il report rappresenta un contributo all'analisi numerica di scenari operativi e incidentali. Consiste nella messa a punto, nell'applicazione e nella validazione di un approccio e di modelli per analisi di sicurezza di reattori veloci di IV generazione. L'attività è svolta in sinergia con *l'International Coordinated Research Project (CRP) on EBR-II Shutdown Heat Removal Tests* promosso dall'IAEA. L'attività è multi-physics e multi-scale e trarrà beneficio dalla disponibilità di dati sperimentali misurati in reattore durante l'esecuzione di test: *protected* (SHRT-17) ed *unprotected* (SHRT-45r) *loss of flow* nel reattore americano di ricerca EBR-II. Il documento presenta l'impianto EBR-II, oggetto delle simulazioni numeriche, descrive il test sperimentale SHRT-17, il modello termoidraulico realizzato per il codice di sistema RELAP5-3D©, la qualifica della nodalizzazione tramite l'analisi di post-test. Visto il livello di dettaglio della strumentazione negli *assemblies* sperimentali XX09 e XX10, installati nel driver del reattore, è stato realizzato un modello CFD attraverso il codice ANSYS CFX per fornire informazioni dettagliate sulla distribuzione di temperature nell'*assembly*, partendo dalle condizioni al contorno fornite dalla termoidraulica e dalla neutronica. Partendo dalle condizioni al contorno fornite dalla termoidraulica di sistema, son stati effettuati calcoli stazionari e di transitorio relativi al test SHRT17. Infine, è stata messa a punto una metodologia per l'analisi del nocciolo, mediante codici di calcolo 3D neutronici. Relativamente al test SHRT-45r, è stato sviluppato un modello neutronico 3D Monte Carlo del reattore, usando come codice di riferimento MCNP6. Ogni pin è stata modellata singolarmente, anche le parti in acciaio del riflettore sono state riprodotte secondo la geometria originale. Da questo modello è stato ottenuto il valore di k_{eff} e la distribuzione di potenza da usare come riferimento per il modello nodale 3D a pochi gruppi. È stato, inoltre, effettuato il calcolo delle sezioni d'urto omogeneizzate a 33 Gruppi, utilizzando il codice di reticolo SCALE. Generando diversi modelli 2D per il fuel, le CR e il riflettore, è stata costruita una libreria di sezioni d'urto per tutto il nocciolo escludendo la zona del blanket. La libreria delle sezioni d'urto è stata poi implementata nel modello 3D sviluppato, usando il codice neutronico PHISICS, tramite il quale sarà possibile effettuare il calcolo accoppiato.

Note: Riferimento CIRTEN CERSE-UNIRM RL 1603/2015

Autori:

A. Del Nevo, I. Di Piazza, C. Parisi (ENEA)

E. Martelli, P. Balestra, F. Giannetti, G. Caruso, A. Naviglio (CIRTEN-UNIROMA1)

Copia n. **In carico a:**

REV.	DESCRIZIONE	DATA		REDAZIONE	CONVALIDA	APPROVAZIONE
1			NOME			
			FIRMA			
0	EMISSIONE	28/09/15	NOME	A. Del Nevo	M. Tarantino	M. Tarantino
			FIRMA			

(Page intentionally left blank)

SUMMARY

The present report is a contribution to the "Numerical analysis of operational scenarios and incidental" activity. It consists in developing, applying and validating an approach and numerical models for the safety analysis of liquid metal Gen. IV reactors.

The activity benefits of the International Coordinated Research Project (CRP) on EBR-II Shutdown Heat Removal tests promoted by IAEA. It is multi-physics and multi-scale and it will require the synergistic effort of different technical skills. The work is based on the availability of experimental tests carried out in EBR-II reactor. These tests are: protected (SHRT-17) ed unprotected (SHRT-45r) loss of flow.

The documents presents the EBR-II and describes the SHRT-17 and the experimental data available. Then, the 3D thermal-hydraulic model of EBR-II by RELAP5-3D© system code is presented, together with the nodalization qualification carried out by means of the post-test analysis.

Considering the highly detailed measurements of temperatures in the SA XX09, a CFD model with ANSYS CFX code was set up and employed for complex 3D simulations of the temperature filed and coolant flow paths. Steady state simulations (at starting of transient) and transient simulation of SHRT17 were also performed starting from the boundary conditions provided by the system code results.

Finally, a methodology was also set-up to carry out neutronic core analysis based on 3D codes. Starting from the SHRT-45r test specifications, including the fuel composition data, an MCNP6 model of the overall core was developed. Every single pin was modeled, including the stainless steel of the reflector, according with the original geometry. The k_{eff} value was calculated as well as the power distribution, which can be used as reference for the 3D nodal model at reduced number of energy groups. Homogenized cross sections were calculated for 33 groups by means of SCALE code. Different 2D models were generated for the fuels, the CR and the reflector. These were used to derive a cross section library for all core, excluding the blanket zone. Then, this library was implemented in the core 3D neutron kinetic code model, PHISICS, which will be used for the coupled calculation of the unprotected transient.

LIST OF CONTENTS

LIST OF FIGURES

LIST OF TABLES

LIST OF ABBREVIATIONS

3D	Three Dimensional
ANL	Argonne National Laboratory
ATC	Annulus Thimble Thermocouple
BAF	Bottom of Active Fuel
BOP	Balance of Plant
CEA	Commissariat à l'énergie atomique et aux énergies alternatives
CFD	Computational Fluid Dynamics
CIAE	China Institute of Atomic Energy
CRP	Coordinated Research Project
DAS	Data Acquisition System
EBR-II	Experimental Breeder Reactor II
EC	European Commission
EU	European Union
FA	Fuel Assembly
FR	Fast Reactor
GEN IV	Generation IV
GFR	Gas-Cooled Fast Reactor
GIF	Generation IV International Forum
GPM	United Sates gallon per minute
HFD	High-Flow Driver
HWCR	High Worth Control Rod
IAEA	International Atomic Energy Agency
IB	Inner Blanket
IFR	Integral Fast Reactor
IHX	Intermediate Heat Exchanger
INCOT	In-Core Instrument Test facility
INL	Idaho National Laboratory
INSAT	Instrumented Subassembly
IPPE	Institute of Physics and Power Engineering
JAEA	Japan Atomic Energy Agency
KAERI	Korea Atomic Energy Research Institute
KINS	Korean Institute for Nuclear Safety
LFR	Lead-Cooled Fast Reactor
LWR	Light Water Reactor
LMR	Liquid Metal Reactor
MCP	Main Coolant Pump
M-G	Motor-Generator set
MSR	Molten Salt Reactor

NK	Neutron Kinetics
OB	Outer Blanket
ORNL	Oak Ridge national Laboratory
OTC	Outlet-Coolant Thermocouple
PPS	Plant Protection System
PS	Primary Side
R&D	Research and Development
SA	Sub-Assembly
SCWR	Supercritical Water Reactor
SDC	Safety Design Criteria
SFR	Sodium Fast Reactor
SHRT	Shutdown Heat Removal Test
SS	Secondary Side
SSC	Structures, Systems and Components
TAF	Top of Active Fuel
TH	Thermal-Hydraulic
SYS	System
TTC	Top-of-core Thermocouple
ULOF	Unprotected Loss-of-Flow
VHTR	Very High Temperature Reactor

1 INTRODUCTORY REMARKS

1.1 Framework

The activity is developed and set-up in synergy of IAEA Coordinated Research Project (CRP) on EBR-II Shutdown Heat Removal Tests (SHRT) [1].

The CRP aims at improving design and simulation capabilities in fast reactor neutronics, thermal hydraulics, plant dynamics and safety analyses through benchmark analyses of a protected and an unprotected loss-of flow test from the EBR-II SHRT program. Activities include core physics and thermal-hydraulics/safety assessments. Investigations of thermal hydraulics characteristics and plant behavior focus on predicting natural convection cooling accurately by evaluating the reactor core flow and temperatures in comparison to experimental data.

The activity has been established to support validation of simulation tools and models for the safety analysis of liquid metal fast reactors. Validated tools and models are needed both to evaluate liquid metal fast reactors passive safety phenomena and to assess reactor designs incorporating passive features into the system response to accident initiators.

Passive safety response in liquid metal fast reactors is the result of reactor design features that shut down the reactor, remove residual heat, and keep the core cooled during accidents. In addition to the Doppler effect, negative reactivity feedback mechanisms can be used to passively shut down the fission process. Negative reactivity feedback mechanisms are based on thermal expansion and contraction of structural materials, which affects neutron leakage in the fast spectrum core. Radial and axial core expansion, subassembly bowing, and control rod driveline expansion are examples of these passive reactivity feedbacks. Coolant density changes in sodium are utilized in the design to produce natural circulation flow, thus to keep the core cooled when forced circulation is lost. Passive heat removal is accomplished through use of natural convection, conduction and vessel wall radiation.

The potential for a liquid metal cooled fast reactor to survive severe accident initiators with no core damage has been extensively demonstrated during landmark shutdown heat removal tests in Experimental Breeder Reactor-II (EBR-II). Two of these tests, i.e. SHRT-17 and SHRT-45r, have been chosen because of the availability of extensive thermocouples and flow rate data at various elevations in two instrumented subassemblies, placed in row 5 of the core (one representing a fuel subassembly and the other a blanket subassembly), plus the range of conditions encountered in both tests. They simulated a loss of pumping power (normal and emergency) to the plant operating at full power and flow.

The objectives are to validate state-of-the-art computer software, to improve participants' analytical and numerical capabilities in fast reactor design and analysis through comparison of numerical predictions with test data from the EBR-II SHRT-17 protected loss of flow and SHRT-45R unprotected loss of flow tests.

1.2 Objective of the activity

ENEA activity addresses to the following objectives:

- To compare best-estimate thermal-hydraulic system code calculations to experimental data, thus to validate RELAP5-3D© system code in simulating sodium fast reactors designs.

- To identify and, as far as possible, to quantify the RELAP5-3D© code limitations and the source of uncertainties in simulating postulated accidents occurring in liquid metal FR designs.

- To improve the understanding of the thermal-hydraulics processes and phenomena observed in EBR-II tests.

- To compare the performances of TH system codes in the domain of interest.

- To develop reliable approaches for the application of TH-SYS codes in safety analysis of new generation FR systems (i.e. LFR), including the coupling with CFD and NK.

The multi-physics approach proposed [2] is based on existing nuclear codes, interacting as depicted in Fig. 1: (ERANOS 2.1 [3]) and MCNP6 [4] codes for (static) deterministic and stochastic neutron transport calculations, SCALE [5] package for cross section generation; PHYSICS [6] neutron kinetic package for 3D core power distribution calculations in steady state and in transient, coupled with RELAP5-3D©[7]; RELAP5-3D© for system analysis; computation fluid dynamic code ANSYS CFX 13 [8] for 3D local simulations; and TRANSURANUS [9] code for fuel pin performance simulations (*not employed in the benchmark activities*).

Neutron physics codes will be applied for simulating the test SHRT-45r, which is an unprotected transient, where the neutronic feedbacks have a crucial role. The RELAP5-3D© notalization, qualified against the test, here discussed, is used for the thermal-hydraulic calculation of the transient. On the opposite, ANSYS CFX-13 is used to perform a detailed simulation of the experimental sub-assemblies XX09 and XX10 for the tests SHRT-17 and SHRT-45r. The three dimensional simulation provides a detailed description of flow paths and temperature distribution inside the fuel assembly and in the subassembly thimble.

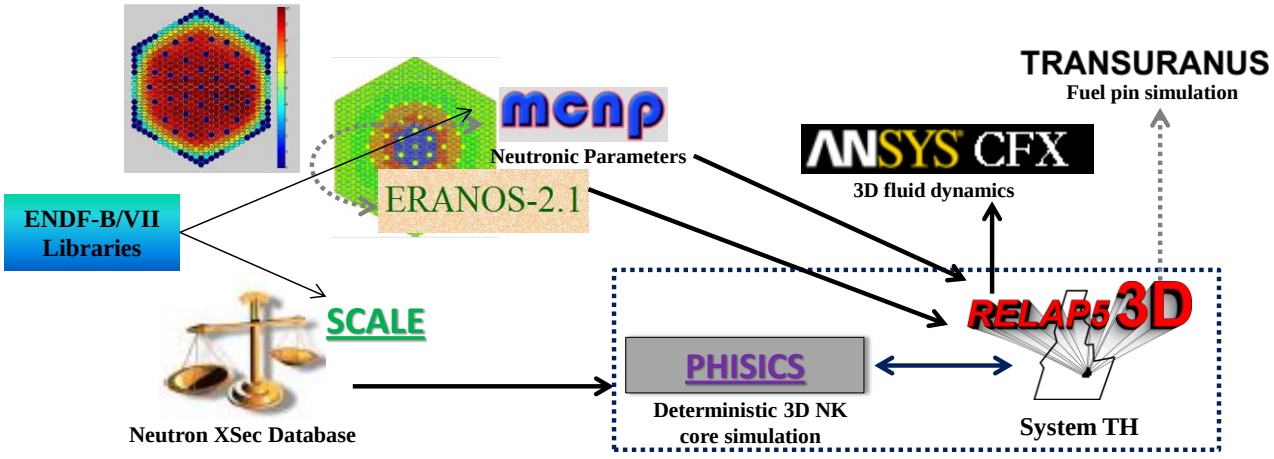

Fig. 1 – Chain of codes proposed for supporting for supporting the design and the safety analysis of Gen. IV liquid metal fast reactors.

2 EBR-II AND SHRT-17

2.1 Introduction

EBR-II [10] [11] [12][13] was operated initially to demonstrate the feasibility of a closed fuel cycle that required the addition only of uranium-238 to the fuel breeding process allowing for sustained operation. To achieve the intended fuel utilization, the initial EBR-II operating period was closely tied to research into pyrometallurgical reprocessing for irradiated nuclear fuel. This period lasted five years. Following the fuel cycle demonstration phase, the focus of EBR-II shifted for much of the next ten years towards irradiation experiments of advanced binary and ternary metal fuels and also advanced oxide fuels. From 1983 and 1994, EBR-II was used for experiments designed to demonstrate the importance of passive safety in liquid metal reactors (LMR).

The Shutdown Heat Removal Test (SHRT) program [11][12] was carried out in EBR-II between 1984 and 1986. The objectives of this program were to support U.S. LMR plant design, provide test data for validation of computer codes for design, licensing and operation of LMRs, and demonstrate passive reactor shutdown and decay heat removal in response to protected and unprotected transients. The protected and unprotected transients tested included loss of flow in the primary and/or intermediate sodium loops as well as a loss of heat sink from balance of plant. Additional tests were performed to examine the response of the system to balance of plant changes and others were performed to characterize reactivity feedbacks.

Passive safety response in sodium fast reactors is the result of reactor design futures that will shut down the reactor, remove residual heat, and keep the core cooled during accidents. In addition to Doppler effect, negative reactivity feedback mechanisms based on thermal expansion and contraction of structural materials, which affect neutron leakage in the fast spectrum core, can be used to passively shut down the fission process. Radial and axial core expansion, subassembly bending, and control rod driveline expansion are examples of these passive reactivity feedbacks. To keep the core cooled when forced circulation is lost, coolant density changes in sodium can be utilized in the design to produce natural circulation flow. Passive heat removal can be accomplished through use of natural convection, conduction and vessel wall radiation.

2.2 EBR-II plant overview

The EBR-II plant is a sodium cooled reactor located in Idaho, it was designed and operated by Argonne National Laboratory for the US Department of Energy [13]. Operation began in 1964 and continued until 1994. EBR-II was rated for a thermal power of 62.5 MW_t with an electric output of approximately 20MW_e [11][12]. Mass flow rates in three cooling loops were rated as [10][11]:

- Primary sodium: 485 kg/s
- Intermediate sodium: 315 kg/s
- Secondary steam: 32 kg/s

All primary system components were submerged in the primary tank, which contained approximately 340 m^3 of liquid sodium at 371°C. An argon cover gas was maintained over the surface of the sodium in the primary vessel to minimize the opportunity for air to contact the

sodium. Fig. 2 shows the primary tank and the other components The primary cooling system consisted of two mechanical centrifugal pumps operated in parallel and pumping a total of 485 kg/s of sodium. The two pumps drew sodium from this pool and provided sodium to the two inlet plena for the core. Subassemblies in the inner core and the extended core regions received sodium from the high-pressure inlet plenum, accounting for approximately 85% of the total primary flow. The blanket and the reflector subassemblies in the outer blanket region received sodium from the low-pressure inlet plenum.

Hot sodium left the subassemblies into a common upper plenum where it mixed before passing through the outlet pipe into the intermediate heat exchanger (IHX). The pipe feeding sodium to the IHX is referred to as “Z-pipe”. Sodium then exited the IHX back into the primary sodium tank before entering the primary sodium pumps again.

Sodium in the intermediate loop traveled from the IHX to the steam generator where its heat was transferred to the balance-of plant (BOP). The steam generator consisted of two parallel superheaters and seven parallel evaporators.

EBR-II was heavily instrumented to measure mass flow rates, temperatures and pressures throughout the system [10][11].

The EBR-II reactor core [1][11][33] vessel grid-plenum assembly accommodated 637 hexagonal subassemblies, which were installed in one of three regions: central core, inner blanket (IB) or outer blanket (OB). Each subassembly position was identified by a unique combination of three parameters: row, sector and position within the sector.

Fig. 3 illustrates the subassemblies arrangement of the reactor and the subassembly identification convention. Subassembly row identification begins at Row 1 for the subassembly in the core-center and moves outward to Row 16.

Two positions in Row 5 contained the in-core instrument subassemblies (INSAT) XX09 and XX10, and one position in Row 5 contained the in-core instrument test facility (INCOT) XY16. The remaining central core subassemblies were either driver-fuel or experimental-irradiation subassemblies of varying types. For SHRT-17 test only the MARK-II A I type driver subassembly was used.

The expanded core region was composed of Rows 6 and 7. This region is also named inner blanket region because originally housed blanket subassemblies. In SHRT-17 test, no blanket subassembly was loaded in this region. Instead, Row 6 contained the driver-fuel and irradiation subassemblies and Row 7 contained reflector subassemblies. The outer blanket region comprised the 545 subassemblies in Rows 8-16, which were either blanket or reflector subassemblies.

Each type of subassembly is discussed in Ref. [11], together with a detailed description of the geometry.

The EBR-II coolant systems model [10][11][12] for the SHRT-17 test included the major components in the primary sodium circuit and the intermediate side of the intermediate heat exchanger. Starting from the outlet of the reactor core, the primary sodium circuit included the upper plenum, reactor outlet piping, auxiliary EM sodium pumps, reactor inlet piping and high- and low-pressure inlet plena.

Fig. 4 illustrates the major components of the EBR-II primary sodium circuit. The two primary sodium pumps took suction from the primary sodium tank and provided sodium to the reactor inlet piping. Both sets of inlet piping provided sodium to the high-pressure and low-pressure inlet plena (Fig. 6). The high pressure inlet plenum provided sodium to the subassemblies in the first 7 rows; while the low-pressure inlet plenum provided sodium to Rows 8-16. Sodium discharged from the right side of the reactor vessel into the reactor outlet piping, known as the 'Z-Pipe'. The shape of this pipe accommodated thermal expansion. The top of the Z-Pipe contained the auxiliary EM pump, which rated to provide up the 0.5% of the nominal pump head. Sodium exited the Z-Pipe and entered the shell side of the intermediate heat exchanger (Fig. 7). Cold sodium was finally discharged into the primary sodium tank. Fig. 4 shows the two primary sodium pumps and their inlet piping.

Simplified geometry was given for the major components of the primary sodium circuit in the benchmark model [11].

The primary tank (Fig. 5) was the outer boundary of the primary sodium circuit and was a vertically cylinder. It encompassed all of the major primary sodium components. The reactor vessel, intermediate exchanger and two primary sodium pumps were modeled as vertically oriented cylinders.

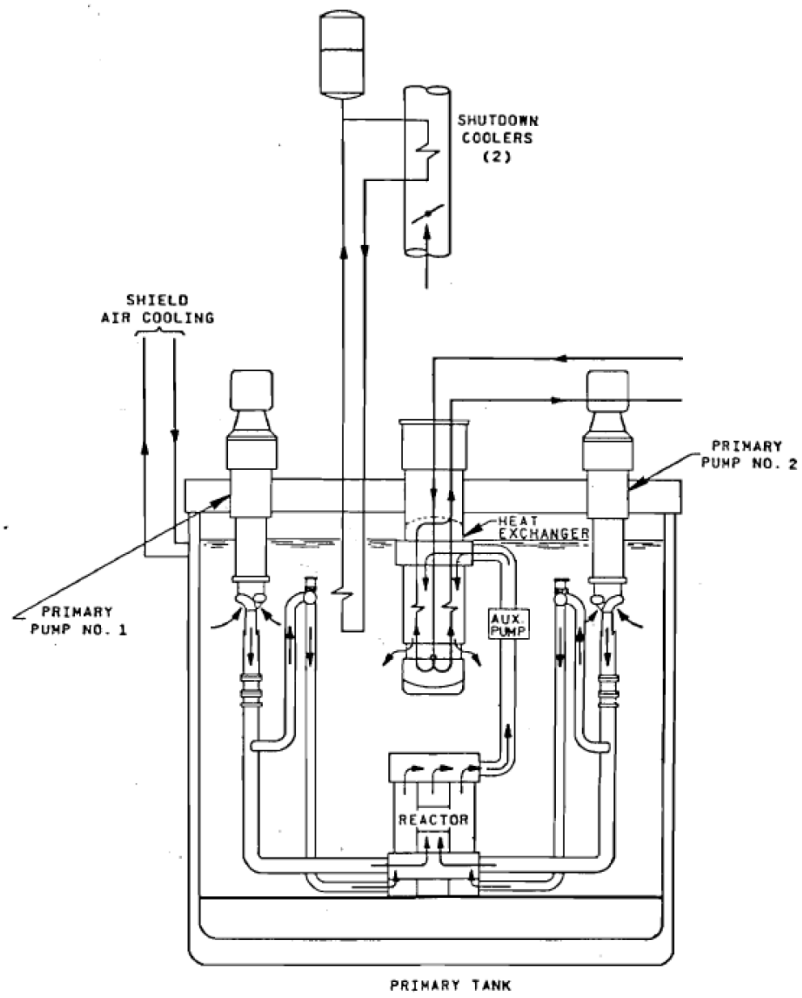

Fig. 2 – EBR-II Primary Tank Sodium Flow Paths.

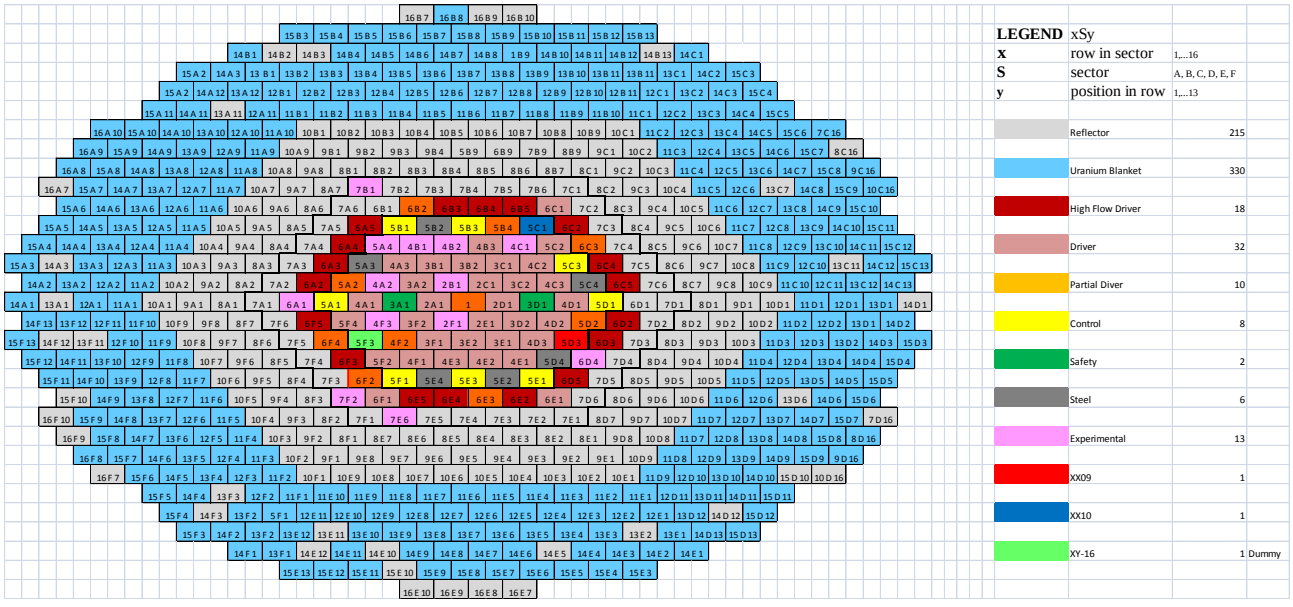

Fig. 3 – EBR-II Core Layout.

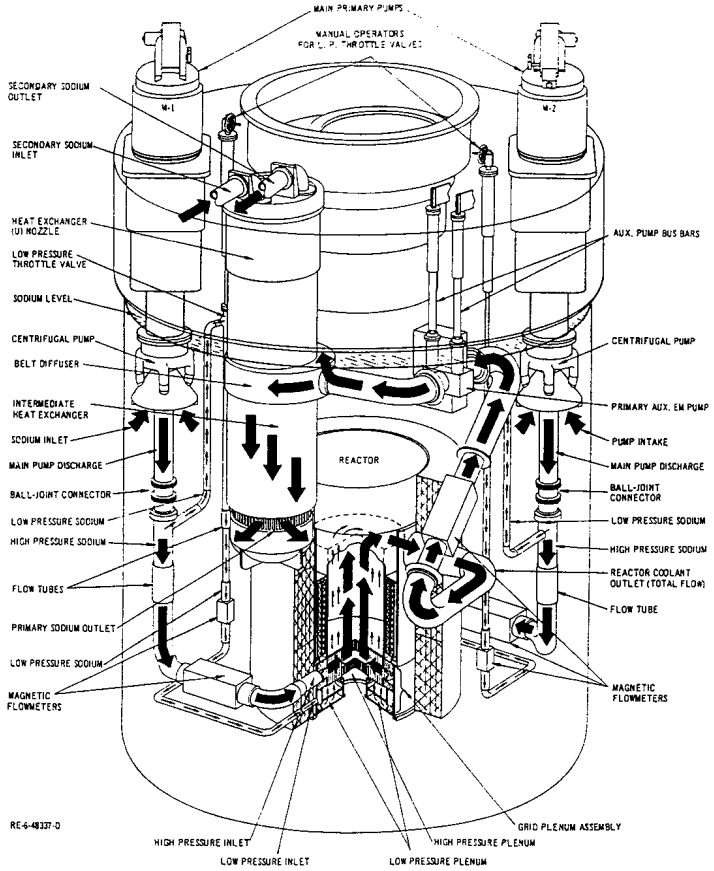

Fig. 4 – EBR-II Primary Tank Layout.

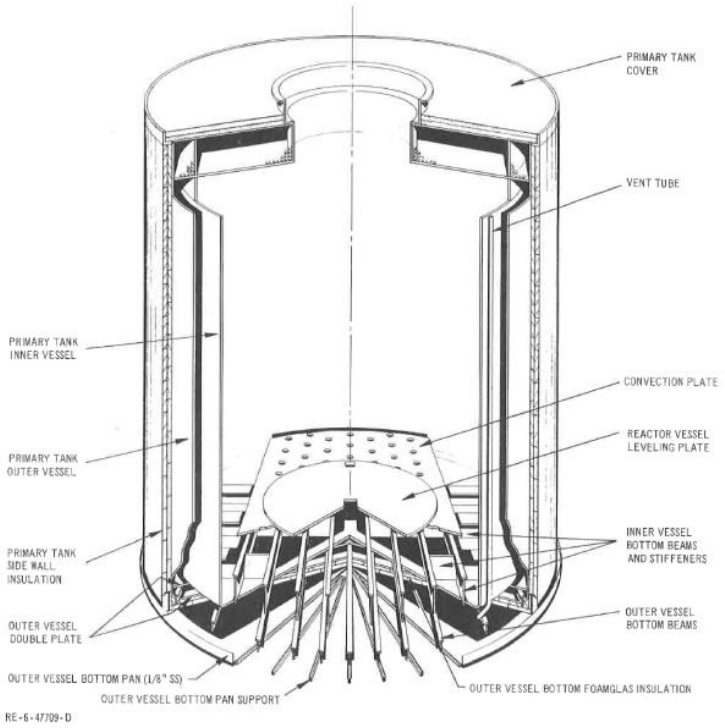

Fig. 5 – EBR-II Primary Tank Vessel.

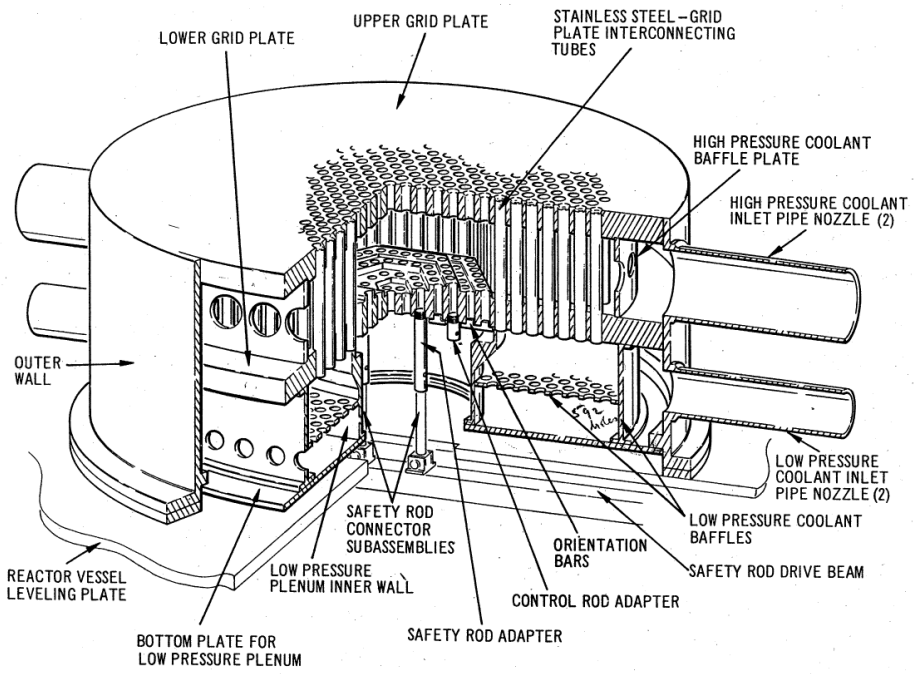

Fig. 6 – EBR-II High - and Low - Pressure Inlet Plena.

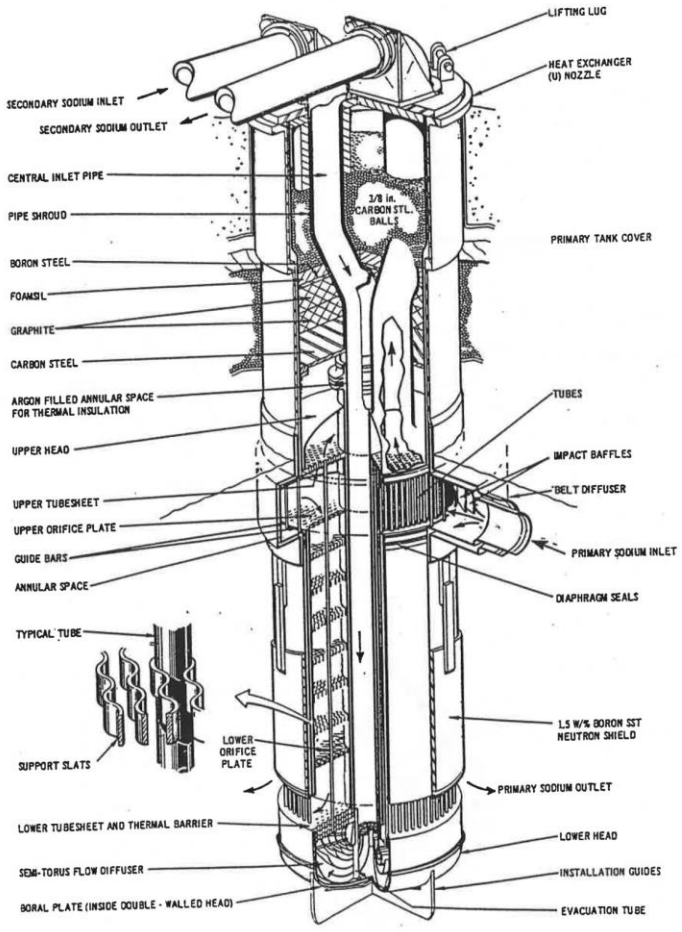

Fig. 7 – EBR-II Intermediate Heat Exchanger.

2.3 DESCRIPTION OF THE SHRT-17 EXPERIMENT

2.3.1 Objectives of SHRT-17

The main objectives of SHRT-17 [1][11][12] are:

- To support U.S. LMR plant design and to provide test data for validation of computer codes for design, licensing and operation of LMRs.
- To demonstrate effectiveness of natural circulation and natural phenomena (thermal expansion of the sodium coolant and thermal inertia of the primary pool sodium) in protecting the reactor against potentially adverse consequences from protected loss-of-flow and loss-of-heat-sink accidents.

2.3.2 Configuration of the facility, boundary and initial conditions of SHRT-17

To initiate the SHRT-17 test, both primary coolant pumps and the intermediate-loop pump were tripped to simulate a protected loss-of-flow accident beginning from full power and flow conditions. In addition, the primary system auxiliary coolant pump that normally had an emergency battery power supply was turned off. The reduction in coolant flow rate caused reactor temperatures to rise temporarily to high, but acceptable levels as the reactor safely cooled itself down at decay heat levels by natural circulation.

Initial Conditions

Primary sodium heat balance calculations are not available for the SHRT-17 test. According to post run-reports for Run 129-C (ANL-EBR-132), the initial power for the SHRT-17 test was 57.3 MW [11].

Tab. 1 and Tab. 2 summarize the initial conditions and transient initiators for the SHRT-17 test.

Transient Boundary Conditions

The pump speeds of the two primary sodium pumps are treated as boundary conditions in the primary sodium circuit. In the intermediate sodium loop, the boundary conditions are the flow rate and temperature of the sodium at the inlet of the IHX. Data is provided for each of the boundary conditions for the 15-minute duration of the test.

Primary sodium pump speeds are illustrated in Fig. 8. Tab. 3 gives the pump parameters to be used for the EBR_II primary side simulation. While EBR-II has two “identical primary pumps, pump #2 has higher frictional torque losses and stops sooner during the coastdown.

The normalized measured fission power for the first twenty seconds of SHRT-17 is illustrated in Fig. 9. No measurements were taken to effectively collect either the total reactor power or the decay heat power during the transient. The resulting decay heat power is plotted with the scaled fission power in Fig. 10 along with the sum of the two for the total reactor transient power.

The boundary conditions for the intermediate sodium loop for the SHRT-17 benchmark are the sodium flow rate and temperature at the inlet to the IHX. The IHX inlet sodium flow rate on the intermediate side during SHRT-17 is depicted in Fig. 12. The corresponding IHX inlet sodium temperature is shown in Fig. 12.

2.3.3 Description of SHRT-17

SHRT-17 was a loss of flow test used to support LMR plant design and to demonstrate effectiveness of natural circulation cooling characteristics. Tab. 8, Tab. 9, Tab. 10 reports the

facility configuration, the imposed sequence of main events and the resulting sequence of main events.

The experimental test started with EBR-II in nominal steady state conditions, thus at full power and flow. The initiating events were the trip of the primary coolant pumps and of the intermediate-loop pump. The reactor was instantaneously scrammed. The primary pump trip mode was a breaker trip, thus the flow coast-down was governed by the kinetic energy stored in the inertia of motor-generator set. Intrinsic differences between the two pump drive units caused a difference in stop times. The auxiliary electromagnetic pump in the primary loop was turned off and did not receive power from battery backups as would occur during a total station blackout. The reduction in coolant flow rate caused reactor temperatures to rise temporarily to high, but acceptable levels, as the reactor safely cooled itself down at decay heat levels by natural circulation. The test stopped after 15 minutes without any operator action any system intervention.

Four phases and related phenomena are identified in the transient, as discussed in section **4**. They are:

- **Phase 1** – effective core cooling by MCP coast-down (0 – 10s): from initiating events to fuel cladding starts to rise;

- **Phase 2** – primary system energy increases and temperatures rise (10 – 100s): from end of Phase 1 up to maximum fuel temperature in the core;

- **Phase 3** – buoyancy forces effective in removing energy from the core, long term cooling in natural circulation (100 – 900s): from end of Phase 2 up to end of transient.

TEST DESCRIPTION	
Initial Power	57.3 [MW]
Initial Primary Coolant Flow Through Core (at 700 K)	456 [kg/s]
Initial Intermediate Coolant Flow (at 579 K)	311.43 [kg/s]
Initial Core Inlet Temperature	624.7 [K]
Primary and Intermediate Pump Coastdown Conditions	Power to motor-generator sets removed
Control Rods	Full insertion at test initiation
Auxiliary EM Pump Conditions	Power to Auxiliary EM Pump removed

Tab. 1 – EBR-II, SHRT-17 Test Description.

INITIAL CONDITIONS	
Core sodium mass flow rate (at 700 K)	456 [kg/s]
Average core inlet temperature	625 [K]
Pressure at discharge of primary sodium pump #1	295785 [Pa]
Pressure at discharge of primary sodium pump #2	288890 [Pa]
Upper plenum pressure	43850 [Pa]
Intermediate sodium mass flow rate (at 579 K)	311.43[kg/s]
EBR-II operated at full power for less than two hours prior to test Calculated initial decay heat Resulting initial fission power	 3.36 [MW] 53.93 [MW]

Tab. 2 – EBR-II, SHRT-17 Initial Conditions.

PARAMETER	RATED CONDITION
N_R (rated speed)	870 [rpm]
H_R (rated head)	43 [m]
Q_R (rated flow)	0.2946 [m^3/s]
NS (specific speed)	31.01/1602 [SI/gp]
I_P (inertia)	16.0 [kg m^2]
T_R (rated torque)	1300.0 [N m]
$T_{f,R}$ (friction torque)	0.0286 T_R (37.2) [N m]

Tab. 3 – EBR-II primary pump parameters.

TIME [s]	PUMP#1 [rpm]	PUMP#2 [rpm]
0	799.0	764.9
2	727.7	695.4
4	566.7	532.6
6.5	407.5	376.6
9	323.2	301.5
12.5	244.1	230.1
17.5	172.5	167.3
24.5	109.2	113.9
33	56.5	74.62
42	0.69	46.54
51	0.76	2.29
90	0.76	2.44
120	0.61	2.44
180	0.76	2.44
240	0.84	2.59
300	0.61	2.44
360	0.61	2.44
420	0.61	2.44
480	0.61	2.44
540	0.76	2.44
600	0.76	2.75
660	0.69	2.44
720	0.69	2.44
780	0.76	2.59
840	0.76	2.44
900	0.92	2.44

Tab. 4 – EBR-II, SHRT-17: Primary Pump Speeds.

TIME [s]	FISSION [MW]	DECAY HEAT [MW]	TOTAL POWER [MW]
0	53.93	3.36	57.29
1	8.24	3.12	11.36
2	6.86	2.95	9.81
3.5	5.61	2.77	8.38
5	4.76	2.63	7.39
7.5	3.82	2.46	6.29
10	3.23	2.33	5.56
15	2.47	2.15	4.62
22.5	1.85	1.95	3.8
30	1.46	1.82	3.28
40	1.1	1.7	2.79
50	0.84	1.6	2.44
60	0.66	1.52	2.19
90	0.38	1.35	1.73
120	0.25	1.24	1.49
180	0.13	1.09	1.22
240	0.1	1	1.1
300	0.1	0.93	1.02
360	0.08	0.88	0.96
420	0.08	0.83	0.92
480	0.08	0.8	0.88
540	0.08	0.77	0.84
600	0.08	0.74	0.82
660	0.08	0.71	0.79
720	0.07	0.69	0.76
780	0.08	0.67	0.75

Tab. 5 – EBR-II, SHRT-17: Total, Fission and Decay Heat Power.

TIME [s]	IHX MASS FLOW RATE [kg/s]
0	311.7
1	234.1
2.5	157.1
6	88.41
16.5	42.16
30	28.34
60	21.29
120	18.20
180	18.29
240	19.03
300	20.58
360	21.74
420	22.03
480	22.37
540	22.08
600	23.56
660	22.17
720	20.47
780	19.82
840	18.88
900	17.24

Tab. 6 – EBR-II, SHRT-17: Intermediate IHX Inlet Sodium Flow rate.

TIME [s]	IHX INLET TEMPERATURE [K]
0	574.3
60	574.2
120	574.0
180	574.1
240	573.9
300	573.5
360	573.2
420	572.9
480	572.6
540	572.5
600	572.1
660	571.3
720	570.0
780	568.5
840	566.7
900	565.3

Tab. 7 – EBR-II, SHRT-17: Intermediate IHX Inlet Sodium Temperature.

SYSTEMS	CHARACTERISTICS	STATUS
Primary and Intermediate Pump	Loop #1 Loop #2	Power to motor-generator sets removed
Control Rods	8 Rods	Full insertion at test initiation
Safety Rods	2 Rods	Full insertion at test initiation
Throttle Valve	Loop #1 Loop #2	Active
Auxiliary EM Pump Conditions	--	Power to Auxiliary EM Pump removed

Tab. 8 – EBR-II, SHRT-17: Facility configuration.

IMPOSED EVENT DESCRIPTION	SYSTEM	SIGNAL (TIME OR SET POINT)	REMARKS
Trip of the MCP and coastdown	MCP	0 s	Coast-down in Fig. 8
Scram	Control and Safety Rods	0 s	Total power in Fig. 10
End of transient	--	900 s	--

Tab. 9 – EBR-II, SHRT-17: imposed sequence of main events.

Ph. W.	DESCRIPTION & PHENOMENA/PROCESSES	EVENT	Exp [s]
Phase I (0 – 10 s)	*Pressure drop at discontinuities* *Wall to fluid friction* *Heat transfer in covered core* *Heat transfer in passive structures and heat losses;* *Pool thermal hydraulics in the tank* *Multidimensional coolant temperatures and flow distributions* *Heat transfer in IHX primary (i.e. bundle zone) and secondary (non-bundle) sides and between IHX primary coolant and passive structures* *Thermal mixing in reactor upper plenum* *Forced circulation* *Pump behavior*	Stop MCP ***[Imposed]***	0
		Initiating event: loss of IHX flow rate ***[Imposed]***	0
		SCRAM ***[Imposed]***	0
		Min. cladding T in XX09 @ TAF	4.5
		Min. cladding T in XX10 @ core TAF	10
		Min. coolant T in UP	12
Phase II (10 – 100s)	*Pressure drop at discontinuities* *Wall to fluid friction* *Heat transfer in covered core* *Heat transfer in passive structures and heat losses;* *Pool thermal hydraulics in the tank* *Multidimensional coolant temperatures and flow distributions* *Conduction in fluid and structures* *Heat transfer in IHX primary (i.e. bundle zone) and secondary (non-bundle) sides and between IHX primary coolant and passive structures* *Thermal mixing in reactor upper plenum* *Transition from forced to natural circulation* *Pump behavior (i.e. coastdown)*	Max. cladding T in XX09 @ TAF	73.5
		Max. cladding T in XX10 @ core TAF	96.5
		Max. coolant T in UP	138.5
		MCP 2 coastdown end [minimum of mass flow rate]	76
Phase III (74 – 900s)	*Pressure drop at discontinuities* *Wall to fluid friction* *Heat transfer in covered core* *Heat transfer in passive structures and heat losses;* *Pool thermal hydraulics in the tank* *Multidimensional coolant temperatures and flow distributions* *Conduction in fluid and structures* *Heat transfer in IHX between primary coolant and passive structures* *1 Φ natural circulation; and* *Stratification in upper plenum*	End of transient ***[Imposed]***	900
		– (Cladding T XX09 @ TAF)	691-705K
		– (Cladding T XX10 @ core TAF)	672-675K

Tab. 10 – EBR-II, SHRT-17: resulting sequence of main events.

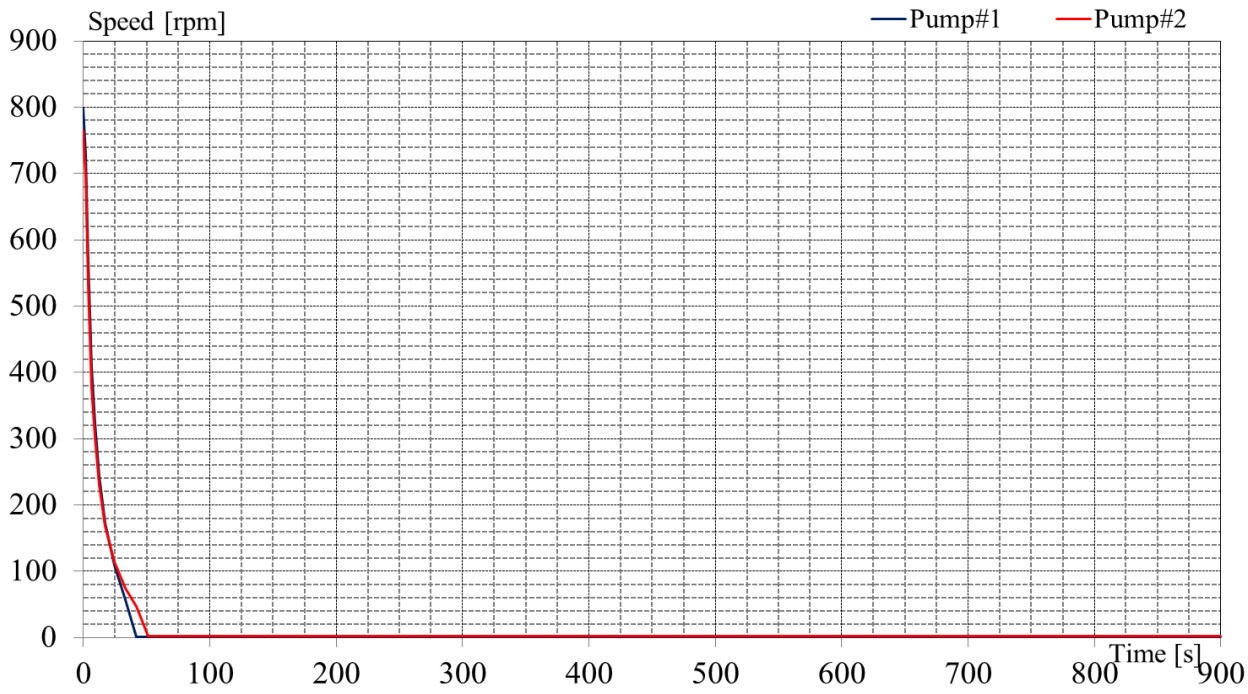

Fig. 8 – EBR-II, SHRT-17: Primary Pump Speeds.

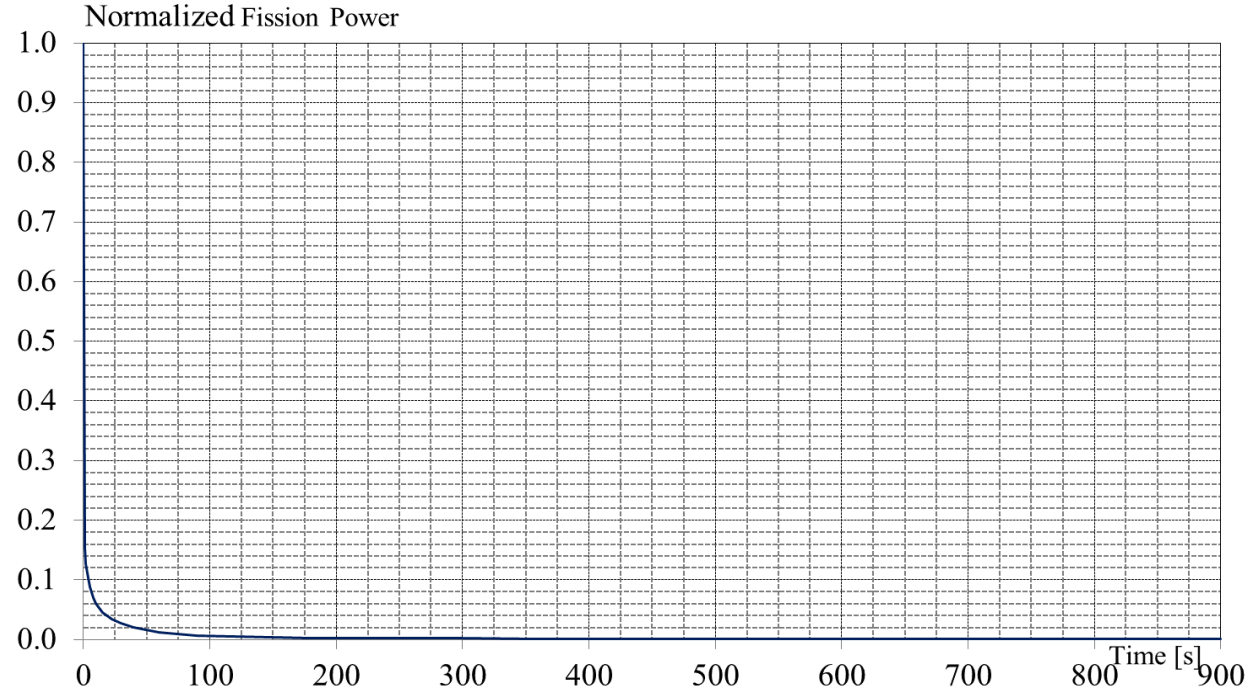

Fig. 9 – EBR-II, SHRT-17: Normalized Fission Power.

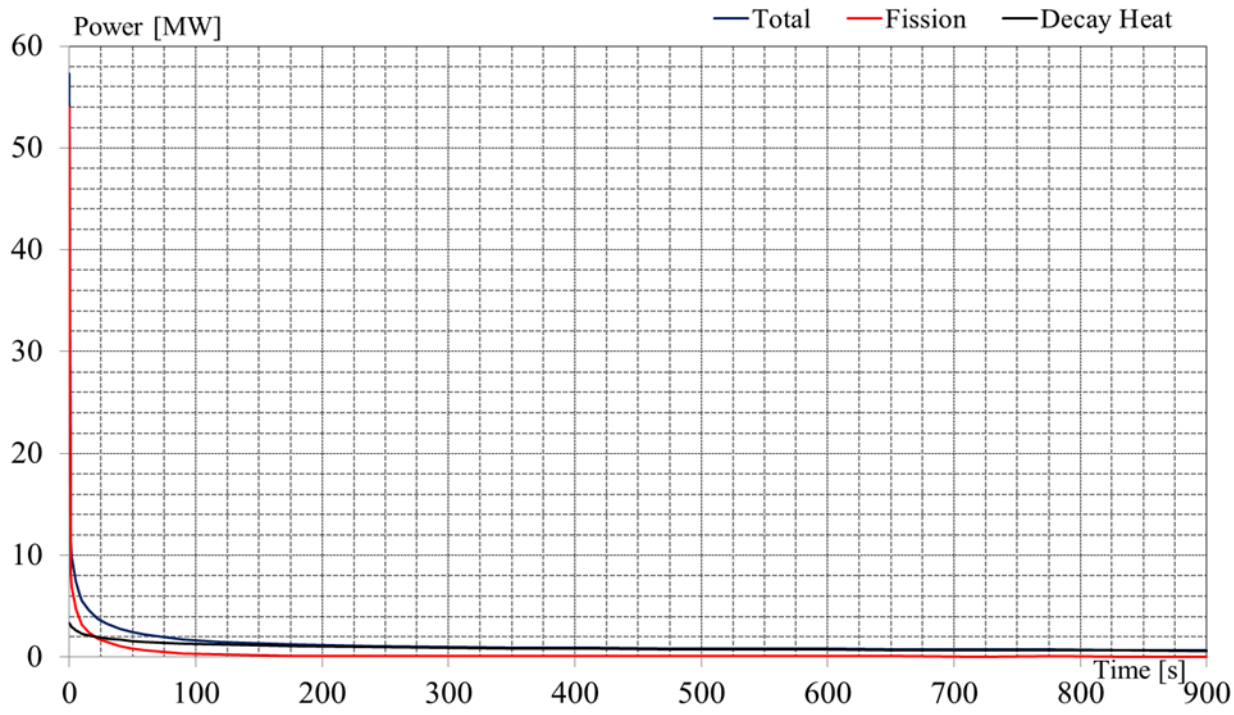

Fig. 10 – EBR-II, SHRT-17: Total, Fission and Decay Heat Power.

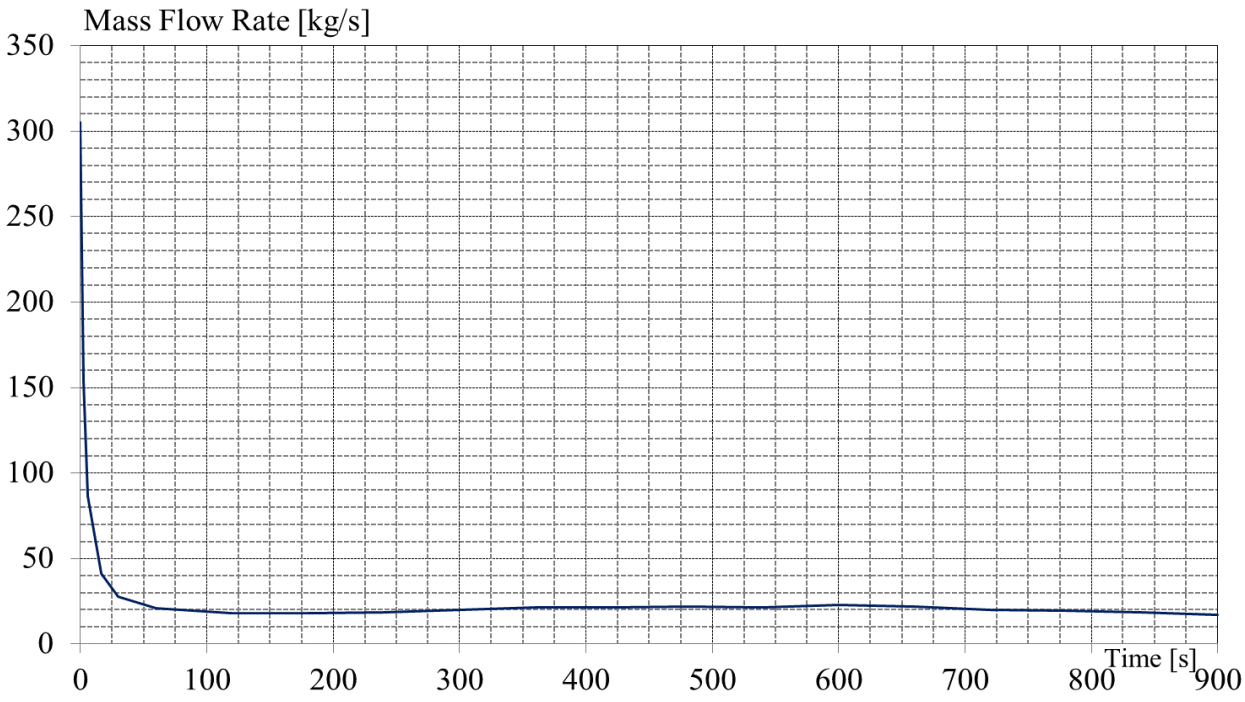

Fig. 11 – EBR-II, SHRT-17: IHX Intermediate Side Inlet Sodium Mass Flow Rate.

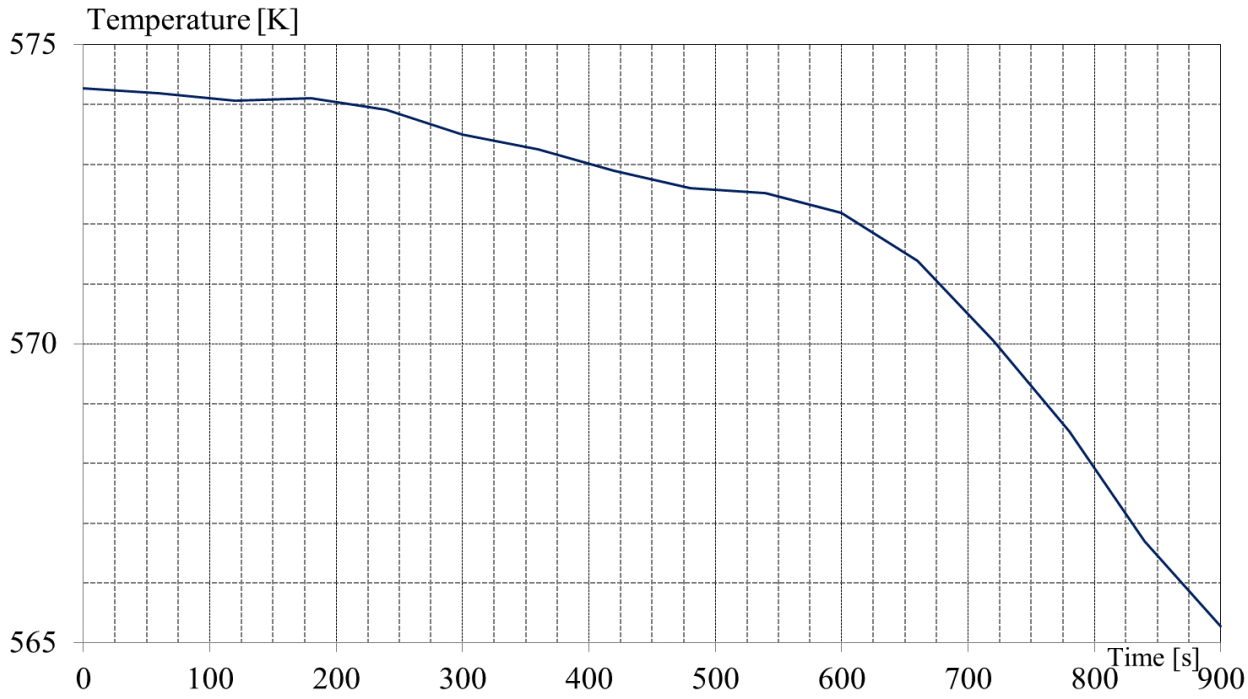

Fig. 12 – EBR-II, SHRT-17: IHX Intermediate Inlet Sodium Temperature.

3 RELAP5-3D© NODALIZATION

3.1 RELAP5-3D©v4.0.3 code

The RELAP5 [27] series of code has been developed at the Idaho National Laboratory (INL) under sponsorship of the U.S. Department of Energy, the U.S. Nuclear Regulatory Commission, members of the International Code Assessment and Applications Program (ICAP), members of the Code Applications and Maintenance Program (CAMP), and members of the International RELAP5 Users Group (IRUG). Specific applications of the code have included simulations of transients in light water reactor (LWR) systems such as loss of coolant, anticipated transients without scram (ATWS), and operational transients such as loss of feedwater, loss of offsite power, station blackout, and turbine trip. RELAP5-3D© [28], the latest in the series of RELAP5 codes, is a highly generic code that, in addition to calculating the behavior of a reactor coolant system during a transient, can be used for simulation of a wide variety of hydraulic and thermal transients in both nuclear and non-nuclear systems involving mixtures of vapor, liquid, non-condensable gases, and nonvolatile solute [7][29][30].

The RELAP5-3D© version contains several important enhancements over previous versions of the code. The most prominent attribute that distinguishes the RELAP5-3D© code from the previous versions the fully integrated, multi-dimensional thermal hydraulic and kinetic modeling capability. This removes any restrictions on the applicability of the code to the full range of postulated reactor accidents. Enhancements include a new matrix solver for 3D problems, new thermodynamic properties for water, and improved time advancement for greater robustness. Enhancements also include all features and models previously available in the ATHENA configuration version of the code, which are as follows: addition of new working fluids (e.g. ammonia, blood, carbon dioxide, DowThermA, glycerol, helium, helium-xenon, hydrogen, lead-bismuth, lithium, lithium-lead, molten salts, nitrogen, potassium, R134a (SUVA®), sodium, sodium-potassium, and xenon) and a magneto-hydrodynamic model [28].

3.2 EBR-II nodalization

A description of the RELAP5-3D© nodalization [2] is summarized below, distinguishing:

- The coolant system, that includes: the pool region, the lower and the top part of the pool; the major components in the primary sodium circuit: pumps, high and low pressure flow lines, throttle valve; the Z-Pipe and the intermediate heat exchanger, primary and secondary side.
- The reactor region, that includes the reactor vessel, including the lower plenum, the upper plenum and the core bypass; the core subassemblies, divided in the central core region (driver subassemblies) and outer blanket region (reflector and blanket subassemblies).

The EBR-II nodalization is shown from Fig. 13 to Fig. 17. The entire input deck consists of 3985 hydraulic volumes, 6428 hydraulic junctions and 5248 thermal structures. More details regarding the adopted code resources have been reported in Tab. 11. Detailed description of the nodalization is available in Ref. [2].

3.3 Nodalization features

The main features of RELAP5-3D© input deck are:

- Recommended common rules involving characteristic dimensions, flow path area, elevations, heat structures and capacities have been taken into account from the EBR-II benchmark data [11].
- Bypass is modeled according to geometric specifications, when available, and mass flow data in steady state.
- Comparisons between EBR-II pump specifications and code modelling characteristics are in *Tab. 12*
- A sliced approach is applied at all systems (i.e. coolant system, reactor core).
- The elevations of the different parts of the plant are maintained in the nodalization.
- Dimension of nodes is set-up according with the expected spatial temperature gradients, relevant geometrical features of the systems and measurement points constraints.
- The node to node ratio is kept uniform, as much as possible, with reference maximum ratio of 1.2 between adjacent sub-volumes.
- The roughness is set 3.2e-5 m with the exception of the core region, where is set 1.0e-6 m as consequence of the nodalization qualification, as reported in Ref. [2].
- The standard RELAP5 wall friction correlations (i.e. laminar and turbulent regions) are modified with Cheng and Todreas formulations to represent wire wrapped rod bundle with optionally form loss coefficient with a Reynolds dependence [17][34].
- K-loss coefficients in junctions have been evaluated or estimated on the basis of geometries, when available.
- Standard RELAP5 liquid metals correlations are used for convective heat transfer for non-bundle and bundle zones, described in Refs. [34] and [26].

3.4 Modeling changes for open calculation

Blind simulation results of test SHRT-17 is reported in Ref. [2].

The open simulation of test SHRT-17 is carried out with few modifications:

- The pressure drops of the primary system are set-up according with the experimental results of the test. Dependence of energy loss coefficients from Re number is taken into account to improve the prediction of the mass flow rate in the subassembly.

- The orientation of the core with respect to the high and low pressure line connections is corrected as in the real configuration, thanks to up-dated information delivered by the benchmark coordinators.

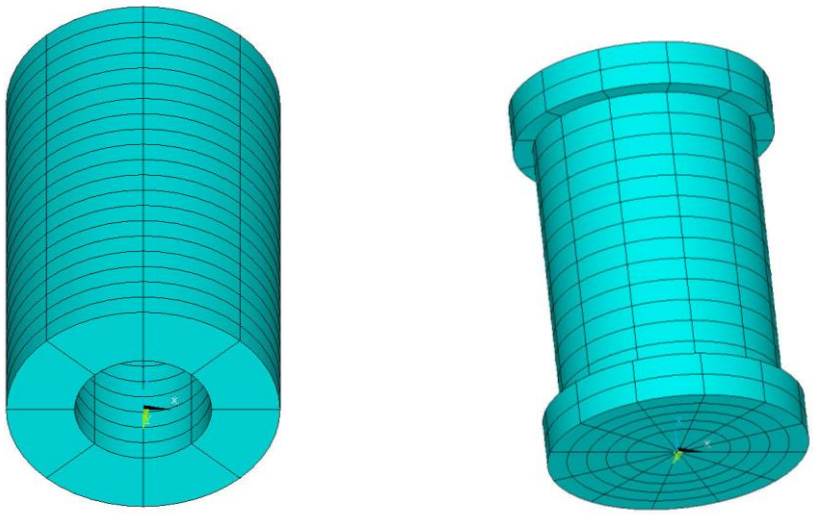

a) *Scheme of the pool region* b) *Scheme of the reactor vessel*

Fig. 13 – EBR-II SHRT-17, RELAP5-3D©: schematization of 3D components.

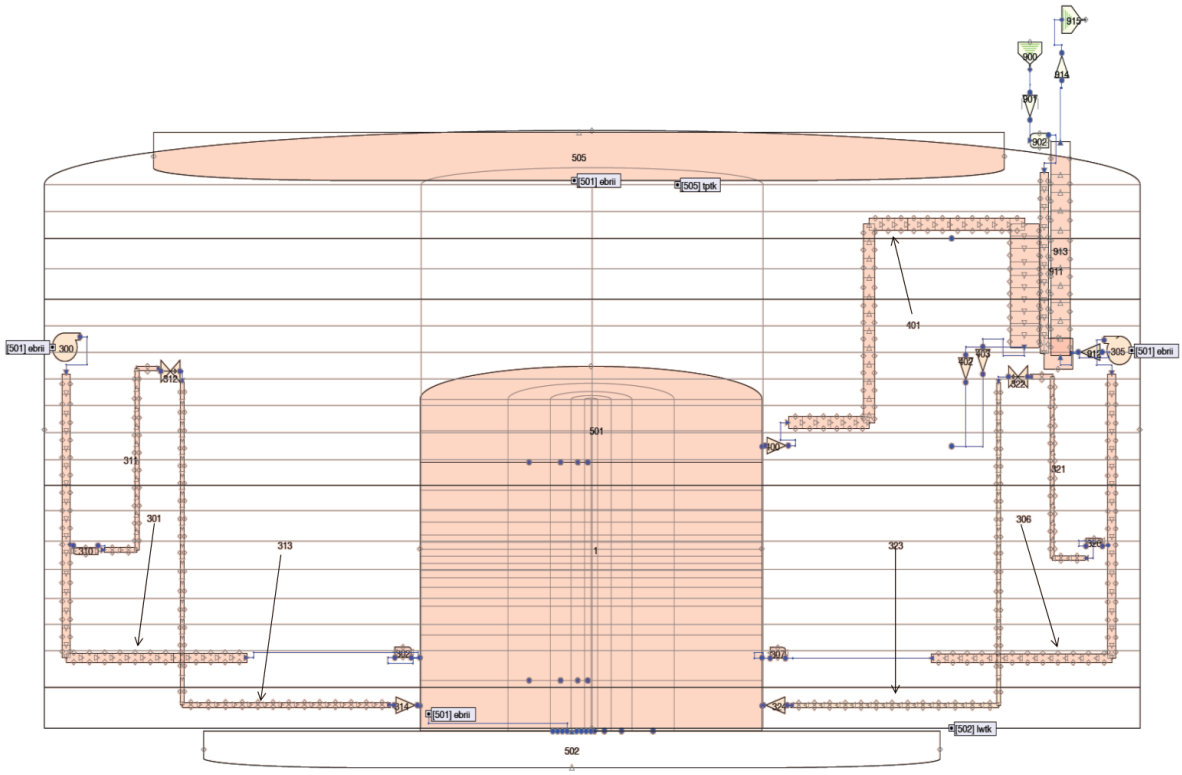

Fig. 14 – EBR-II SHRT-17, RELAP5-3D©: plant scheme.

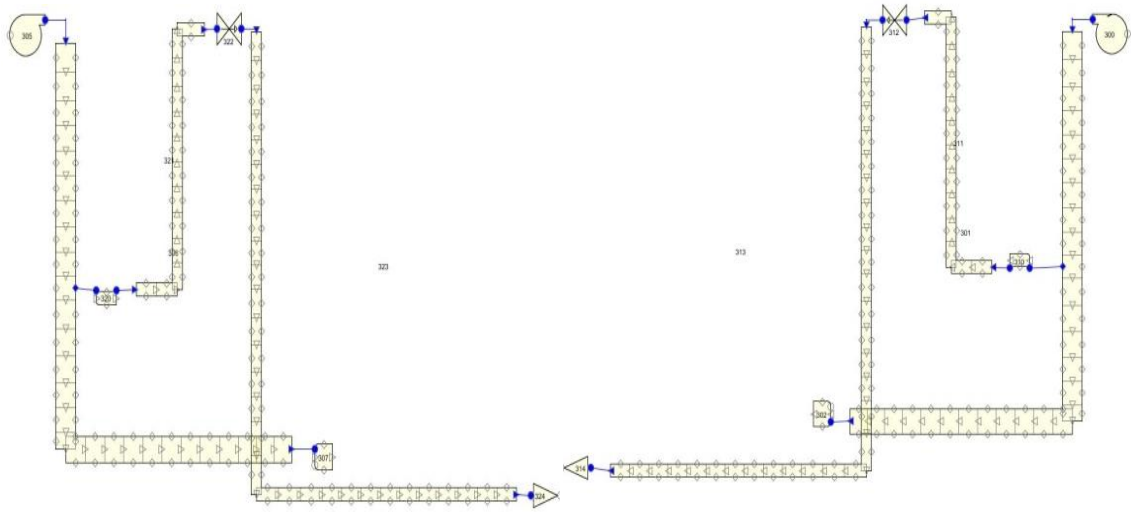

a) Pump#1, *b) Pump#2,*

[1] High and Low pressure flow lines#1

[2] High and Low pressure flow lines#2

Fig. 15 – EBR-II SHRT-17, RELAP5-3D©: scheme of pumps, high and low pressure flow lines.

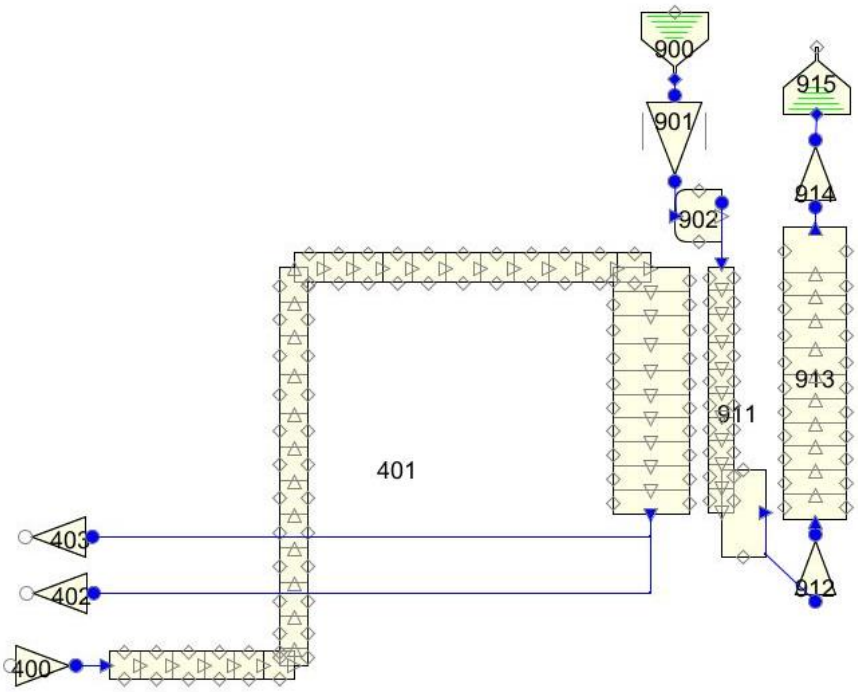

Fig. 16 – EBR-II SHRT-17, RELAP5-3D©: scheme of Z-PIPE, IHX primary and secondary side.

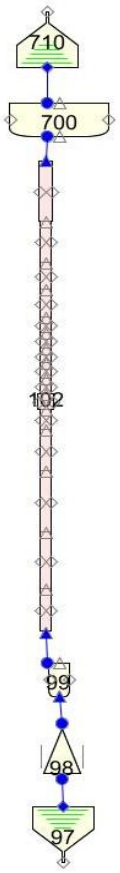

Fig. 17 – EBR-II SHRT-17, RELAP5-3D©: MARK-II AI fuel assembly

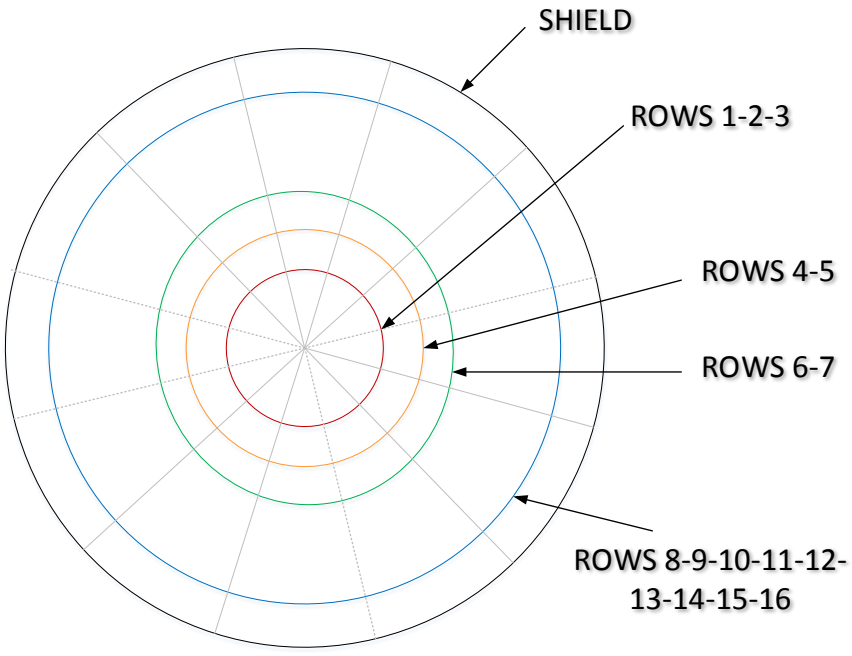

Fig. 18 – EBR-II SHRT-17, RELAP5-3D©: plane view of reactor core subdivision.

#	QUANTITY	Value
1	Tot. No. of HYDRAULIC volume	3985
2	Tot. No. of HYDRAULIC junction	6428
3	Tot. No. of HYDRAULIC volume in the core	2460
4	Tot. No. of heat structures	5248
5	Tot. No. of mesh points in the heat structures	31236
6	Tot. No. of core active structures (radial x axial)	8 x 5

Tab. 11 – EBR-II nodalization:adopted code resources.

PARAMETER	UNIT	RATED CONDITION	RELAP5-3D
Speed	[rad/s]	91.10	91.10
Head	[kPa]	358.530	328.5
Flow	[kg/s]	250.2	251.40 / 251.34
Torque	[Nm]	1300.0	1204.1

Tab. 12 – EBR-II SHRT-17, RELAP5-3D©: pump parameter.

4 QUALIFICATION OF EBR-II NODALIZATION AGAINST SHRT-17 TEST

Results of RELAP5-3D© simulations are presented: the blind calculation (Ref. [2]), performed on the basis of initial and boundary conditions delivered to the benchmark participants, and the open calculation, after the availability of the experimental data trends.

The mass flow rate distribution in the core sub-assemblies (i.e. core, extended core and blanket/reflector zones) has been set up using steady state data in isothermal conditions released to benchmark participants. These data provide mass flow rates in core sub-assemblies at rated pump operation. Detailed subassembly power distribution was also provided to benchmark participants with the reactor core at full power. Then, total core fission and decay heat powers versus time were given in benchmark specifications. The other boundary conditions used to set up the code simulations of SHRT-17 test were: MCP speed versus time; IHX secondary side mass flow rate and temperature versus time.

The initial conditions of the experiment at the end of steady state calculation are compared in Tab. 13. Steady state and initial conditions are achieved accordingly with the specifications for blind and open simulations. Few minor deviations are observed among the code results and the experimental data.

The comparison of the resulting sequences of main events is reported in Tab. 14. Selected experimental and calculated parameter trends are reported below and discussed (see also Ref. [35]).

Three phases and related phenomena are identified in the transient (see section 2.3.3).

Phase 1 – effective core cooling by MCP coast-down (0 – 10s): from initiating events to fuel cladding starts to rise.

Phase 2 – primary system energy increases and temperatures rise (10 – 100s): from end of Phase 1 up to maximum fuel temperature in the core.

Phase 3 – buoyancy forces effective in removing energy from the core, long term cooling in natural circulation (100 – 900s): from end of Phase 2 up to end of transient.

The initiating events of the test are the primary pumps and the intermediate pump trips (Phase 1). The reactor SCRAM occurs and the transient evolves without any system intervention or any operator/external action, thus such as a station blackout. The core temperatures (cladding and coolant, see Fig. 19) decrease for about 10 s (9 seconds considering the cladding temperatures at TAF of subassembly XX09, Fig. 23), due to sharp decrease of nuclear fission power, and mass flow rate, with the pump coasting-down, is still above 30% of initial value (see Fig. 42, Fig. 43, Fig. 44, Fig. 45 and Fig. 46).

Correct prediction of this phase is mainly connected with the energy distribution in the core structures, the thermal inertia and, then, the evaluation of the pressure drop in the system (i.e. dominated by the subassembly inlet orifices and friction losses in wire wrapped fuel bundle) and the pump coast-down. The main parameters trends of blind (Ref. [2]) and open simulations are satisfactory during this phase, because the convective heat transfer between the core structures and

the coolant is correctly calculated by the code, the flow distribution in core subassemblies is still proportional to the initial distribution and the conduction in the fluid is still negligible.

When the coolant pump flow rate decreases below 30% of nominal mass flow rate, the unbalance between total core power (fission and decay heat) and energy removed by the primary coolant flow causes a sharp increase of cladding and coolant temperatures in the subassemblies (phase 2). The maximum cladding temperatures experienced by the experimental subassemblies XX09 and XX10 at top of active core are observed at 73 s and 96 s, respectively (see Fig. 23 and Fig. 29). Code predictions are driven by the pump inertia, the pressure drops calculated in the subassemblies inlet orifices and in the wire wrapped fuel bundles.

The latest is based on Cheng and Todreas formula specified in the input deck. This means that the code follows this formula in laminar and turbulent regions. Larger errors are in the transition region, because Cheng and Todreas formulation has the transition region function of P/D, whereas in RELAP5-3D is a constant range $2200 < Re < 3000$ [34].

The energy loss coefficients at subassemblies inlet orifices are set up on the basis of the experimental data trends of mass flow rates at nominal steady state. However, it is expected that RELAP5-3D© has the capability to model the Reynolds dependent energy loss coefficients of these geometries, with some limitations in the laminar region, as discussed in Ref. [34].

Timing and rates of coolant and cladding temperature increases in the core are qualitatively and quantitatively well predicted in code simulation (see XX09 from Fig. 22 to Fig. 26; XX10 from Fig. 28 to Fig. 32). The blind simulation was affected by an underestimation, see Ref. [2]. This was connected with the faster increase of mass flow rate, following the pumps coast-down end, and with the flow stabilization to an higher value.

The open calculation evidenced an excellent simulation of the mass flow rates measured in high and low pressure lines (Fig. 45 and Fig. 46), as well as of the mass flow rates in available experimental subassemblies XX09 and XX10 (Fig. 47 and Fig. 48). Experimental cladding and coolant temperatures are simulated with satisfactory accuracy, in particular when the safety relevant parameters are considered (see Fig. 21 to Fig. 25 and Fig. 27 to Fig. 31). Nevertheless, some quantitative differences are observed and hereafter discussed.

Considering that the mass flow rates are correctly predicted, the coolant flows from high and low pressure feeding pipes towards the corresponding lower plena, delivering the sodium towards the different sub-assemblies. In this zone, complex three dimensional coolant flow distribution is roughly simulated by the coarse MULTID component of RELAP5-3D©. Then, once the natural circulation is the prevailing driving force of primary flow, the thermal conductivity in the core thermal structures and in the fluid becomes relevant.

The reference blind and open calculations do not account for axial thermal conduction in heat structures (i.e. only radial conduction is calculated by the code). However, the code has the capability to calculate the axial conduction in the heat structure, but it does not have the same capability for the conduction in the fluid. This would result in a conservative prediction of the code simulations with respect to temperatures of heat structure. Indeed, sensitivity analyses were carried out to evaluate the effect of the axial conduction model implemented in RELAP5-3D© (see Ref. [35]).

Moreover, considering the conduction in the coolant, it will affect the temperature distribution of subassemblies in radial and axial directions (see Fig. 33, Fig. 34, Fig. 35, Fig. 36, Fig. 37 and Fig. 38). This level of detail is beyond the objectives of the present simulation and the capabilities of RELAP5-3D© nodalization. The conduction in the coolant affects the temperature distribution upstream, downstream the active fuel and of core bypass region. This effect is highlighted by the coolant temperature change from the high pressure line, upstream the reactor zone (Fig. 41) and the coolant temperatures in XX09 and XX10 at flow meter (see Fig. 21 and Fig. 27). Looking at Fig. 21 and Fig. 27, it is evident that the coolant temperature is higher than in the code results, but the experimental thermocouples in XX09 (two at about 15-20 cm of distance) measure the same temperature, on the opposite in XX10 a coolant temperature difference is observed. For sake of clarity, it is highlighted that conduction of fluid is treated as infinite, when a computational volume is concerned, and zero, when adjacent computational volumes are considered. Considering the experimental subassemblies XX09 and XX10, they are both placed in the fifth ring of the reactor core. According with the MULTID discretization, 3 subassemblies of fourth ring and 4 of the fifth exchange energy with the corresponding radial and azimuthal bypass stack of hydraulic volumes. This means that only one temperature is assumed (infinite fluid conduction) for the hydraulic volume and no exchange of energy is possible between adjacent bypass volumes without transport of mass (no fluid conduction). This explain why, the XX09 cladding and coolant temperatures are accurate in the active zones and less accurate downstream, whereas in XX10, the temperature at mid core is overestimated and excellent prediction of the experimental temperatures otherwise. The thimble coolant temperatures at top of sub-assemblies are overestimated in both XX09 and XX10 as well.

Considering the upper plenum of the reactor zone, the measured temperature trends are connected with the mixing, induced by the forced circulation during the phase 1 of the test, the onset of thermal stratification is in phase 2, which, then, becomes the prevailing process after 100 seconds from the starting of transient. The correct prediction of coolant thermal mixing and stratification phenomena cannot be accurately predicted by RELAP5-3D© code. It is influenced by the nodalization scheme, and thus by the user effect. Improved prediction of thermal stratification can be achieved increasing the number of axial meshes in the upper plenum, and improving the knowledge of the flow paths occurring in this zone. Performances of open simulation is reported in Fig. 39.

Phase 2 ends after about 100s, when total core power (i.e. mainly decay heat) is efficiently removed in all subassemblies by natural circulation flow.

The coolant from reactor core is transported towards the Z-pipe (Fig. 20) at the IHX inlet and outlet (Fig. 40). During phase 3, the natural circulation is stabilized. Coolant temperature at core outlet and thermal structures in the core zone are cooled down. The results of the simulation predict correctly these trends. Improved quantitative accuracy is observed in open calculation, thanks to a better simulation of natural circulation flow.

The experiment is stopped after 900s, with the maximum coolant temperatures at subassemblies XX09 and XX10 equal to 691-705K and 672-675K, respectively. The blind (open) simulation predicts these temperatures 674K (700K) and 665K (676K).

In summary, the simulation demonstrate that RELAP5-3D© has the capability to predict the main phenomena and processes relevant to safety of the test. The trends of primary mass flow rate are well predicted (open calculation). Analogous consideration is applicable to coolant and cladding

temperatures of primary system. Improvements might be possible if knowledge of EBR-II features/characteristics is improved too (e.g. inlet sub-assemblies geometry details and characterization, better understanding and quantification of the cooling induced by the IHX structures close to the Z-pipe inlet).

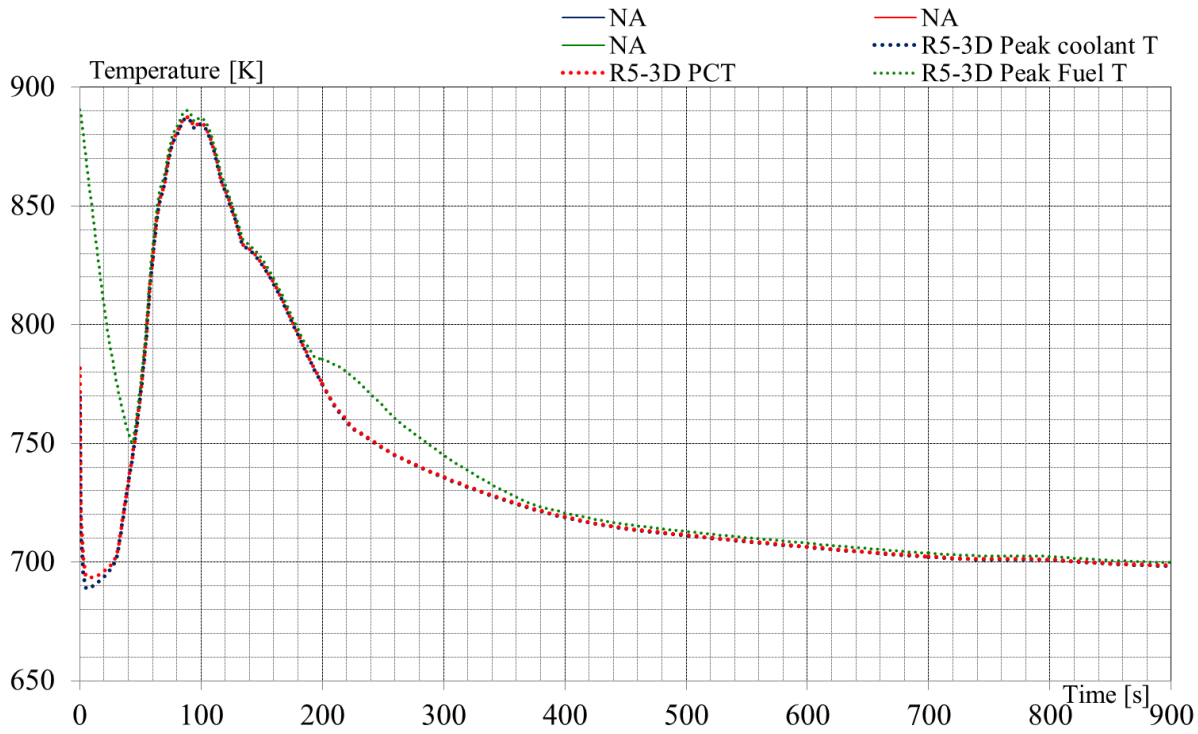

Fig. 19 – EBR-II SHRT-17, RELAP5-3D©: envelop of fuel centerline temperatures, PCT, and coolant temperatures in the core .

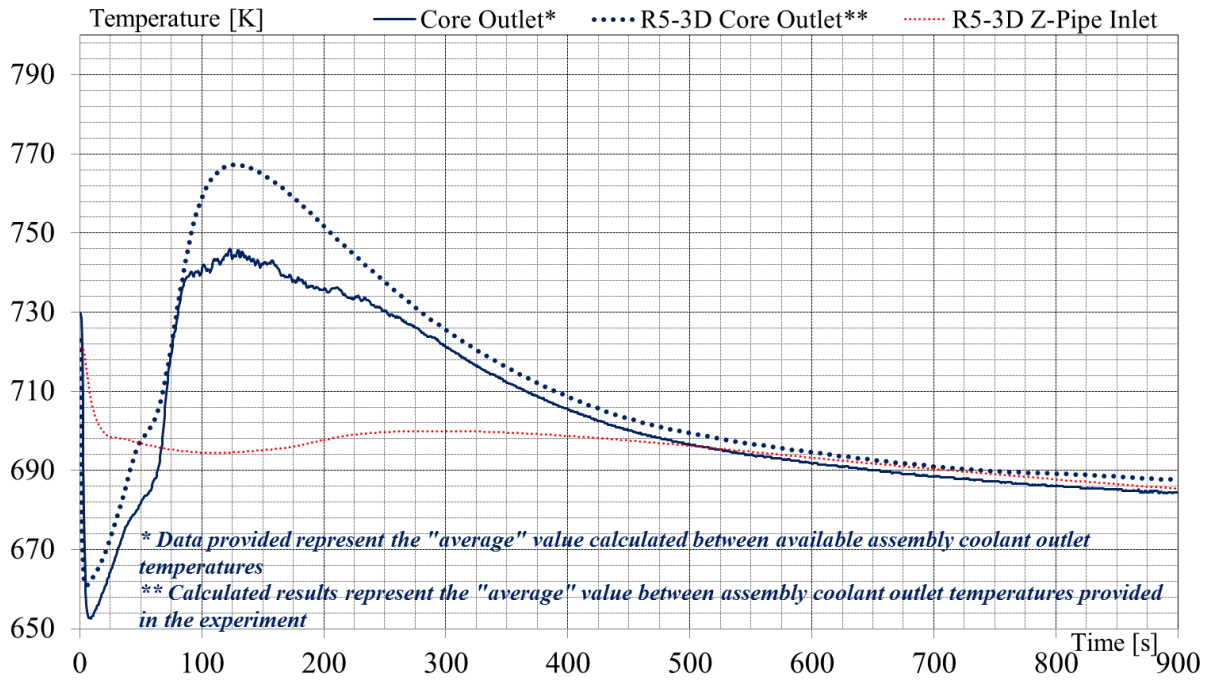

Fig. 20 – EBR-II SHRT-17, RELAP5-3D©: averaged coolant outlet temperature and Z-pipe inlet coolant temperature .

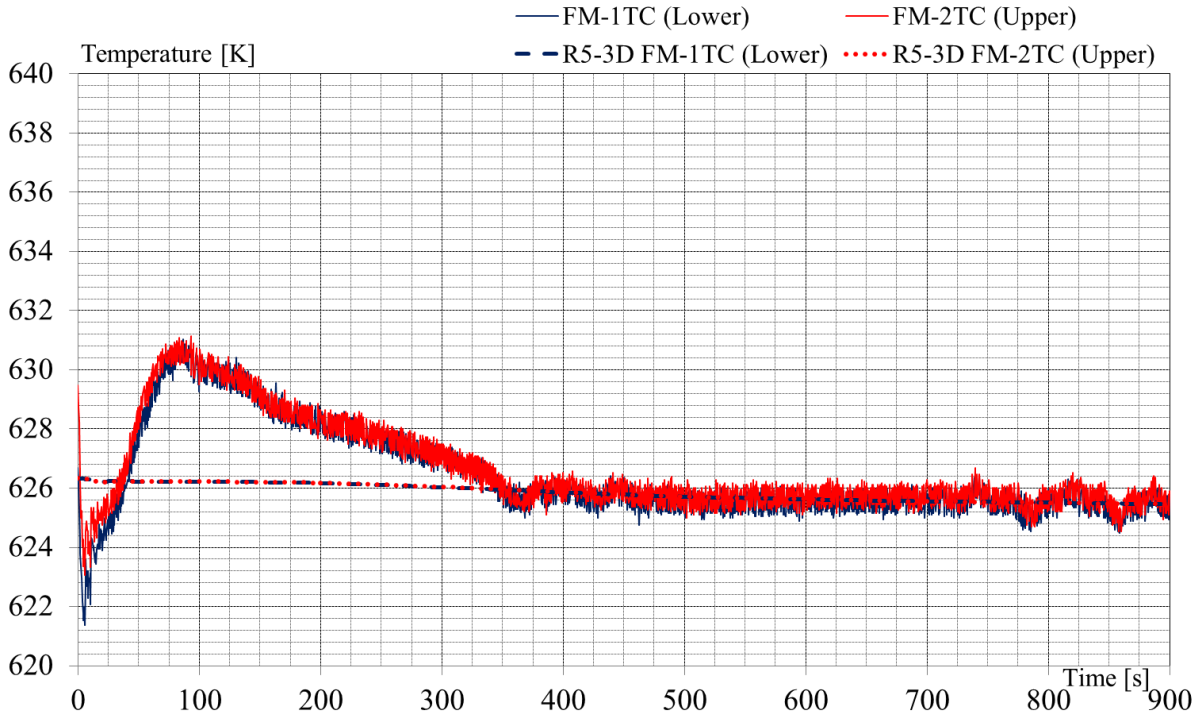

Fig. 21 – EBR-II SHRT-17, RELAP5-3D©: FA XX09 coolant temperature at flowmeter (0.25 and 0.4m below BAF).

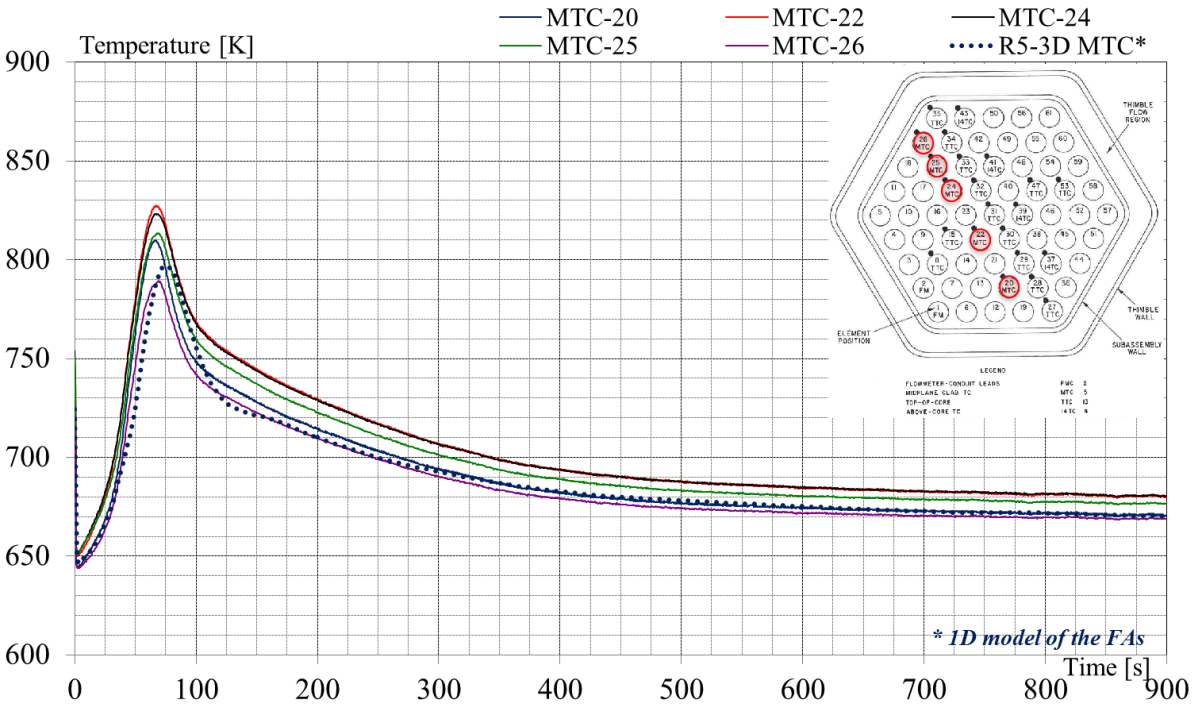

Fig. 22 – EBR-II SHRT-17, RELAP5-3D©: FA XX09 cladding temperatures at middle of active core.

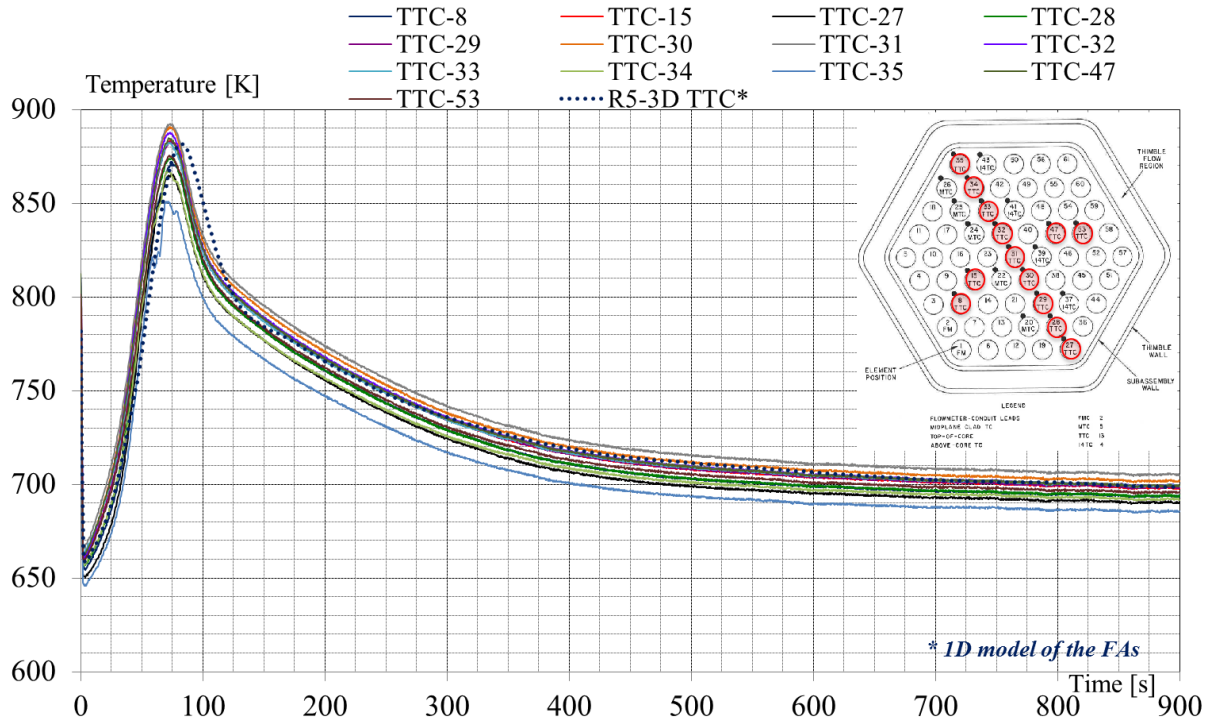

Fig. 23 – EBR-II SHRT-17, RELAP5-3D©: FA XX09 cladding temperatures at top of active core.

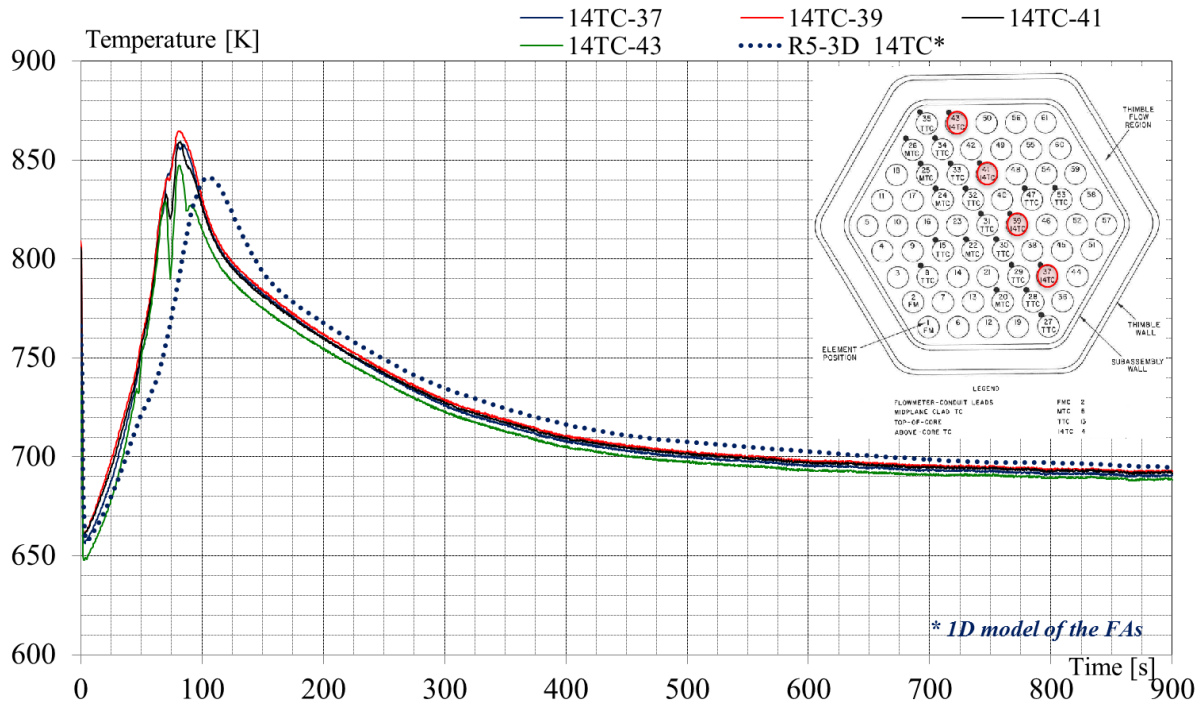

Fig. 24 – EBR-II SHRT-17, RELAP5-3D©: FA XX09 cladding temperatures at top of wire wrapped fuel bundle.

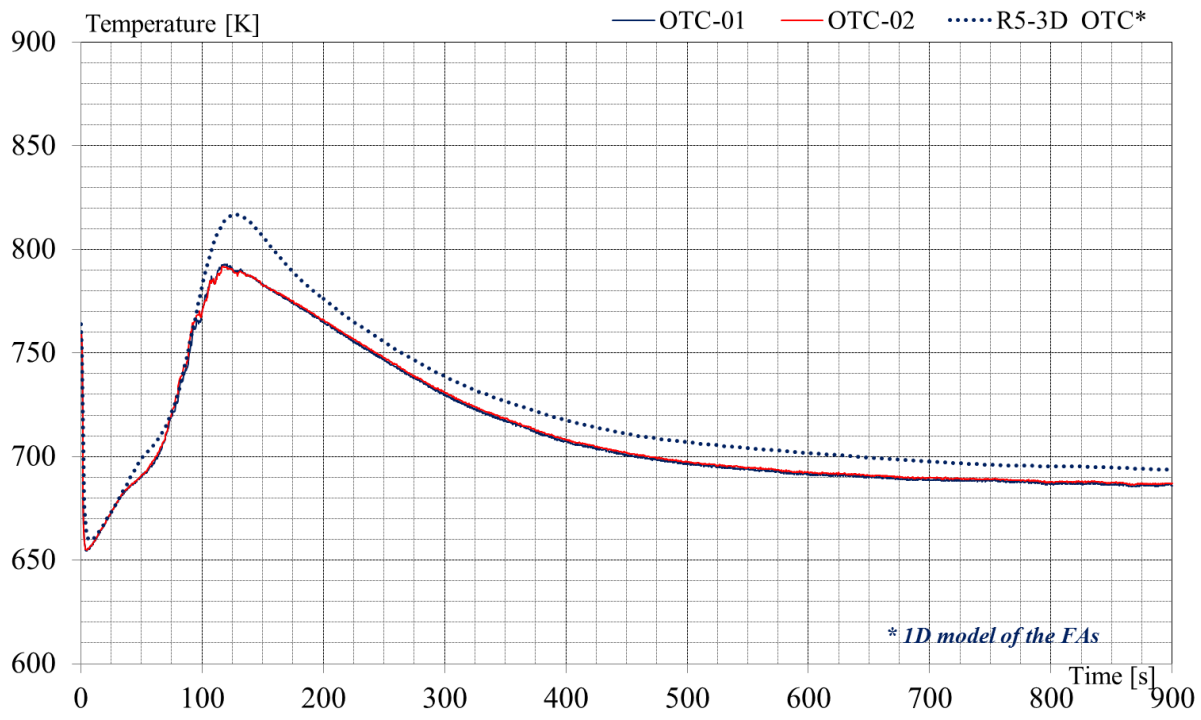

Fig. 25 – EBR-II SHRT-17, RELAP5-3D©: FA XX09 coolant temperatures at outlet.

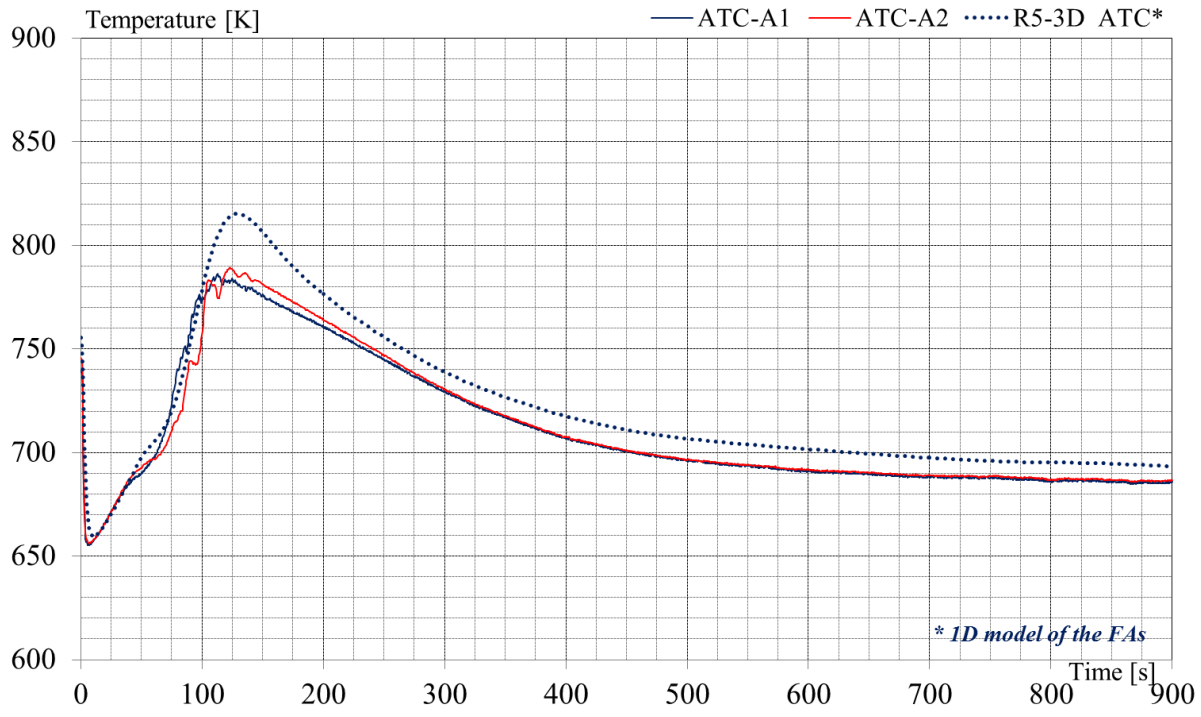

Fig. 26 – EBR-II SHRT-17, RELAP5-3D©: FA XX09 coolant temperatures at outlet of thimble channel.

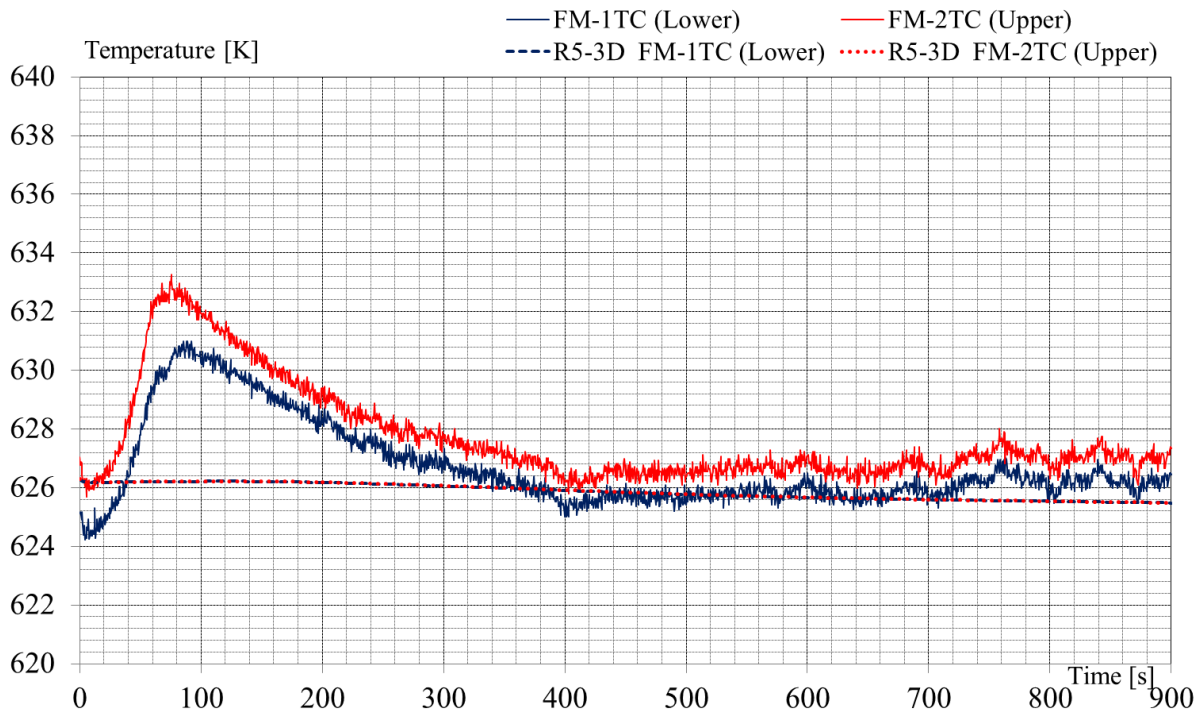

Fig. 27 – EBR-II SHRT-17, RELAP5-3D©: FA XX10 coolant temperature at flowmeter (0.25 and 0.4m below BAF).

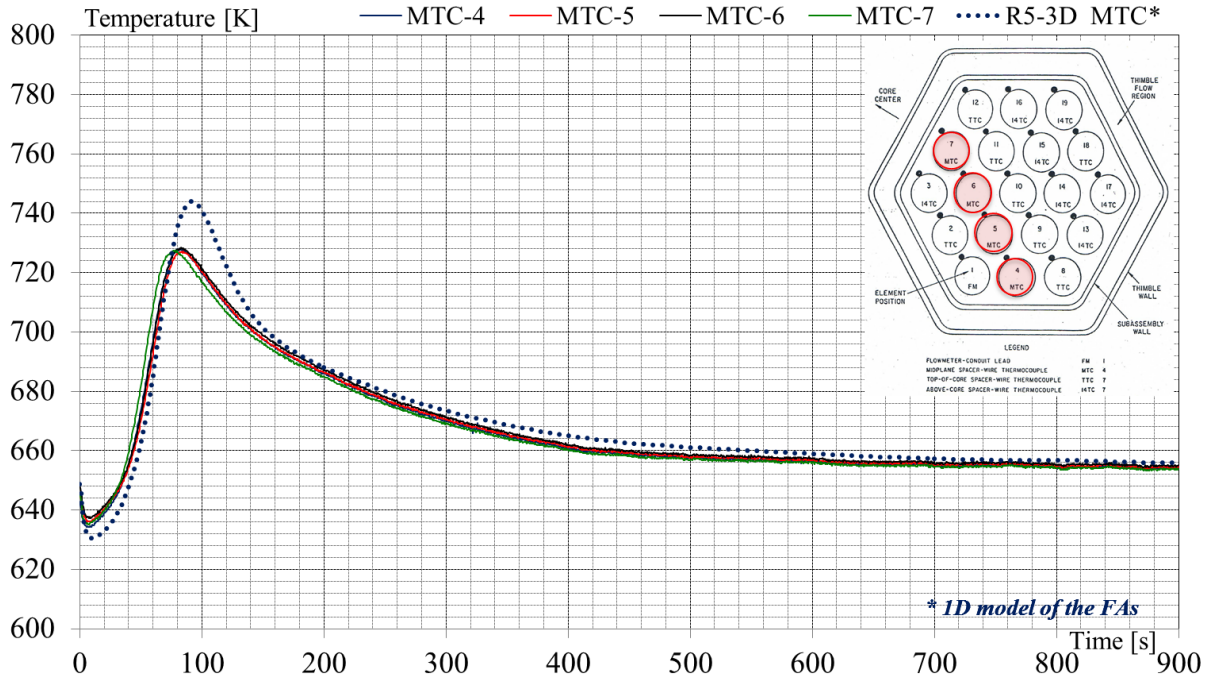

Fig. 28 – EBR-II SHRT-17, RELAP5-3D©: FA XX10 cladding temperatures at middle of active core.

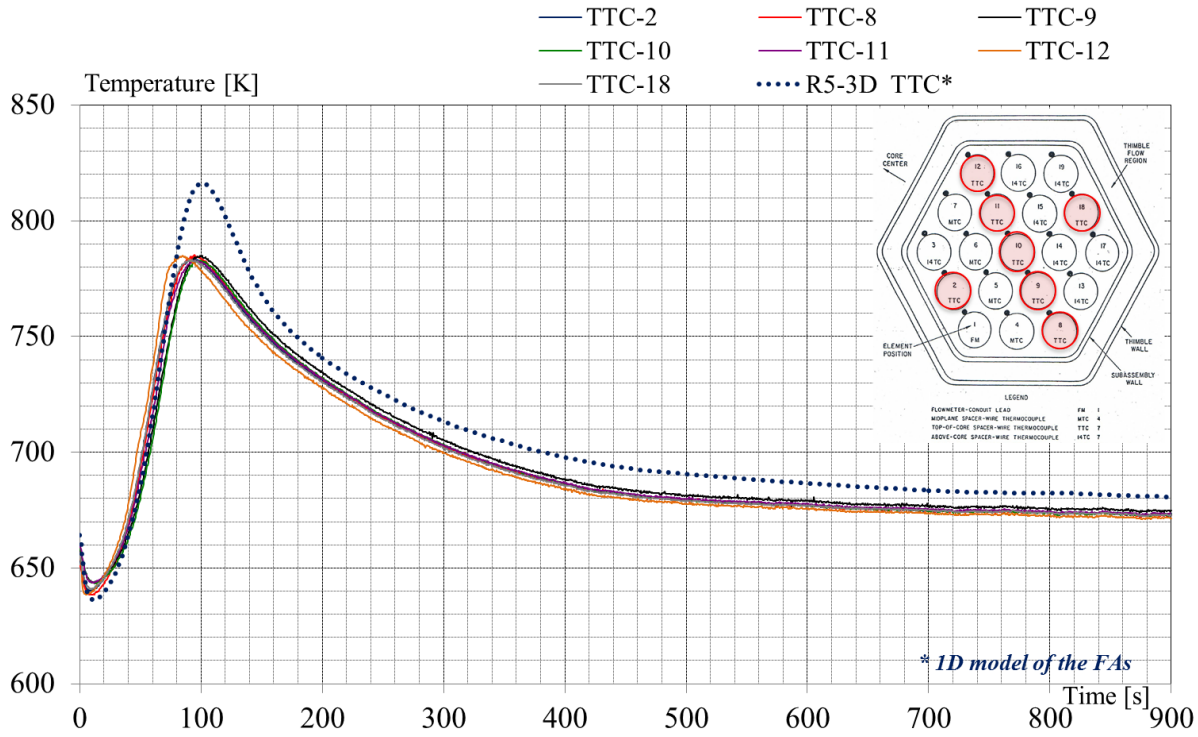

Fig. 29 – EBR-II SHRT-17, RELAP5-3D©: FA XX10 cladding temperatures at top of active core.

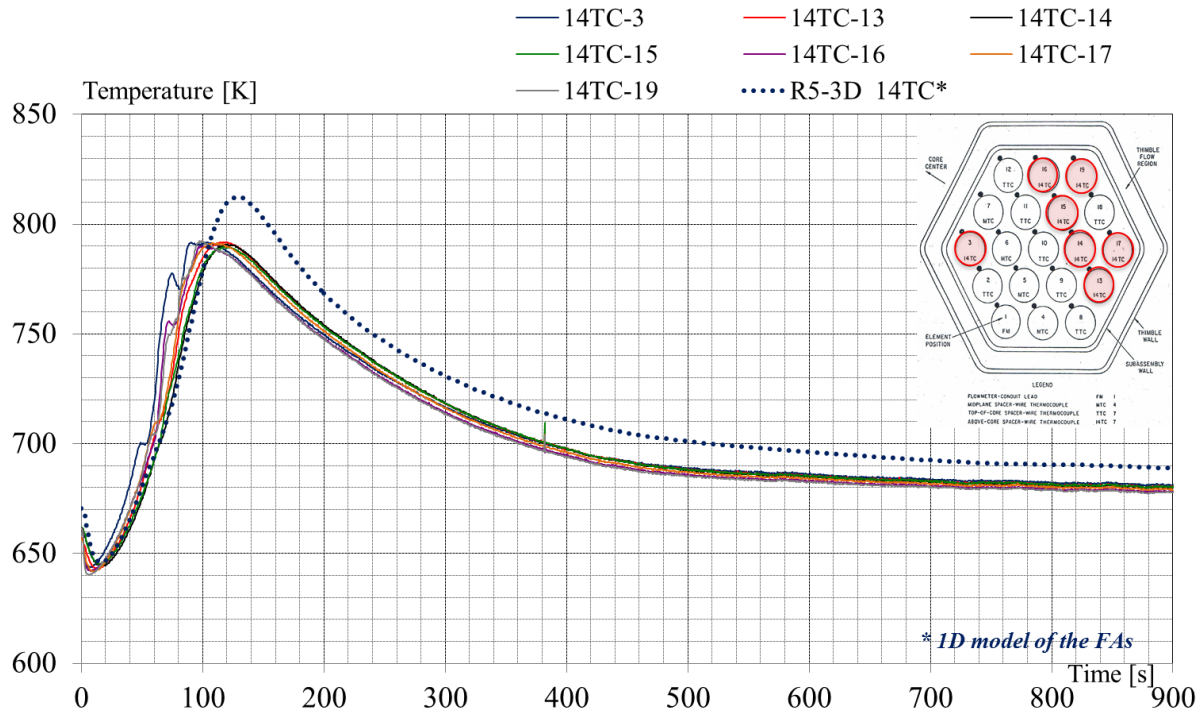

Fig. 30 – EBR-II SHRT-17, RELAP5-3D©: FA XX10 cladding temperatures at top of wire wrapped fuel bundle.

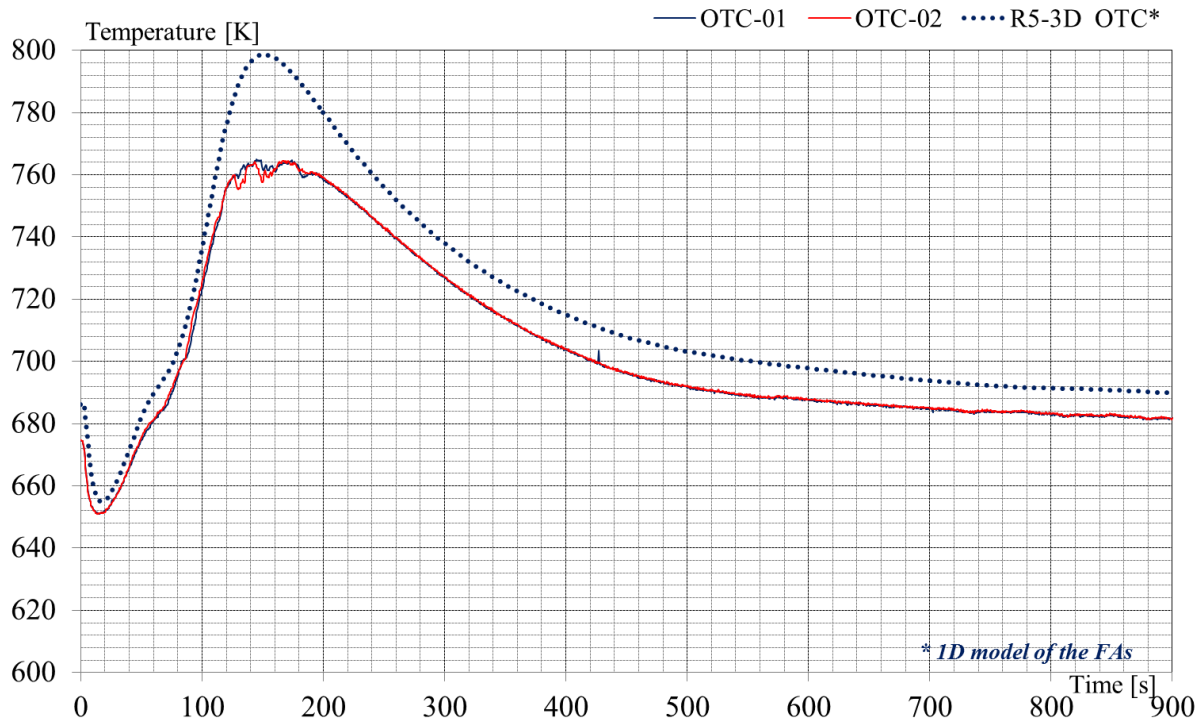

Fig. 31 – EBR-II SHRT-17, RELAP5-3D©: FA XX10 coolant temperatures at outlet.

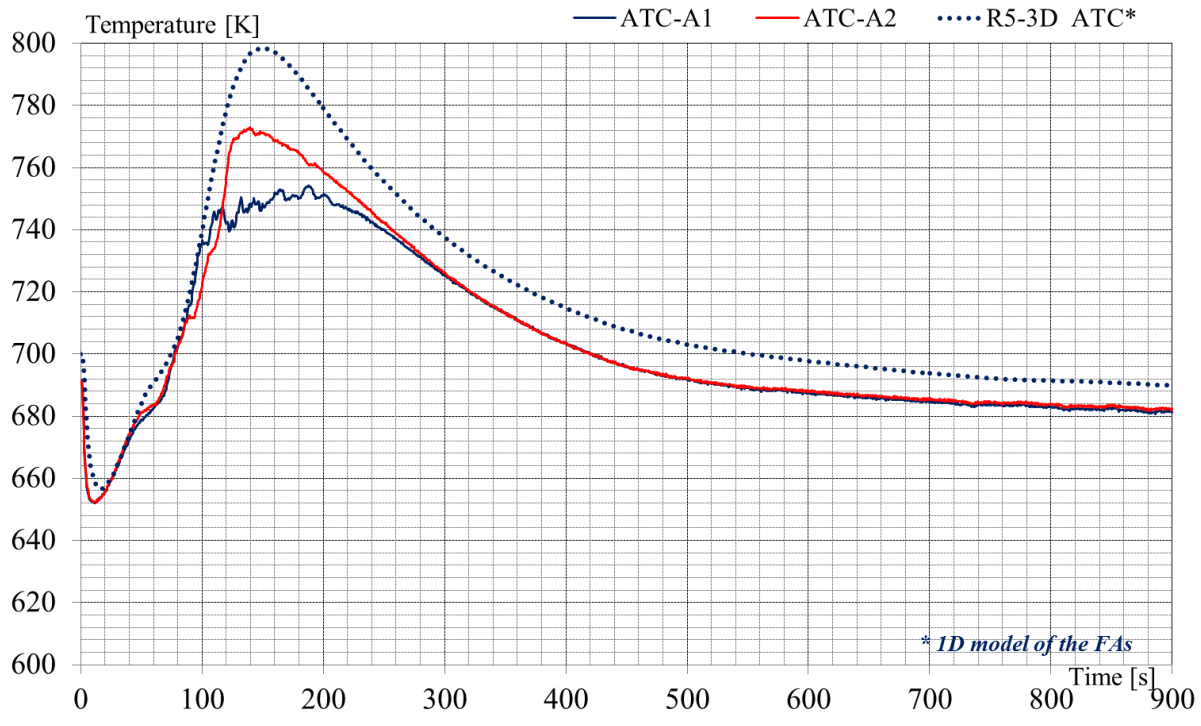

Fig. 32 – EBR-II SHRT-17, RELAP5-3D©: FA XX10 coolant temperatures at outlet of thimble channel.

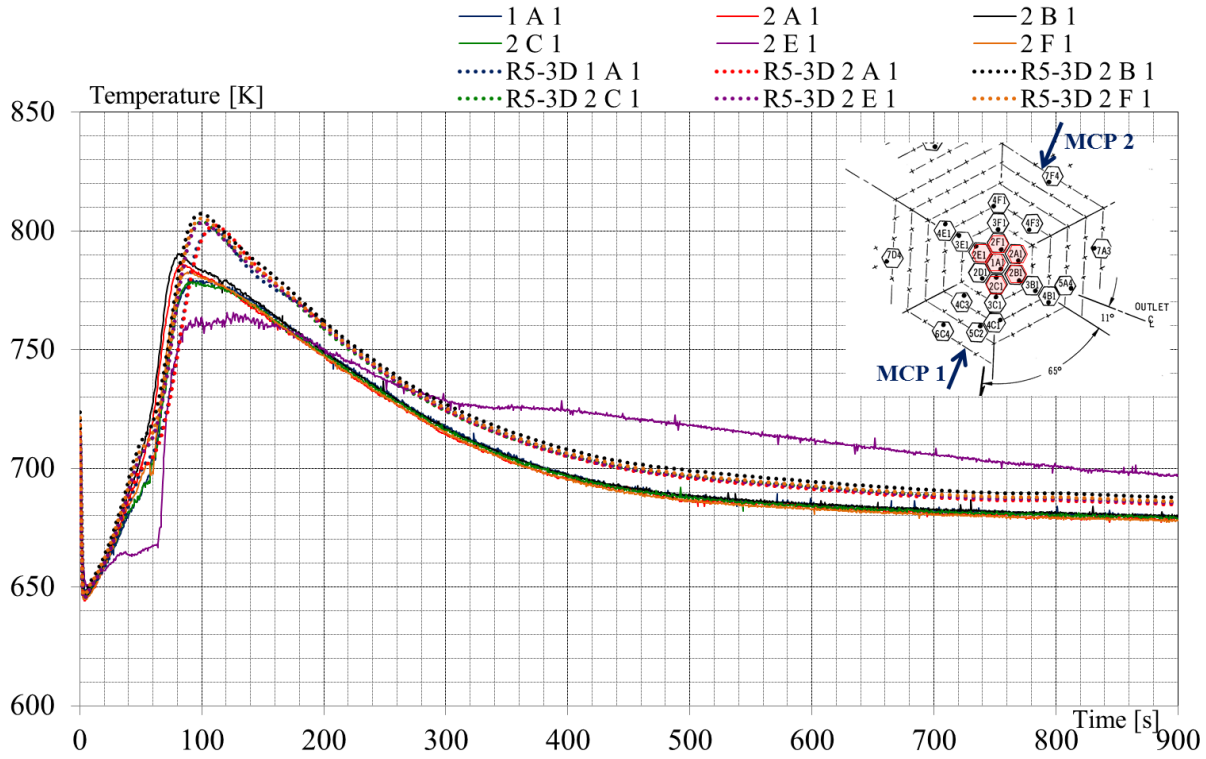

Fig. 33 – EBR-II SHRT-17, RELAP5-3D©: selected SA, ring 1 and 2 coolant outlet T.

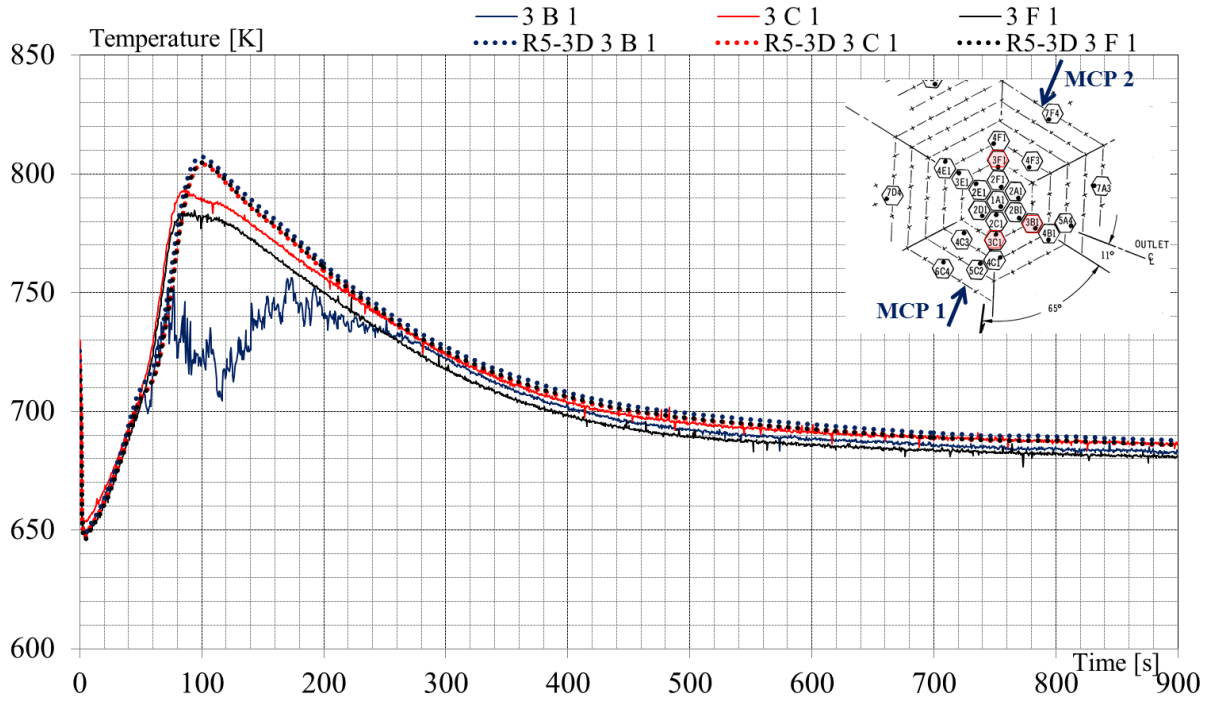

Fig. 34 – EBR-II SHRT-17, RELAP5-3D©: selected SA, ring 3 coolant outlet T.

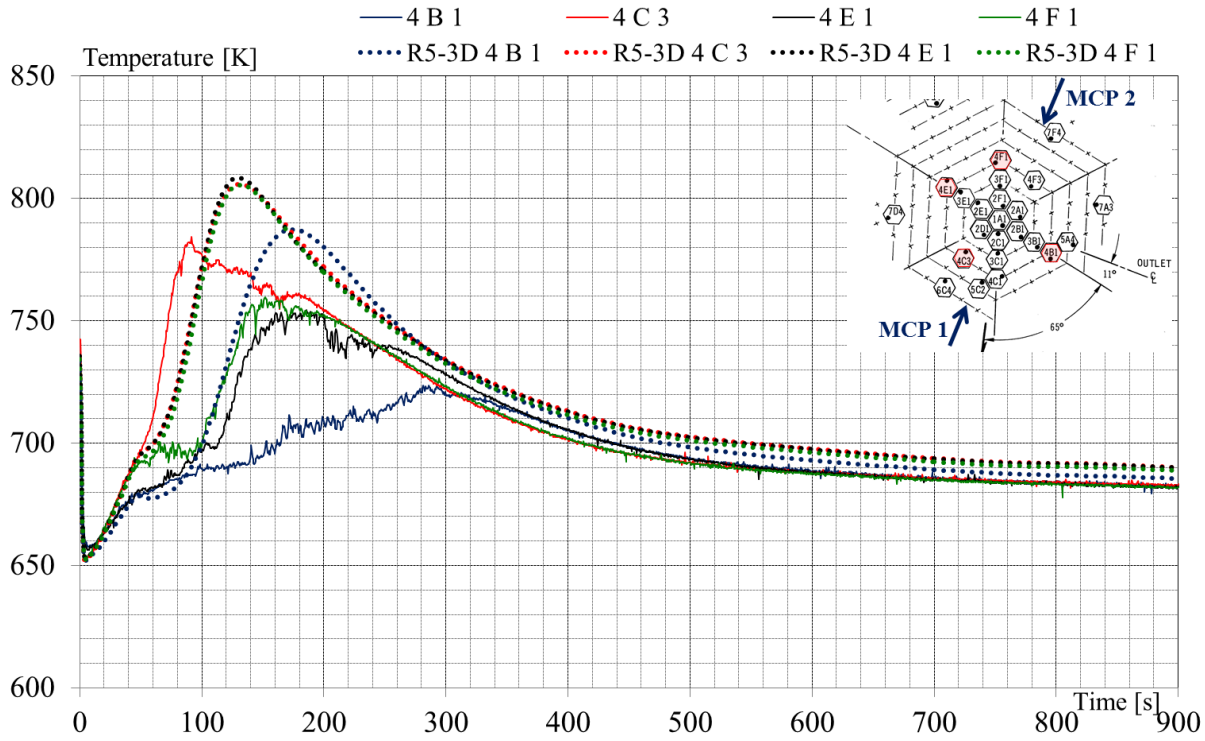

Fig. 35 – EBR-II SHRT-17, RELAP5-3D©: selected SA, ring 4 coolant outlet T.

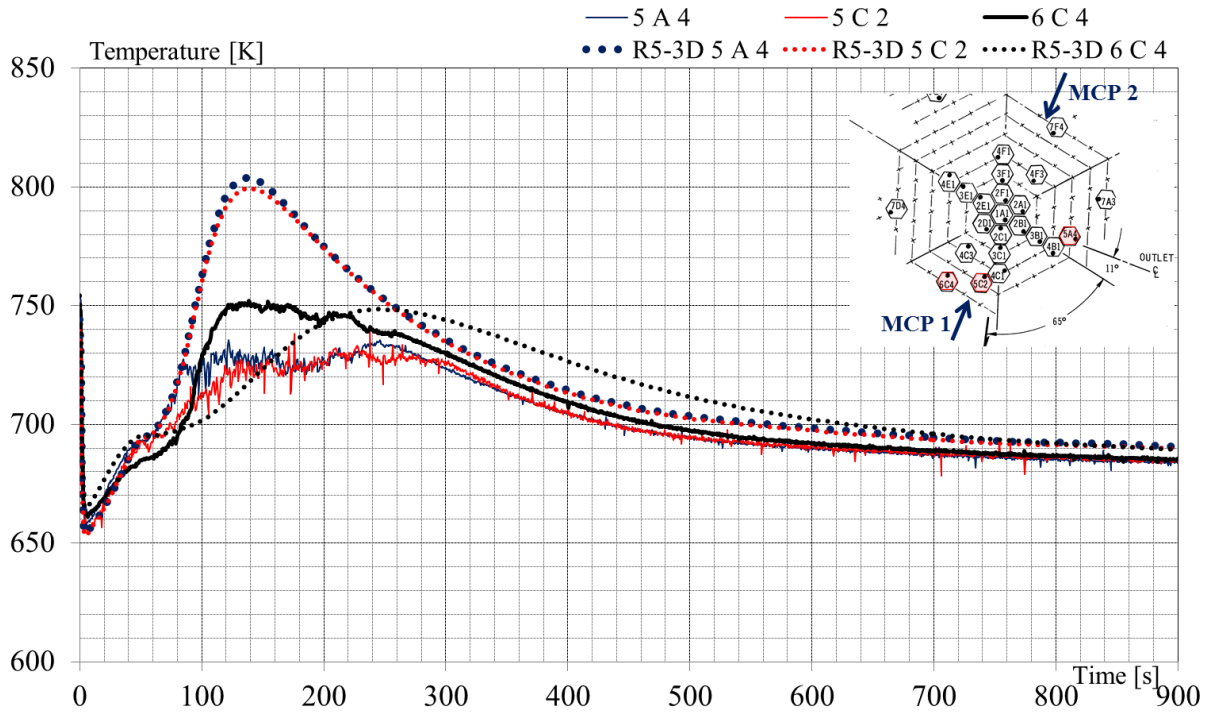

Fig. 36 – EBR-II SHRT-17, RELAP5-3D©: selected SA, ring 5 and 6 coolant outlet T.

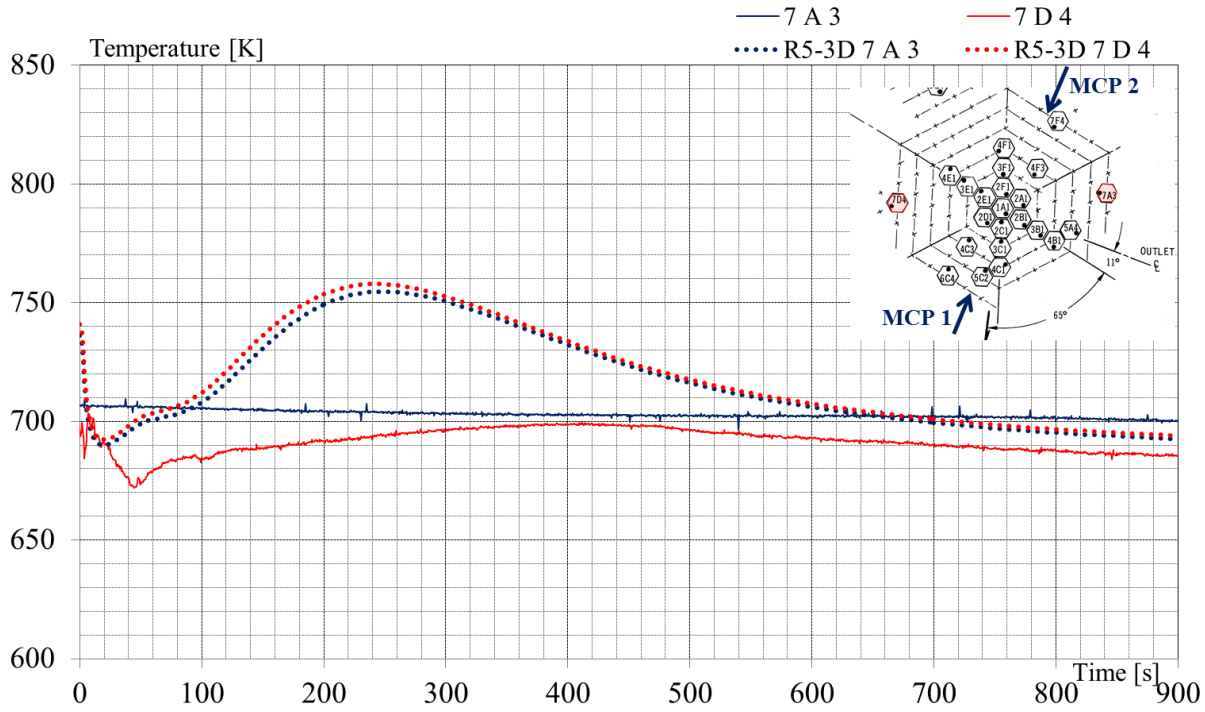

Fig. 37 – EBR-II SHRT-17, RELAP5-3D©: selected SA, ring 7 coolant outlet T.

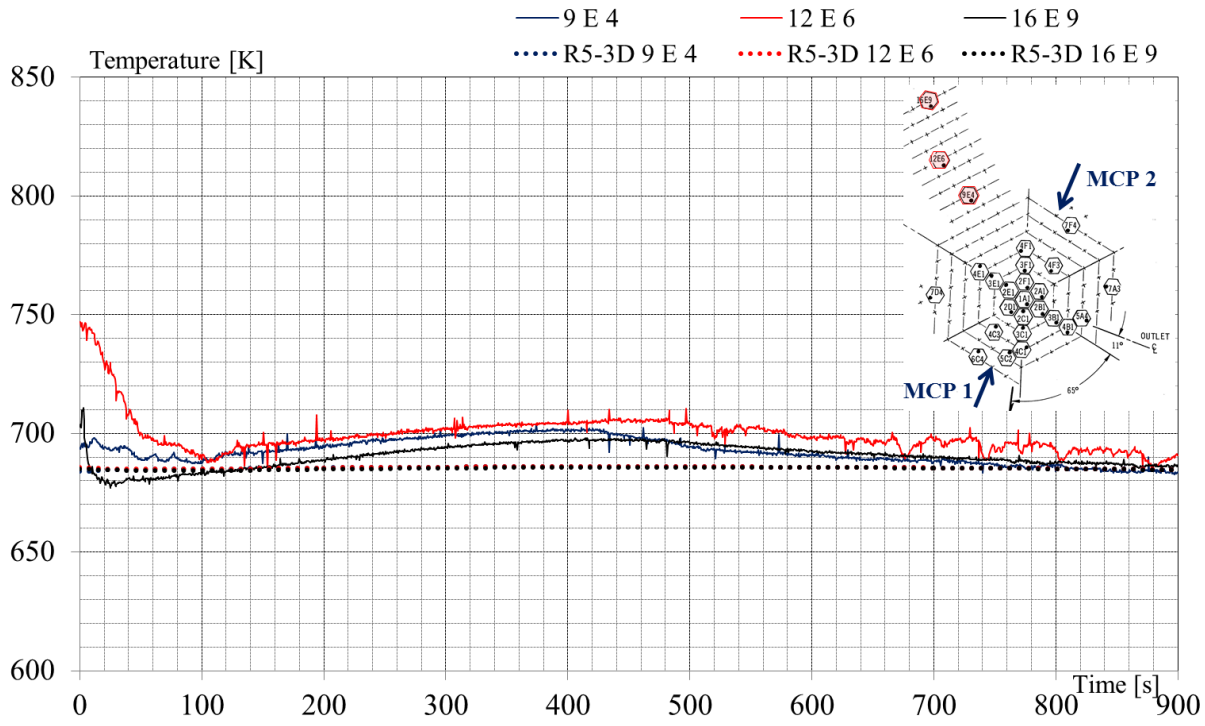

Fig. 38 – EBR-II SHRT-17, RELAP5-3D©: selected SA, ring 9, 12, 16 coolant outlet T.

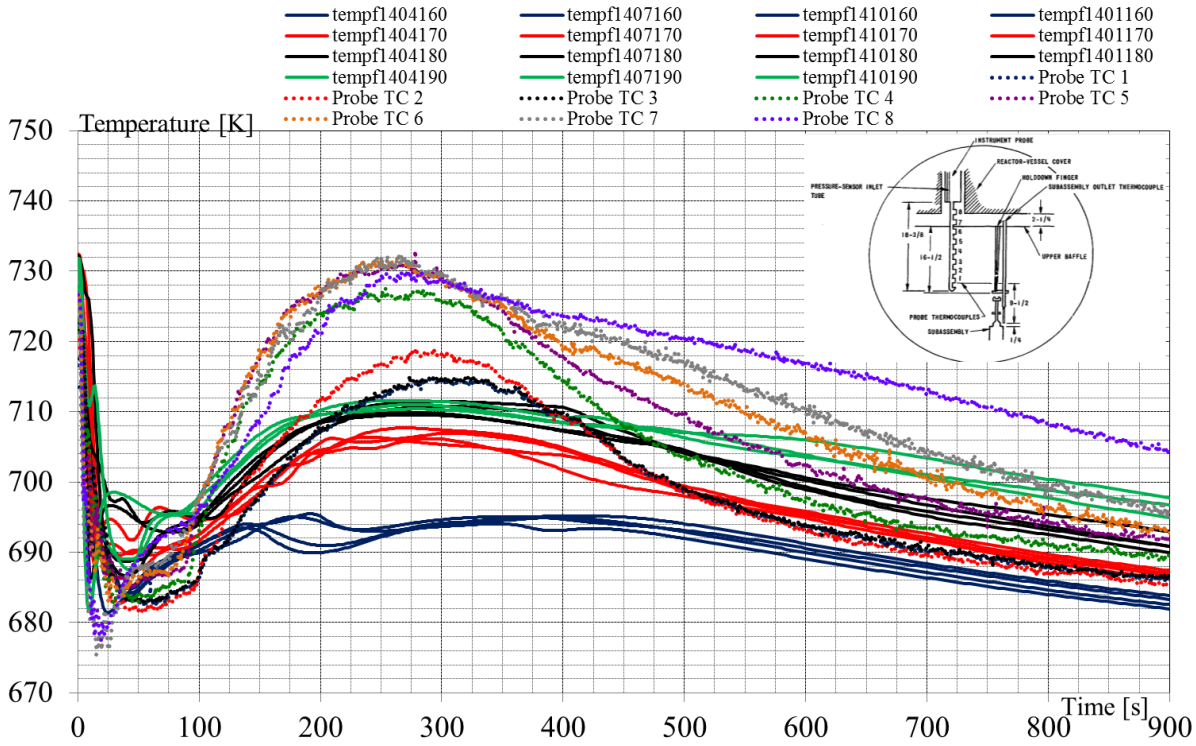

Fig. 39 – EBR-II SHRT-17, RELAP5-3D©: upper plenum coolant temperatures.

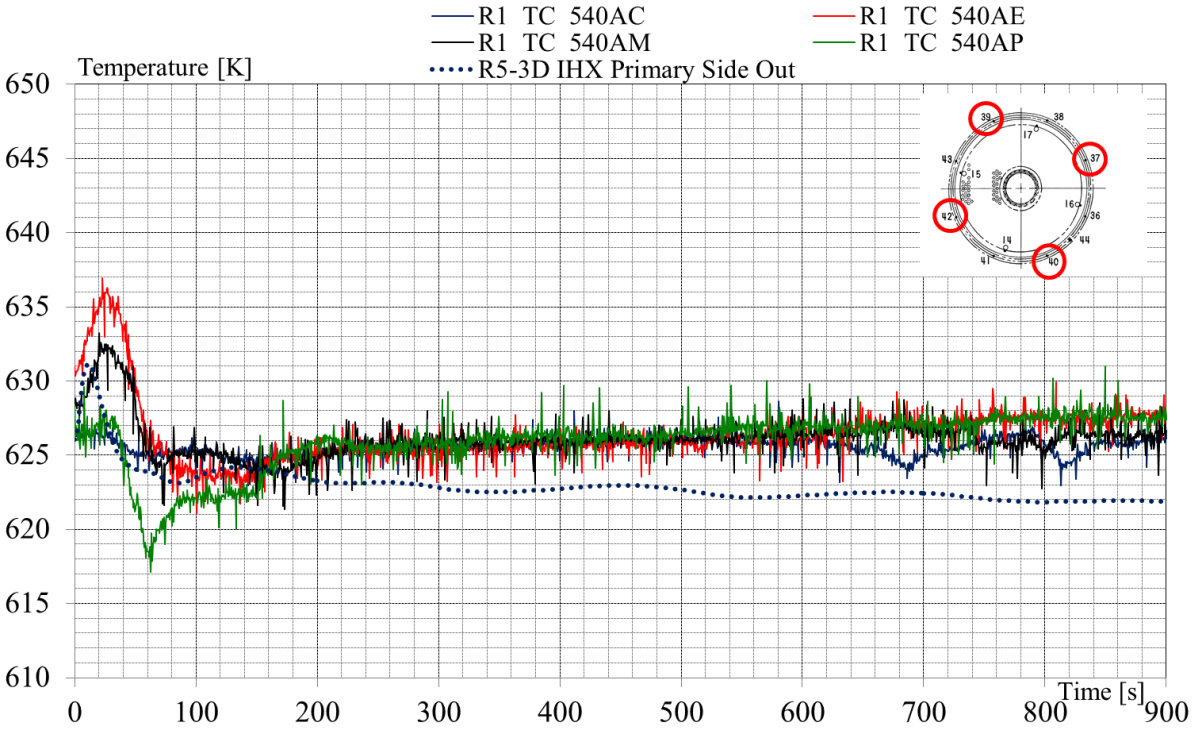

Fig. 40 – EBR-II SHRT-17, RELAP5-3D©: IHX primary side coolant outlet tempeartures.

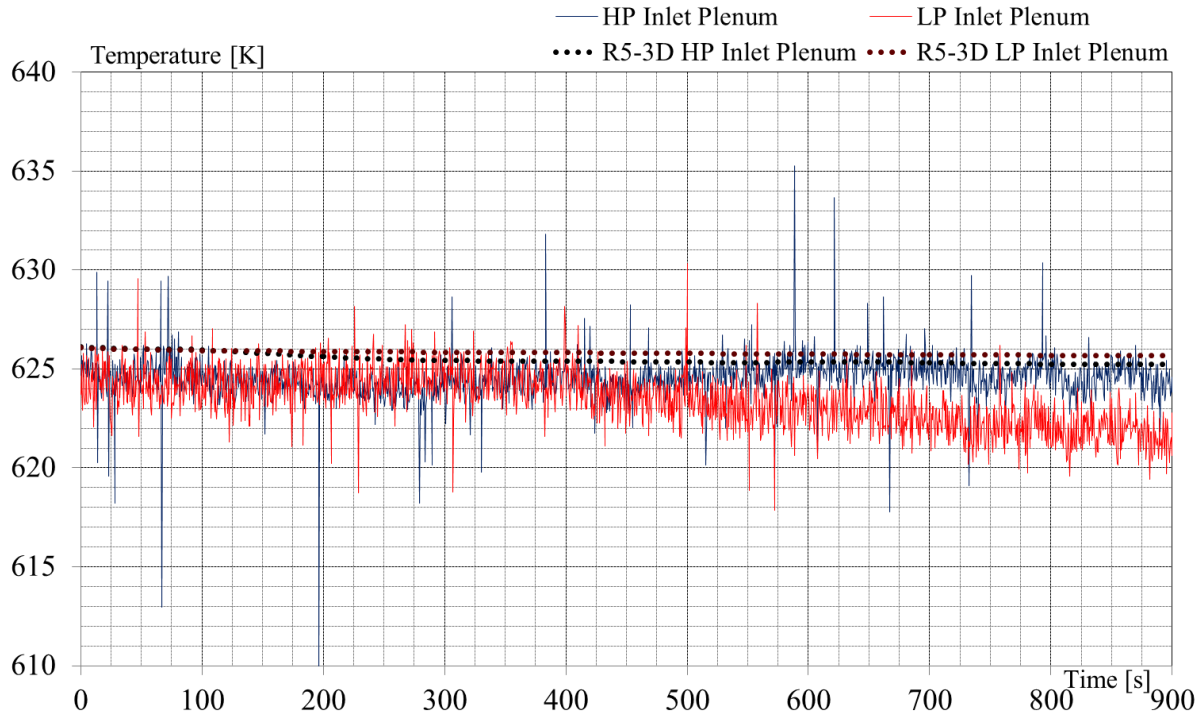

Fig. 41 – EBR-II SHRT-17, RELAP5-3D©: high and low pressure inlet lower plenum coolant temperatures.

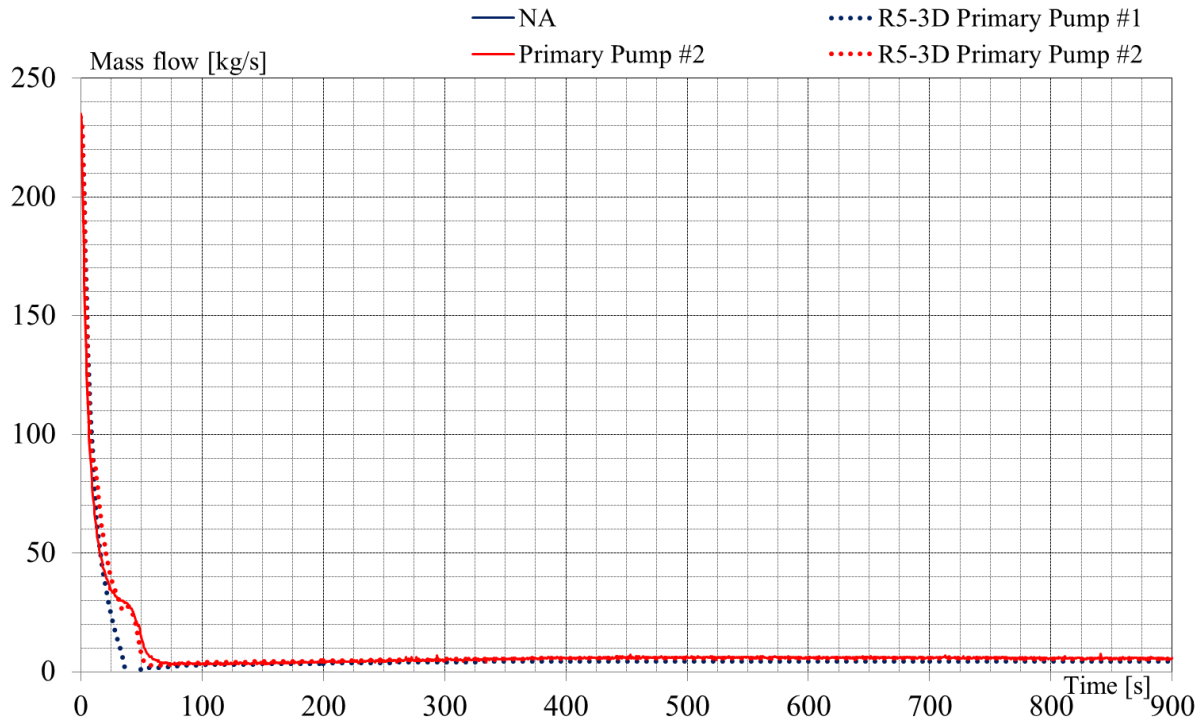

Fig. 42 – EBR-II SHRT-17, RELAP5-3D©: primary pump mass flow rate (overall transient).

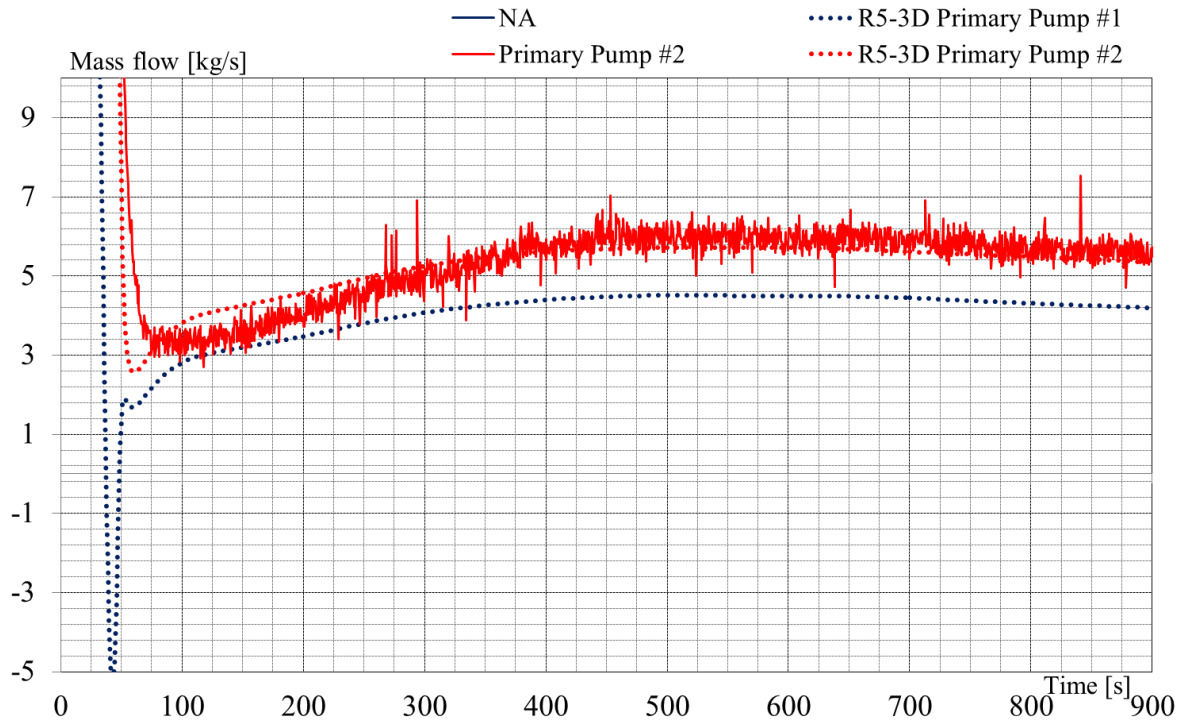

Fig. 43 – EBR-II SHRT-17, RELAP5-3D©: primary pump mass flow rate (zoom 1).

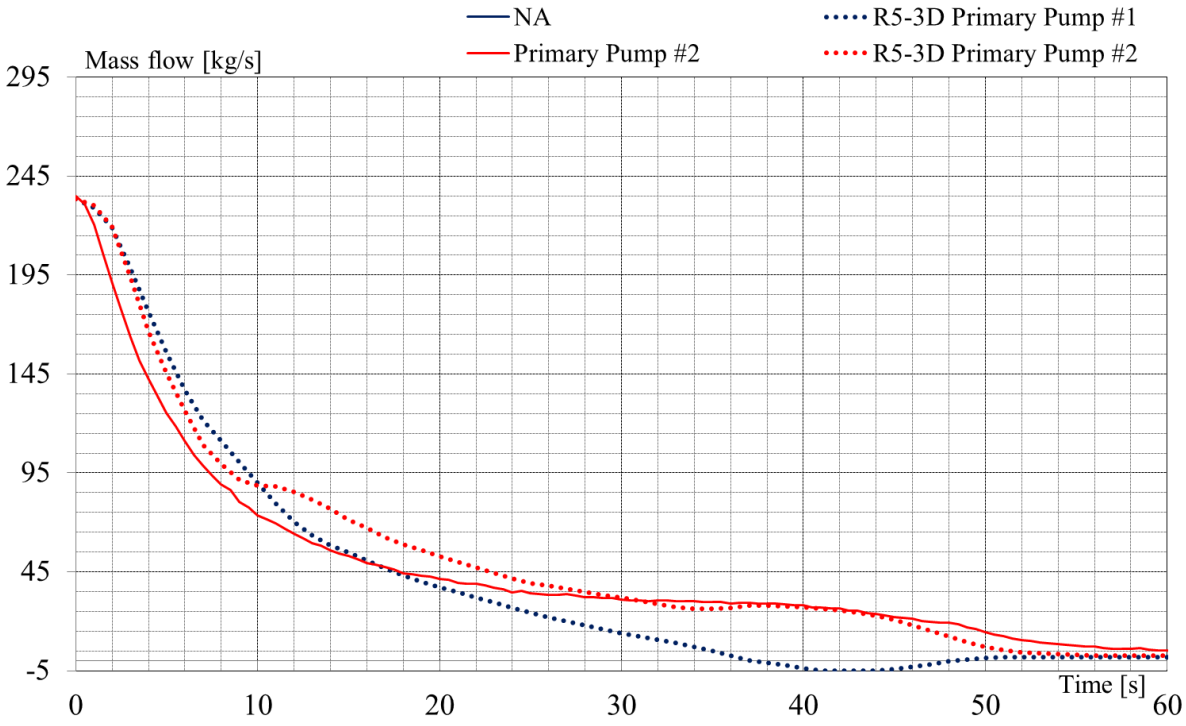

Fig. 44 – EBR-II SHRT-17, RELAP5-3D©: primary pump mass flow rate (zoom 2).

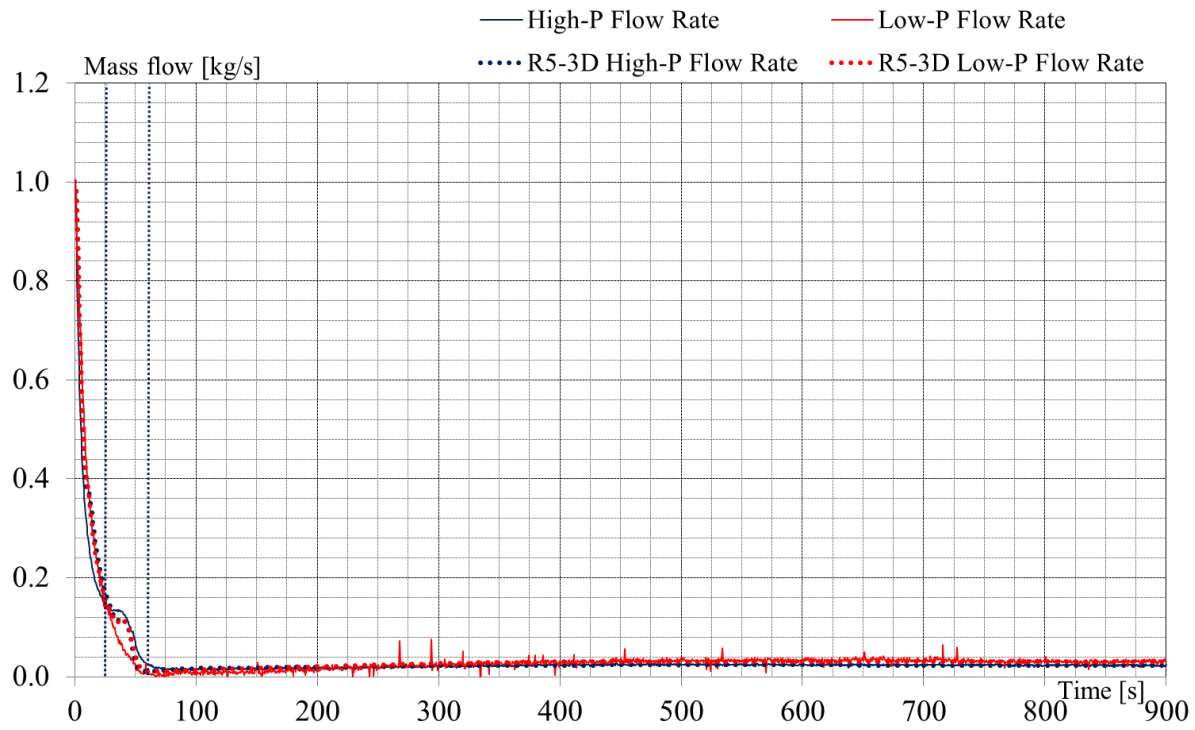

Fig. 45 – EBR-II SHRT-17, RELAP5-3D©: high and low pressure lines #2 mass flow rate.

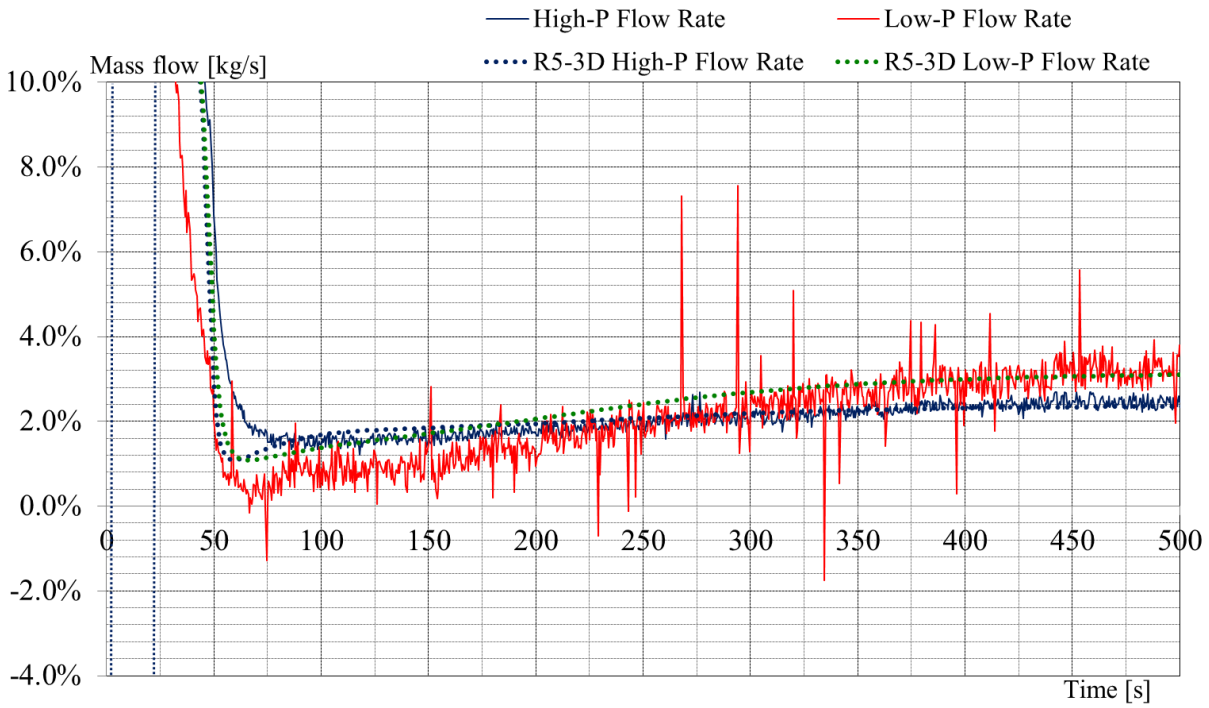

Fig. 46 – EBR-II SHRT-17, RELAP5-3D©: primary pump mass flow rate (zoom 1).

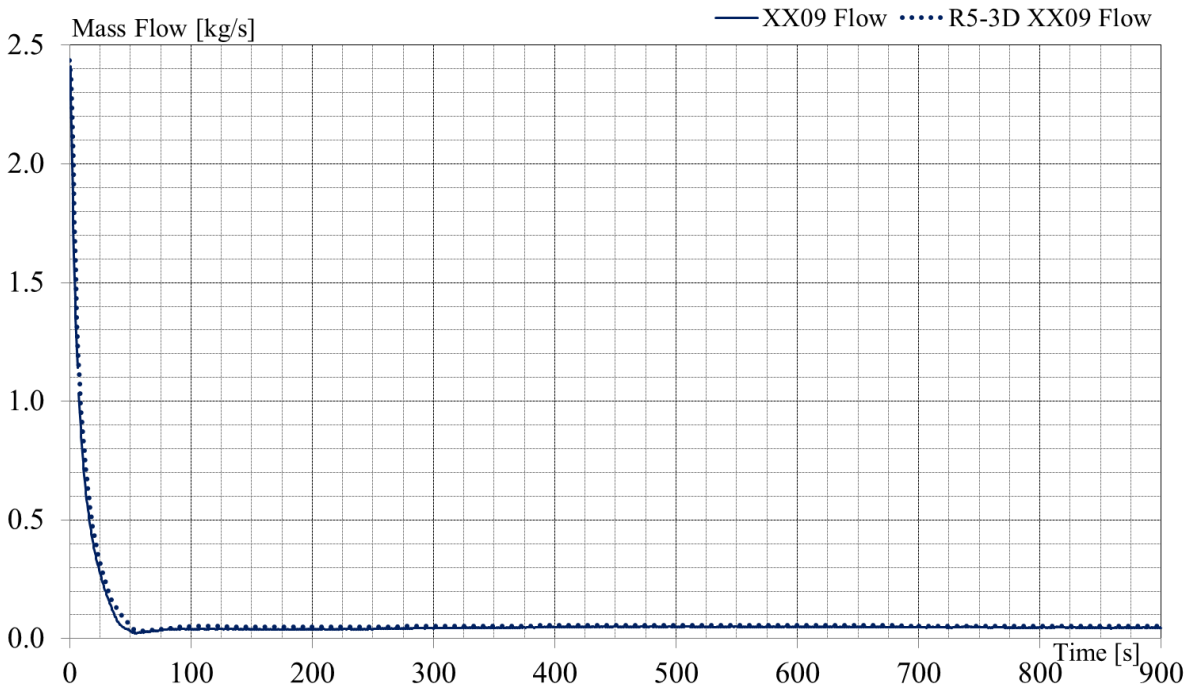

Fig. 47 – EBR-II SHRT-17, RELAP5-3D©: FA XX09 mass flow rate.

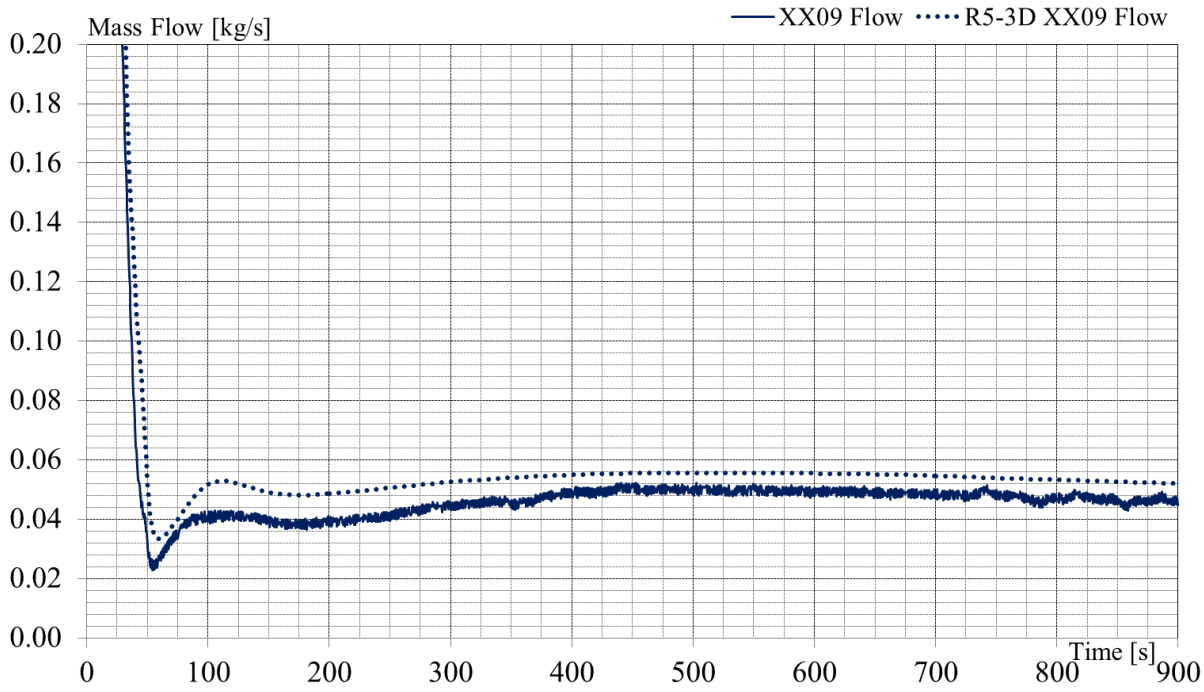

Fig. 48 – EBR-II SHRT-17, RELAP5-3D©: FA XX09 mass flow rate (zoom1).

#	Parameter	Unit	Exp	Blind Calc	Open Calc
1	Core Driver thermal power	MWth	52.28	52.28	52.28
2	Core Blanket thermal power	MWth	5.02	5.02	5.02
3	Core inlet temperature	K	624.15	625.6	625.9
4	Core outlet temperature	K	--	730.3	720.9
5	IHX SS inlet coolant temperature	K	574.2	574.2	574.2
6	MCP1 mass flow rate	kg/s	233.5	231.2	233.8
7	MCP2 mass flow rate	kg/s	233.2	230.9	233.8
8	Core Driver mass flow rate	kg/s	387.0	384.6	389.9
9	Core Blanket mass flow rate	kg/s	65.2	66.0	65.9
10	IHX SS mass flow rate	kg/s	311.4	311.4	311.4
11	Primary pressure @ MCP out	kPa	441.2	452.5	473.0
12	Primary pressure @ Upper Plenum	kPa	213.9	217.1	210.6

Tab. 13 – EBR-II SHRT-17, RELAP5-3D©: steady-state comparison.

Ph. W.	EVENT	Exp [s]	Blind Calc [s]	Open Calc [s]
Phase I (0 – 10 s)	Stop MCP ***[Imposed]***	0	0	0
	Initiating event: loss of IHX flow rate ***[Imposed]***	0	0	0
	SCRAM ***[Imposed]***	0	0	0
	Min. cladding T in XX09 @ TAF	4.5	4.0	4.0
	Min. cladding T in XX10 @ core TAF	10	16	13
	Min. coolant T in UP	12	6	6
Phase II (10 – 100s)	Max. cladding T in XX09 @ TAF	73.5	67	81
	Max. cladding T in XX10 @ core TAF	96.5	88	110
	Max. coolant T in UP	138.5	89	131
	MCP 2 coastdown end [minimum of mass flow rate]	76	62	60
Phase III (74 – 900s)	End of transient ***[Imposed]***	900	900	900
	– (Cladding T XX09 @ TAF)	691-705K	674K	700K
	– (Cladding T XX10 @ core TAF)	672-675K	665K	676K

Tab. 14 – EBR-II SHRT-17, RELAP5-3D©: sequence of main events.

5 CFD SIMULATIONS OF LM COOLED WIRE-SPACED FUEL ASSEMBLY XX-09

5.1 CFD: Model and methods

The general purpose code ANSYS CFX 15 was used for all the numerical simulations presented here. The code employs a coupled technique, which simultaneously solves all the transport equations in the whole domain through a false time-step algorithm. The linearized system of equations is reconditioned in order to reduce all the eigenvalues to the same order of magnitude. The multi-grid approach reduces the low frequency error, converting it to a high frequency error at the finest grid level; this results in a great acceleration of convergence.

The SST (Shear Stress Transport) k-ω model by Menter is extensively used in this context. It is formulated to solve the viscous sub-layer explicitly, and requires several computational grid points inside this latter. The model applies the k-ω model close to the wall, and the k-ε model (in a k-ω formulation) in the core region, with a blending function in between. It was originally designed to provide accurate predictions of flow separation under adverse pressure gradients, but it has since been applied to a large variety of turbulent flows and it is now the default and most commonly used model in CFX-15 and other CFD codes.

The SST model adopts the eddy diffusivity approach for momentum transport. Regarding heat transfer, the *k*-ω family turbulence model adopted in this context, uses, coherently with the classical turbulence theory, the well-known analogy between turbulent transport of momentum and energy, i.e. a Reynolds analogy re-proposed at a turbulence level; for the turbulent thermal diffusivity Γ_t:

$$\Gamma_t = \frac{\mu_t}{Pr_t}$$

where Pr_t is the turbulent Prandtl number, which is of the order of 1 for liquid metals and it has been kept constant and fixed to 1.0 for Sodium in this case.

5.1.1 CFD model of XX09 fuel assembly

A full 3D CFD computation of the XX09 instrumented Fuel Assembly has been performed in order to validate the code, comparing the CFD results with the benchmark results.

The model is geometrically built on the nominal sizing of the pin, the wire and the wrappers dimensions. A collapsed model was adopted for wires and pins simulation, avoiding the contact point issue involved in heat transfer phenomena between this two bodies. A nominal interference of 0.05 mm was imposed on wire-pin centre-to-centre distance.

5.1.2 Description of the model

The model developed can be seen in Fig. 49. The whole model has 11.5 million nodes and 47.8 million elements and it was specifically designed with a compromise between number of nodes and accuracy for transient analysis. It includes:

- The fuel (red) into the active length (L_{active}=343 mm) of the pins (59/61 pins have the fuel inside);
- The clad (grey) of the active pins (only in the active length);

- The fluid Na region (light blue) into the pin bundle (from the inlet section of the active region to the top of the pins);
- The solid structure of the hexagonal wrapper (yellow) between the pin bundle and the thimble region;
- The fluid Na thimble region (blue);
- The solid structure of the hexagonal wrapper (orange) between the thimble region and the bypass region shared with the other assemblies of the core;
- The bypass fluid region (purple) shared with the other assemblies of the core, simulated as a thin fluid region with symmetric boundary conditions on its external surfaces.

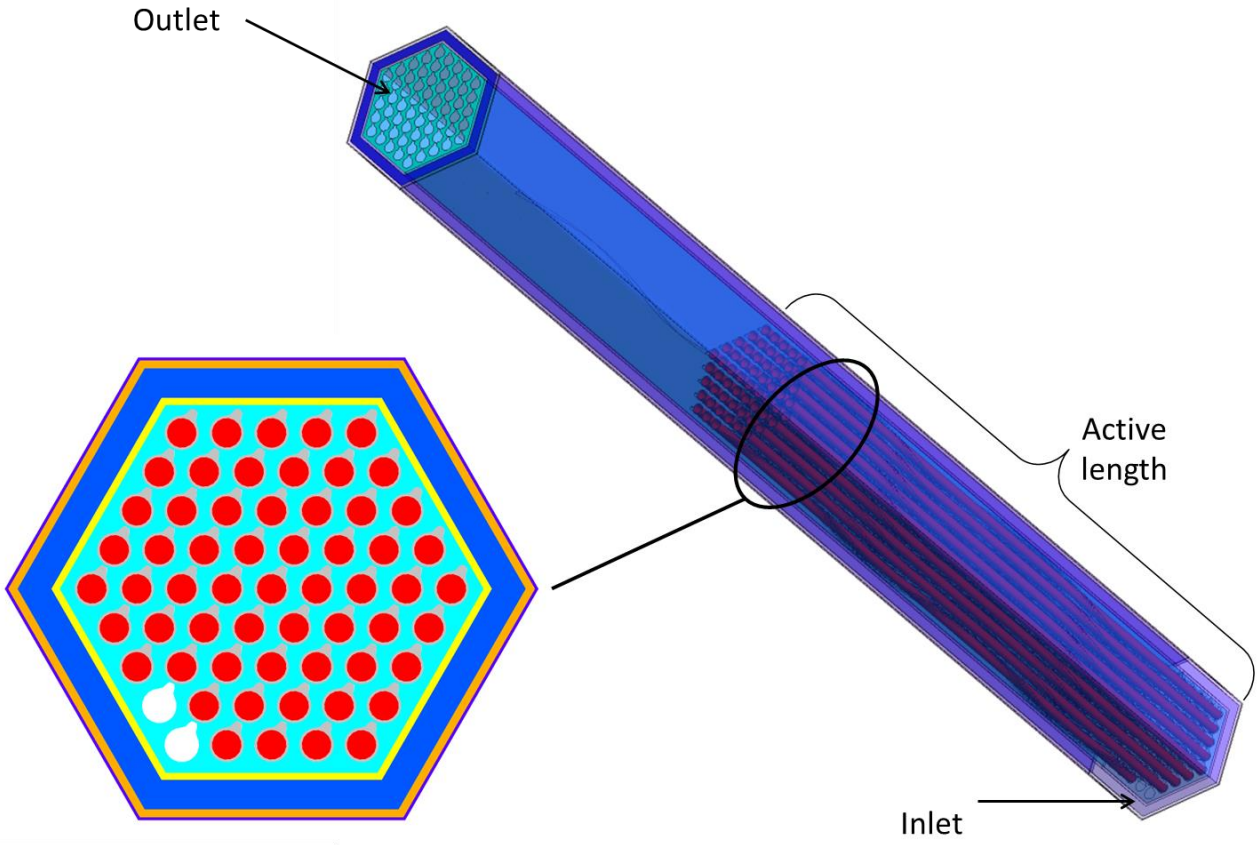

Fig. 49 – Layout of the CFD model.

As it is shown in Fig. 50, unstructured tetrahedral mesh elements were adopted for all the bodies of the model except for the fuel where the elements are semi-structured. The working fluid is Na with variable properties resumed in Tab. 15 consistent with the RELAP5-3D© physical properties. Every buoyancy effect into the sub-channels is neglected because the influence of the phenomena on the final results is negligible from a preliminary dimensionless analysis ($Ri_{tr} \ll 1$).

The material implemented for the pin clad and the two wrappers is SS AISI304, the main properties are reported in Tab. 16.

The fuel properties implemented are provide in the benchmark specification document.

All the interfaces between different domains (fluid-solid or solid-solid) are connected with a general interpolation scheme (for heat transfer simulation).

Sodium properties ([T]=K)	
ρ [kg / m^3]	1014-0.235·T
C_p [J / kg / K]	$-3\cdot10^6\cdot T^{-2}+0.0004454\cdot T^2+1658$
μ [Pa s]	$\exp(556.835\cdot T-6.4406)\cdot T^{-0.3958}$
k [W / m / K]	-0.047·T+104

Tab. 15 – The sodium properties implemented in the CFD simulation.

AISI 304 properties (T= 350 °C)	
ρ [kg / m^3]	7854
C_p [J / kg / K]	434
k [W / m / K]	20

Tab. 16 – Main properties of AISI 304.

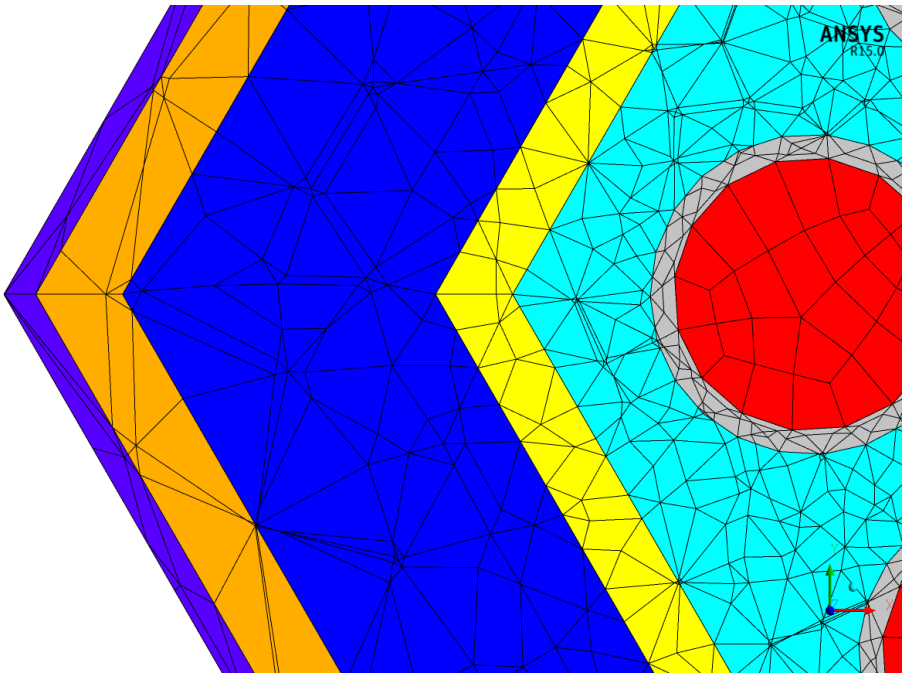

Fig. 50 – Detailed view of the computational mesh.

5.2 Steady state simulation.

5.2.1 Boundary Conditions

As preliminary study, a steady state simulation was implemented, evaluating the accuracy of the model developed with a first comparison with steady state experimental results. The steady state scenario simulated is the reference/unperturbed state of XX09 at reference time t= 0 s of SHRT-17 Test.

The boundary conditions adopted are part from the benchmark data and part from RELAP5 simulation data.

For the fuel, a volumetric heat source with a sinusoidal shape and a peak factor of 1.3 was imposed into the domain (Q = 464416.5 kW from benchmark data).

For the fluid domain into the pin bundle (Sodium), a mass flow rate of 2.436 kg/s (from RELAP5 data) was imposed on the inlet surface of the domain with an inlet temperature of 626.35 K (from benchmark data) and an outlet/zero relative pressure was imposed on the outlet surface.

For the fluid domain in the thimble region (Thimble), a mass flow rate of 0.256 kg/s (from RELAP5 data) was imposed on the inlet surface of the domain with an inlet temperature of 626.35 K (from benchmark data) and an outlet/zero relative pressure was imposed on the outlet surface.

For the external fluid domain (Bypass), a mass flow rate of 0.0067 kg/s (from RELAP5 data) was imposed on the inlet surface of the domain with an inlet temperature of 626.35 K (from benchmark data) and an outlet/zero relative pressure was imposed on the outlet surface, the symmetric boundary condition on the external surfaces of the domain still remains.

As convergence criteria, RMSs of continuity, momentum and energy equations have to be lower that 10-6.

5.2.2 Results

The pins of the XX09 FA were instrumented with wall thermocouples displaced at three different height/planes (one wire pitch distant each other):

- MTC plane : 172 mm from the beginning of the active length;
- TTC plane : 322 mm from the beginning of the active length;
- 14 TC plane (non-active region) : 480 mm from the beginning of the active length.

The location of those thermocouples is shown in Fig. 51.

Post-processing temperature distributions obtained with the CFD simulation on the same thermocouple locations , show a really good agreement with the experimental values . In particular, Fig. 52shows a 3D view of the CFD temperature field in the pins and the detailed field in the 3 measuring planes monitored by thermocouples.

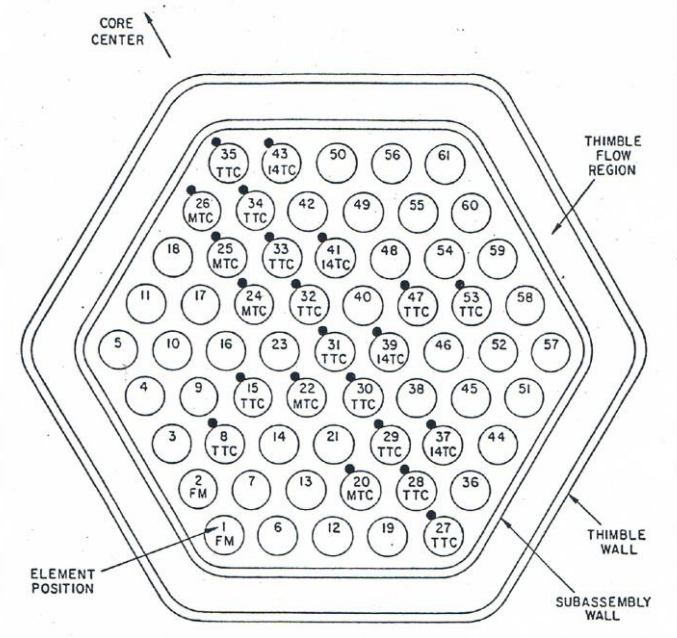

Fig. 51 – Thermocouples position in XX09 Fuel Assembly.

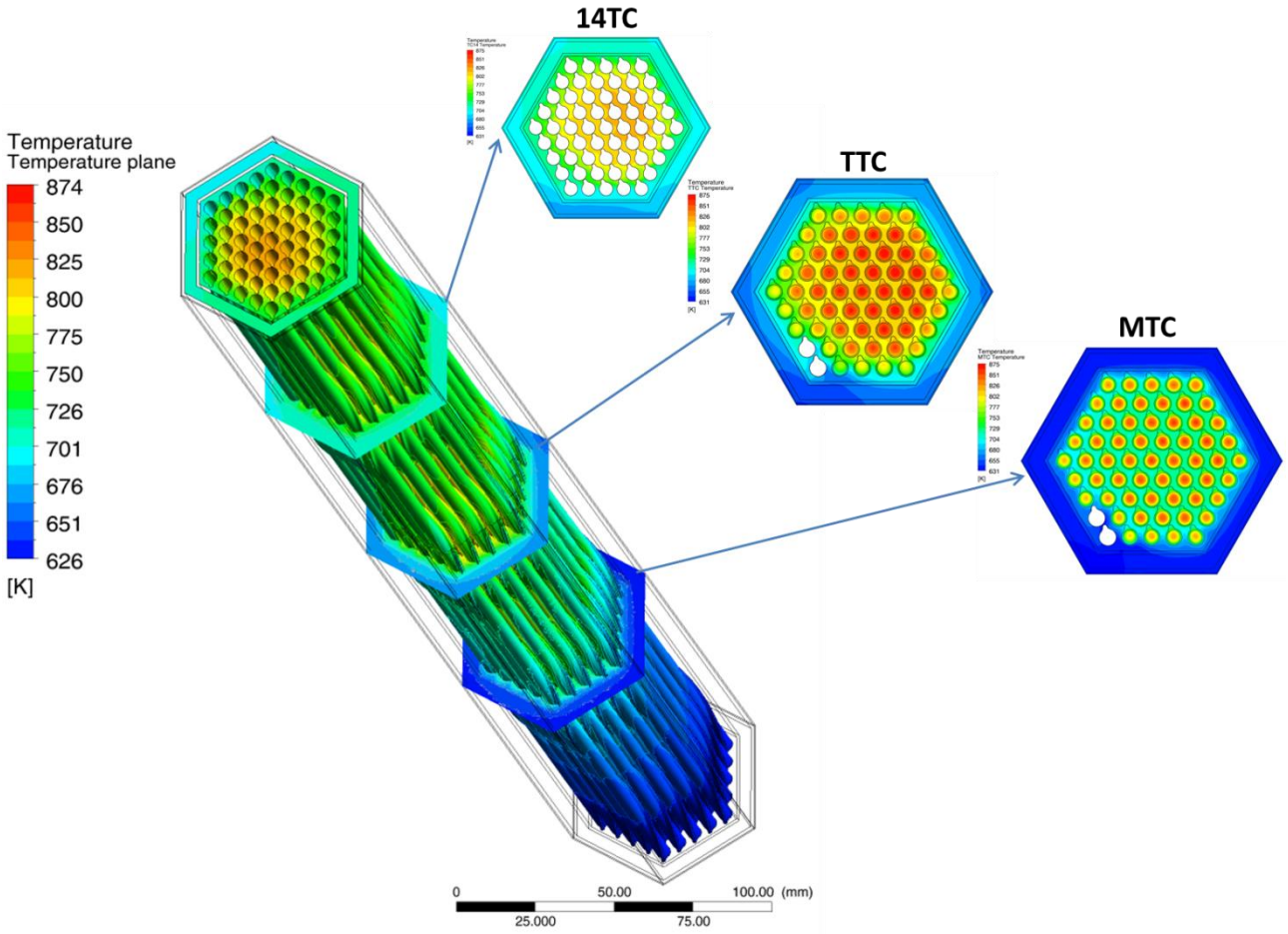

Fig. 52 – Layout of the post-processing of the CFD steady-state simulation.

Fig. 53 shows a graphical comparison of experimental vs. CFD data in the same monitoring points at the three different measuring section: MTC (a), TTC (b), 14TC(c).

Some differences with the experimental values still remains especially for the radial temperature profile depicted on TTC plane by TTC-27…35, probably due to a not symmetric thermal behavior of the neighboring Fuel Assemblies during the test (challenging for the simulation) that influenced the bypass flow temperature. In the CFD model, on the external surfaces of the bypass region, a symmetric boundary condition was imposed; therefore asymmetric effects from the neighboring fuel assemblies are not kept into account. In any case, the comparison show a good agreement and the physical problem seems to be captured by the simulation.

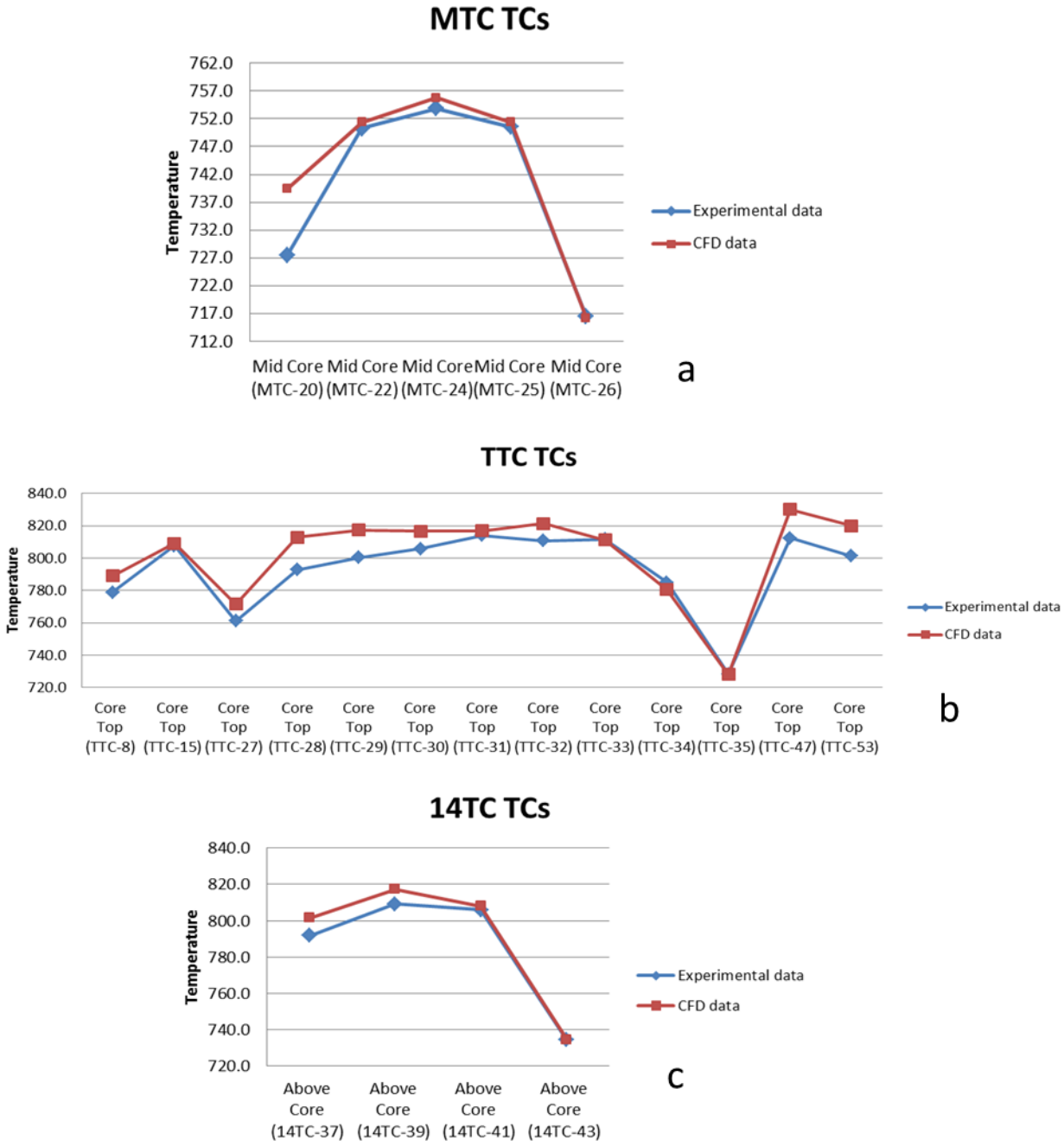

Fig. 53 – Comparison of the CFD results with SHRT-17 experimental values.

5.3 Transient simulation.

5.3.1 Boundary Conditions and computation details

The CFD model developed for the XX09 Fuel Assembly showed to be accurate and reliable in a steady state scenario.

The next step will test the accuracy in the simulation of a transient scenario (SHRT-17 benchmark experiment $0 < t < 100$ s).

The mass flow rates behavior during the transient imposed at the inlet surfaces of Sodium, Thimble and Bypass were calculated with RELAP5-3D© system code. The inlet temperature behavior and the thermal power of XX09 Fuel Assembly during the transient were given as known data of the benchmark.

The results of the previous (steady state) simulation were implemented as initial values for the transient simulation.

For the time interval 0-10 s, a small time step of 0.01 s was adopted because the power gradient in this stage is remarkable. For the time interval 10-100 s, an higher time step (0.025 s) was sufficient to capture the physical phenomena.

As convergence criteria, RMSs of continuity, momentum and energy equations have to be lower that 10^{-5} in each time step iteration (15 maximum iterations on a time step). The simulation was time-marching and the complete solution was saved each second, while temperature values in the monitoring TC points were saved each time step.

5.3.2 Results

A long CFD detailed simulation was performed for the first 100 s of the SHRT-17 protected accident of XX09 FA of the EBR2 reactor. Most of the integral data considered as boundary conditions were taken from the RELAP5 simulation of the transient in the whole primary side. Therefore, a single-way coupling was carried out in the present study. This single-way coupling will capture most of the complex physics involved.

Fig. 54 shows a comparison of CFD and experimental results for the mid-core plane MTC for transient simulation in the range 0-100 s. The agreement is good with a peak in the clad temperature around 810 K at 65 s about. There is a small shift of the curve on the right with a short delay (3-4 s) on the maximum clad temperature.
Fig. 55 and Fig. 56 show results for the top-of-the core plane TTC. The agreement with experimental results is very good for $t<45$ s. For $t>45$ s, there is an error with an overestimation of the maximum clad temperature and a delay of about 10-15 s.

Fig. 57 shows results for the mixing region 14TC. For this measuring plane, the agreement is good for $t<70$ s for all the thermocouples, while for $t>70$ s there an overestimation of the peak (60 K) and a short delay (5 s). The reason of the overestimation by CFD analysis is currently under investigation and the influence of asymmetric boundary conditions by the different neighboring fuel assemblies will also be considered in the future.

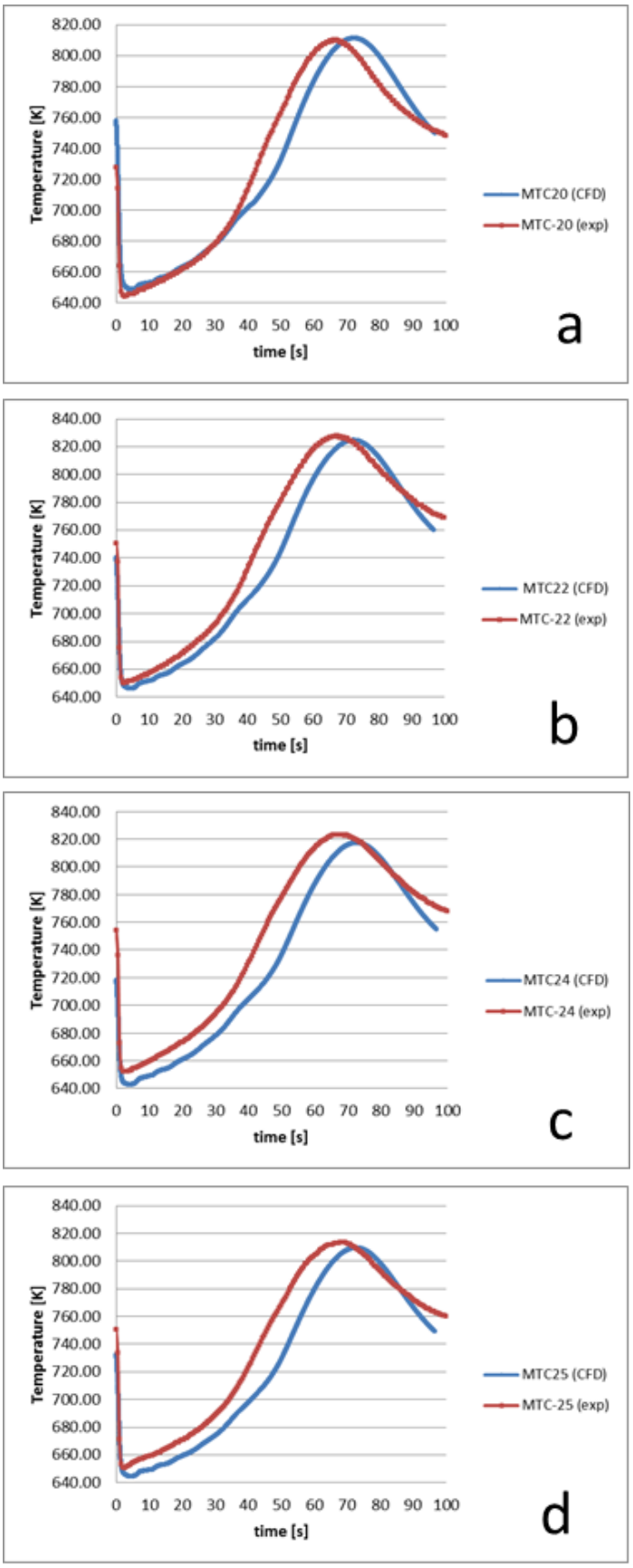

Fig. 54 – Comparison of CFD and experimental results for the mid-core plane MTC.

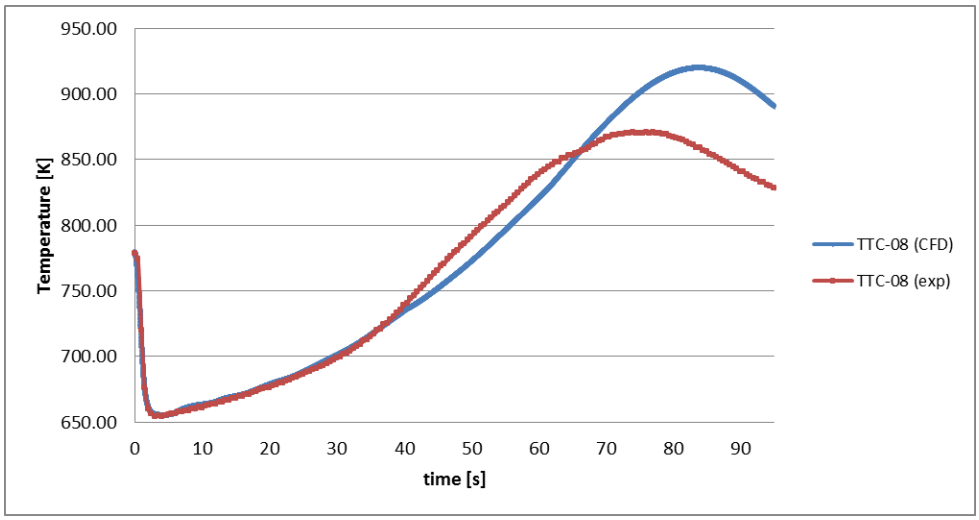

Fig. 55 – Comparison of CFD and experimental results for the top-core plane TTC TTC-08.

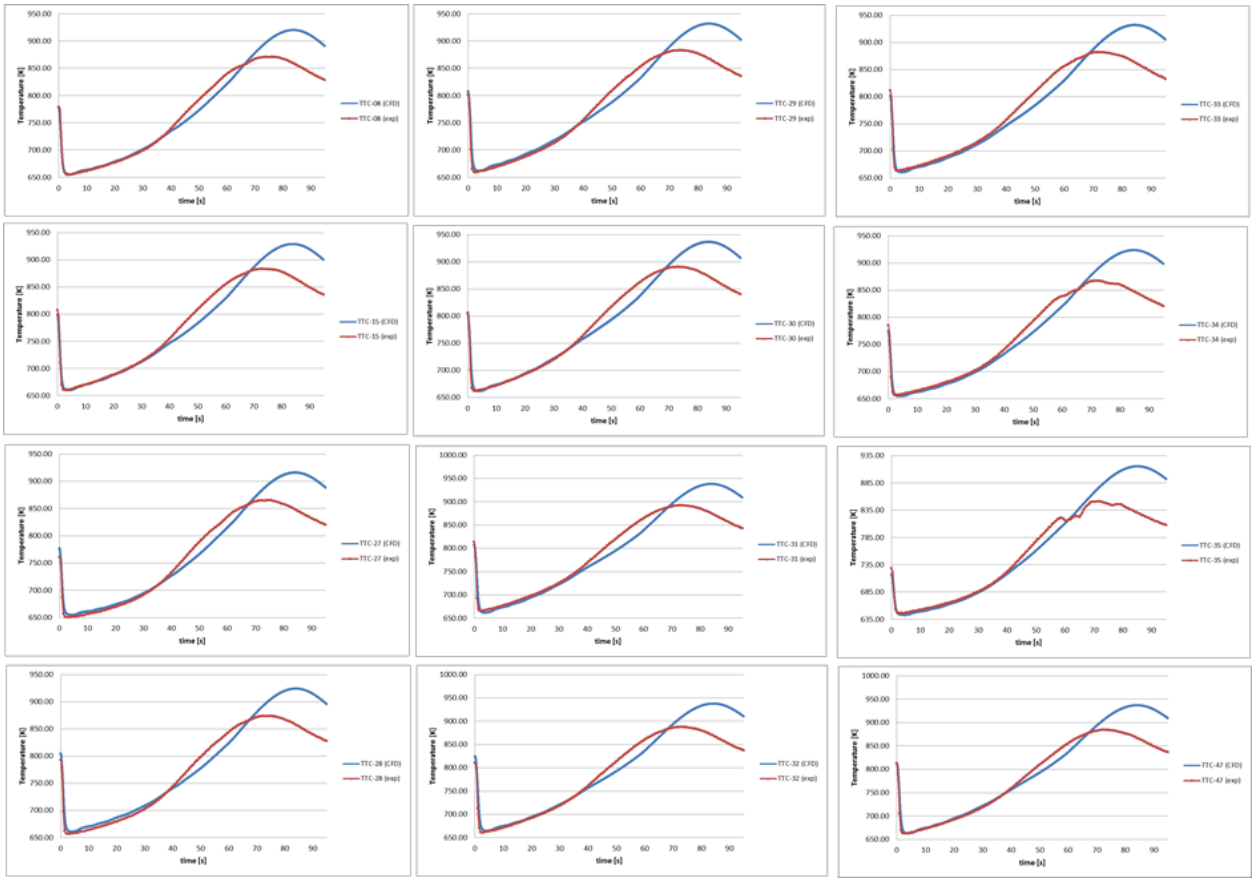

Fig. 56 – Comparison of CFD and experimental results for the top-core plane TTC (all the thermocouples).

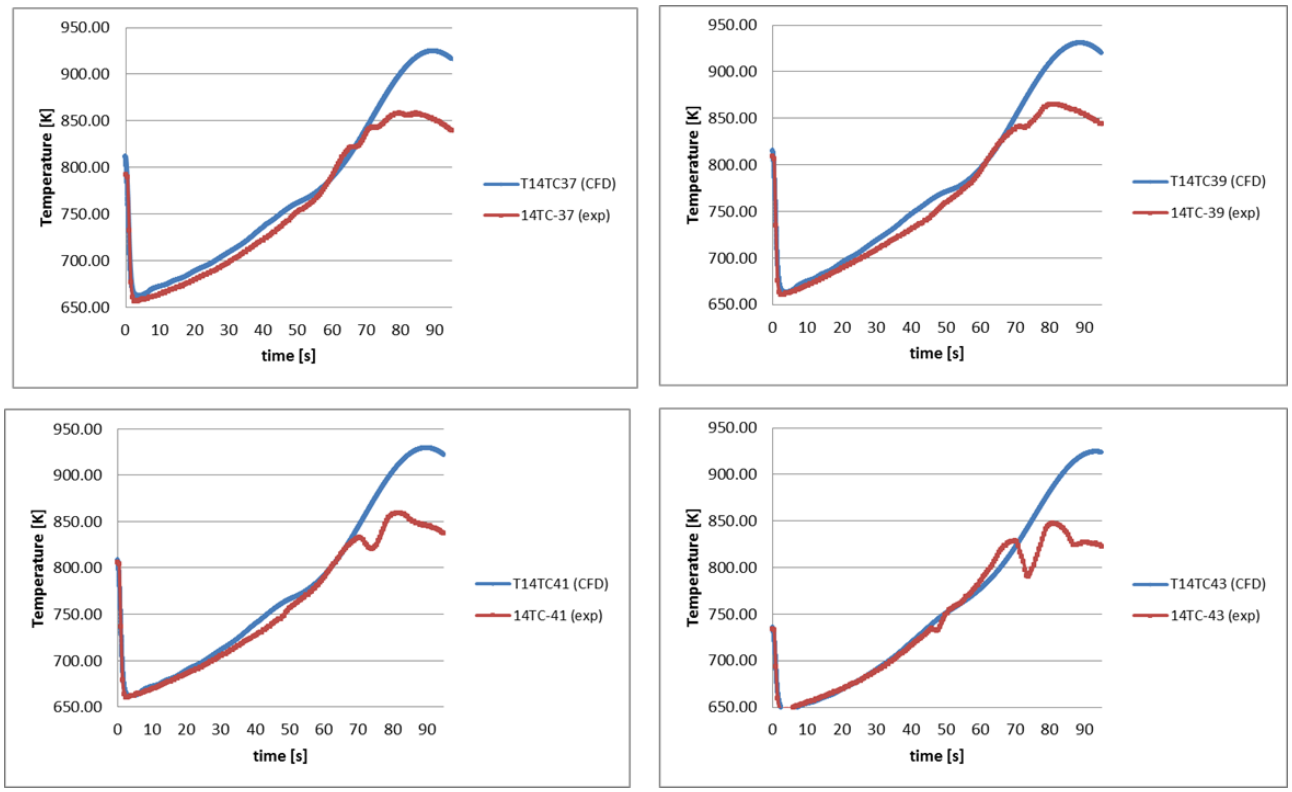

Fig. 57 – Comparison of CFD and experimental results for the out-of-core plane 14TC.

5.3.3 Conclusive remarks

A CFD analysis was carried out on the XX09 EBR2 FA. The numerical model includes the conjugate heat transfer effects and the radial heat transfer through the wrap, the thimble and the by-pass. A one way coupling with RELAP5-3D data was implemented and tested on the SHRT-17 protected accident.

For the stationary case at nominal mass flow rate a good agreement was obtained between CFD and experimental results in all the monitoring points.

The SHRT-17 transient was simulated for the first 100 seconds. CFD results show globally a good agreement with the experiment. The agreement in the MTC plane is very good for all the monitoring points. For TTC (top of the core) and 14TC (mixing region) planes, the agreement is good for t<45,70 s respectively, but there is a delay and a clad peak temperature overestimation of 50-70 K. The reason of this discrepancy is currently under investigation.

6 MCNP NEUTRONIC MODELLING

6.1 Model Description

Static neutronic modelling of EBR-II core was achieved performing Monte Carlo simulations. The purpose of such activity was to obtain a detailed reference solution by evaluating neutronic parameters such as keff , reactivity coefficients, power and flux distributions. These data were used for validating the multi-group cross section libraries and the PHISICS code deterministic model.

The tool chosen for the static neutronic analysis is the Monte Carlo neutron transport code MCNP6 [46], developed by Los Alamos National Laboratory (USA). ENEA acquired the code license and installed it on CRESCO high performance computing (HPC) machine [47] during 2014. The code allows to perform neutron transport calculations with detailed geometry modelling (up to the pin level), including fuel depletion calculations. Capabilities of MCNP6 on SFR simulation were tested in the framework of the PELGRIMM EU FP7 Project [48] (see Fig. 58).

EBR-II core is a quite heterogeneous system, requiring simulation of the different hexagonal sub-assemblies (S/A) composing the core (61 S/A), the inner blanket (66 S/A) and the outer blanket (510 S/A), the Control and Safety S/A, etc. The core configuration that was modeled is shown in Fig. 59.

MCNP6 allowed to perform a neutron transport simulation without introducing significant geometry simplifications.

Detailed S/A modelling was performed, up to the pin level. Example of the different S/A models are shown in Fig. 60 from (a) to (e).

A sketch of the whole core is shown in Fig. 63 (x-y plane). Driver is identified by yellow hexagons, stainless steel reflector by light-blue hexagons, uranium blanket by dark-blue hexagons and sodium boundaries by green hexagons.

A detailed view of the driver and of the core periphery (interface with the stainless steel reflector) is shown in Fig. 62.

Lower and upper parts of the core were also modeled in detail, in order to take into account realistic axial neutron leakage effects. H-shaped cylindrical plugs and sodium volumes are shown in Fig. 63, Fig. 64, Fig. 65.

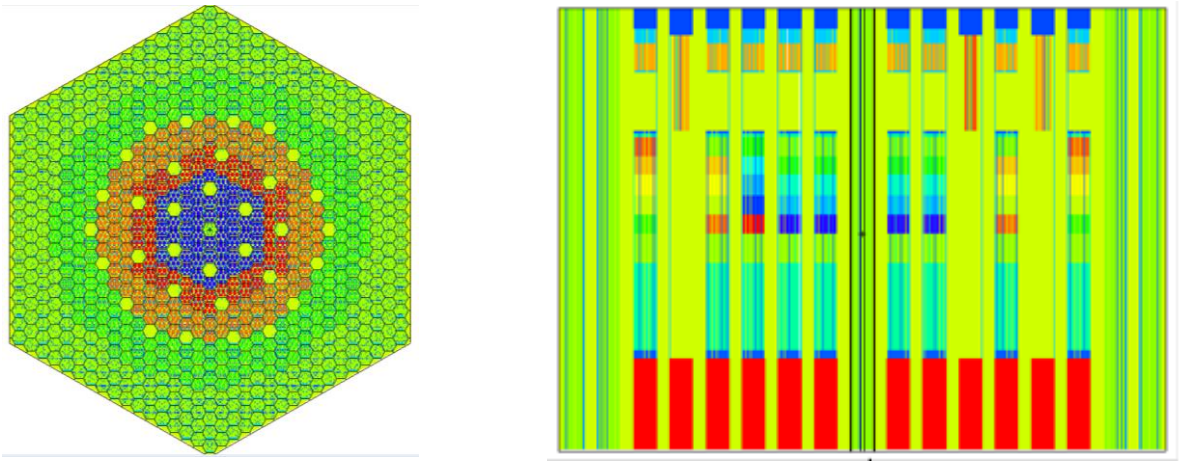

Fig. 58 – MCNP SFR Core Neutronic Modelling.

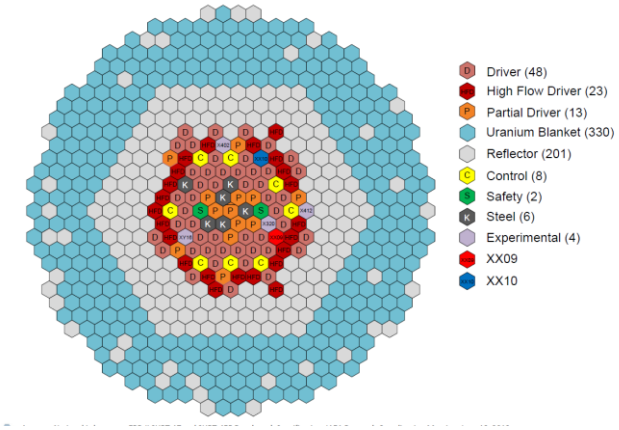

Fig. 59 – Core Neutronic Modelling.

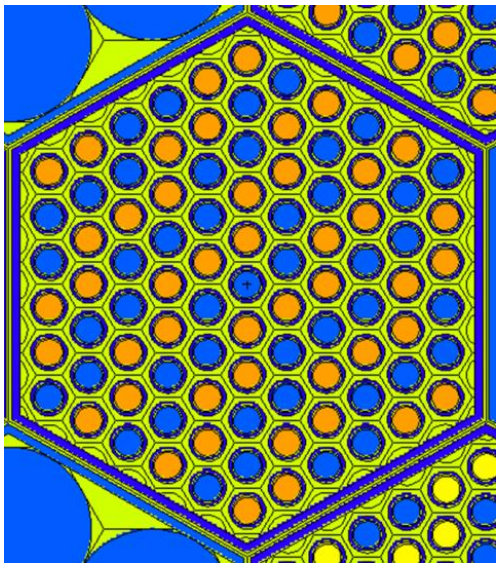

(a) Half-Worth Driver

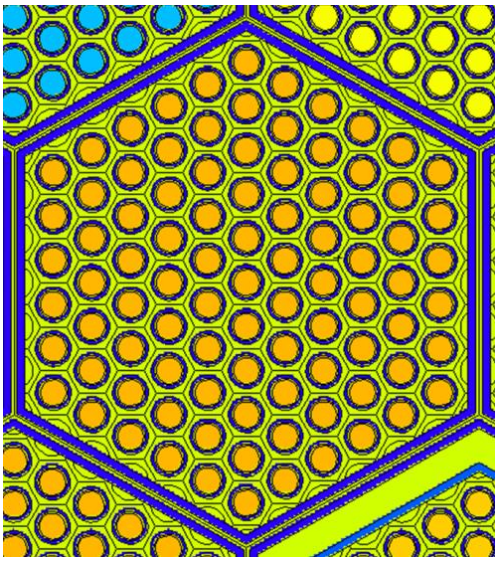

(b) Driver

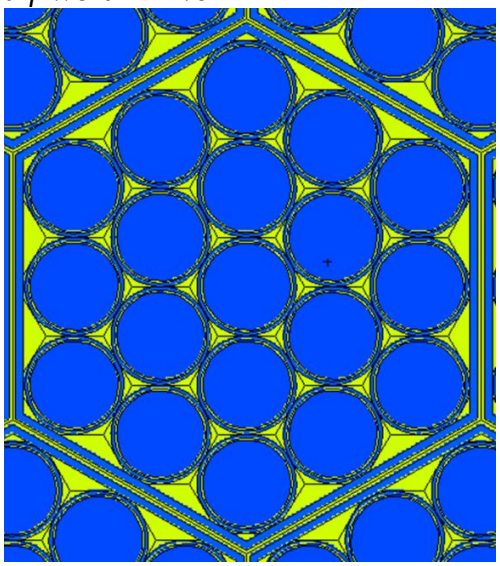

(c) Outer Blanket

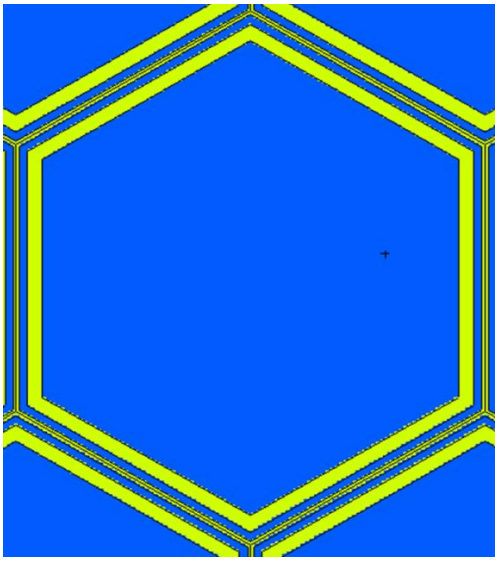

(d) Stainless Steel Reflector

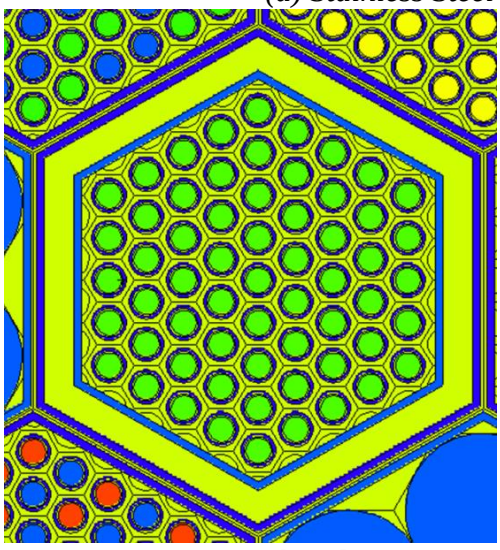

(e) Control Rods

Fig. 60 – MCNP6 S/A Modelling.

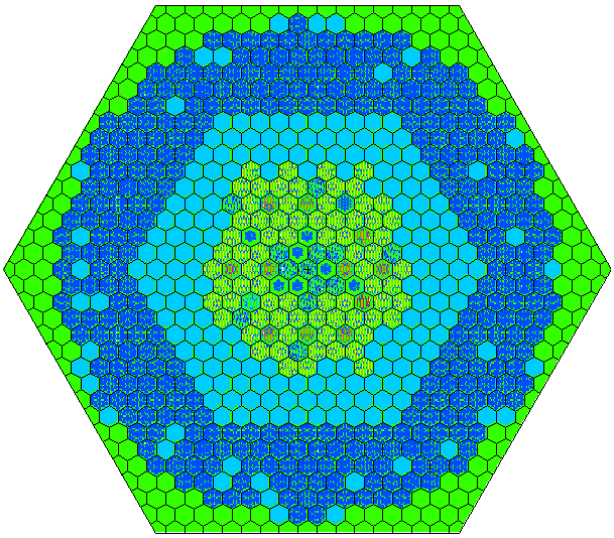

Fig. 61 – Core – Radial View (x-y plane).

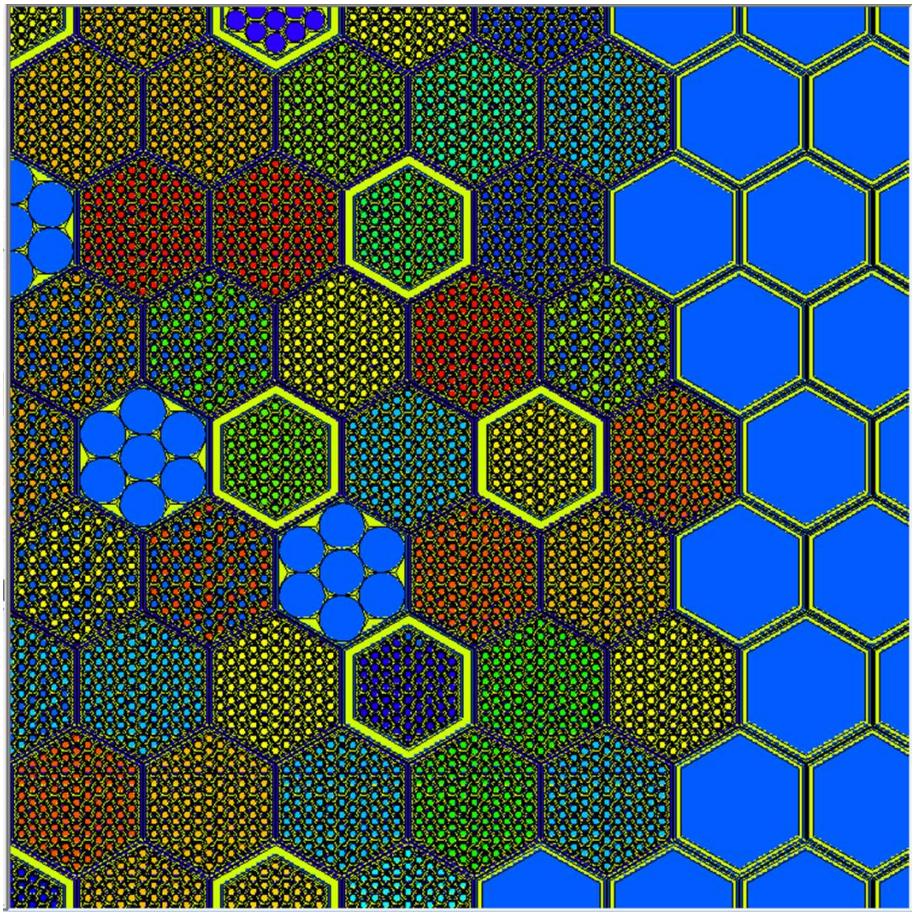

Fig. 62 – Detail of core modelling – Driver / SS reflector interface.

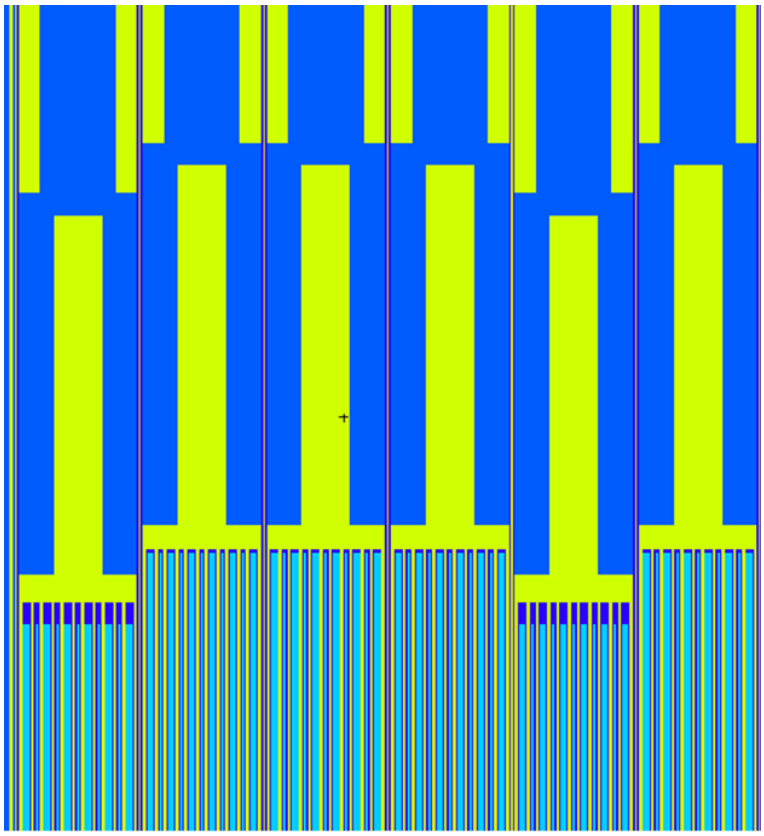

Fig. 63 – Top Reflector Modelling – S/A Steel Plugs.

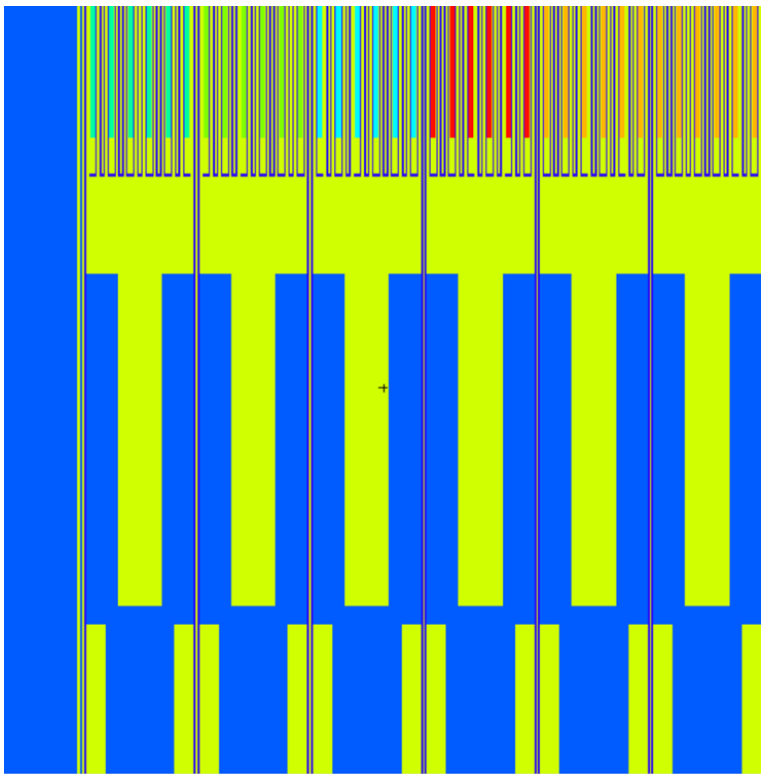

Fig. 64 – Bottom Reflector Modelling – S/A Steel Plugs.

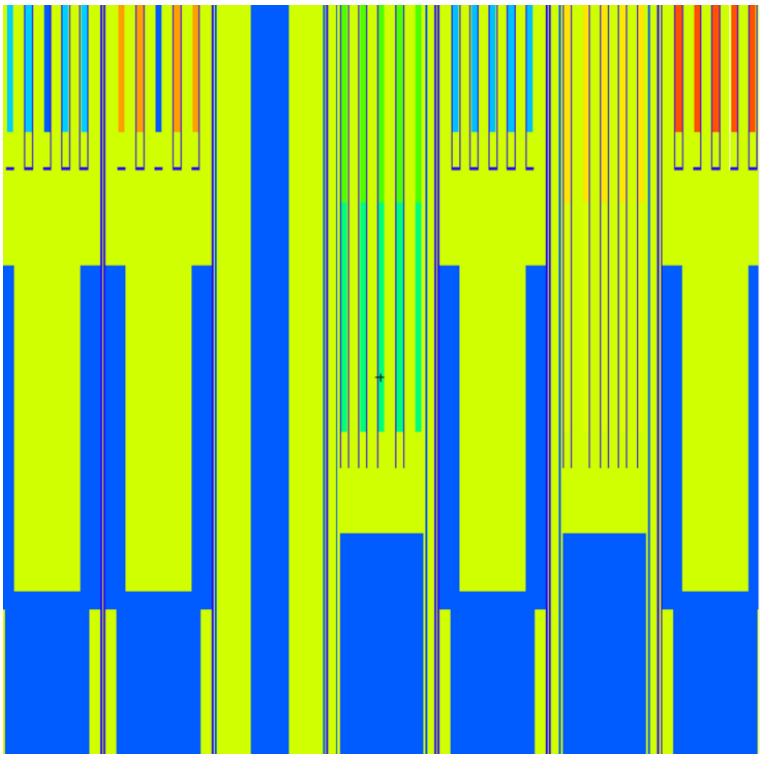

Fig. 65 – Bottom Reflector Modelling for CR – S/A Steel Plugs.

6.2 Materials modelling

A three-axial-layers, assembly-by-assembly material characterization was given by the benchmark organizers. Such large amount of data could not be used in the MCNP model because of memory and computational power limitations. Therefore, a material homogenization procedure was set up, grouping materials according to the burnup level and to S/A type. The three-axial-layer material discretization was kept. Sensitivities were run in order to identify the minimum number of materials not affecting the criticality calculations (keff) more than 100 pcm. 78 materials (75 for the core and 3 for the uranium blanket) resulted in a good compromise for achieving a realistic simulation.

6.3 Calculation parameters

In order to achieve a rapid fission source and keff convergences, preliminary calculations with few neutron histories (NH) were run. This was done for getting a good initial source distribution. Then, production calculations were performed using at least 25 Million of NH (MNH), performing 50000 NH simulations per 500 cycles. ENDF/B-VII.1 [49] continuous-energy cross sections libraries, included in the MCNP6 release, were used. The temperature effects on the cross sections were simulated using the MAKXSF [50] code.

6.4 Criticality calculations

Final criticality calculations are given in Tab. 17. Reference results were obtained considering and not considering the effect of the Uranium blanket. The last one value (no Uranium Blanket) was obtained for validation purposes of the SCALE-PHISICS-RELAP5-3D© deterministic solution (see further).

RUN	Result	Statistical Uncertainty (pcm)
Full Model	1.0392	±13
Driver + SS Reflector (no Uranium Blanket)	0.9875	±13

Tab. 17 – MCNP6 criticality calculations

7 PHISICS NEUTRONIC MODELLING

The EBR II 3D deterministic neutronic model was built using the advanced simulation code "Parallel and Highly Innovative Simulation for INL Code System" (PHISICS) [6] developed by the Idaho National Laboratory (INL). This code was selected because it has many necessary features for a simulation of a fast neutron system (EBR-II) which are not included in the default RELAP5-3D© nodal code (NESTLE). The PHISICS nodal solver, "Intelligent Nodal and Semi-structured Treatment for Advanced Neutron Transport" (INSTANT) [51] allows to use transport or diffusion approximation and the number of energy groups is limited only by the hardware capabilities. For the angular discretization is possible to use up to 33 orders, and several nodes geometry are available such as Cartesian 2/3D , Hexagonal 2/3D, Triangular and Wedges. This powerful tool is coupled with RELAP5-3D© to generate a state of the art software platform to perform safety analysis on the existent LWR fleet as the analysis of advanced reactor designs with an unlimited degree of accuracy. This code is compiled on "Falcon" and "Fission" HPC machines which are provided by the INL through remote connections.

7.1 Neutronic codes description

The reference tool chosen to produce the EBR II XSec library is the SCALE 6.1.2 package [52], developed by "Oak Ridge National Laboratory" (ORNL) under contract with the "U.S. Nuclear Regulatory Commission" (NRC). The SCALE control module TRITON and the related 2D deterministic transport code for lattice calculation "NEWT" are used to generate few-group homogenized XSec libraries for transport and diffusion transient calculations.
Because EBR II is a fast neutron system, the use of the default 44-group XSec library, derived using a thermal weighting spectra from the ENDF/B-V, is not recommended. Therefore the 238-group XSec library based on the ENDF/B-VII was used, as recommended in [53]. For the self-shielding calculations the CENTRM module was used. CENTRM calculates problem-dependent, group-averaged cross section, using as weight the flux calculated by solving the 1D Boltzmann transport equation with continuous-energy Xsec library.

7.2 EBR II broad-group nodal XSec library generation

NEWT calculate the flux solving the 2D transport equation using 238 energy group, after that it collapses the XSec in the space and in the energy domains using the obtained flux solution. Result of each calculation is one set of broad-group XSec. Generally, LWR XSec are collapsed in energy two groups (thermal and fast group). For a fast spectrum reactor, in which the most of fission events occur out of the thermal range, a more detailed energy mesh is required. For the present work, the 33 energy group structure used in the ERANOS code [54] and given in Tab. 18, is adopted.

Since EBR-II has a lot of sub-assemblies (SA) with different geometry (e.g., see in Fig. 66, SA with dummy rods, experimental SA, Control rods, etc.,), many 2D SCALE models were developed and used to calculate the multi-group Xsec libraries.

Since the studied system is a critical system, for each model the "B1" critical spectrum search is computed after the transport calculations. Homogenized constants are then generated using as a weight a critical spectrum.

Energy group	Upper Energy (eV)	Energy group	Upper Energy (eV)
1	1.96E+07	18	3.35E+03
2	1.00E+07	19	2.03E+03
3	6.07E+06	20	1.23E+03
4	3.68E+06	21	7.49E+02
5	2.23E+06	22	4.54E+02
6	1.35E+06	23	3.04E+02
7	8.21E+05	24	1.49E+02
8	4.98E+05	25	9.17E+01
9	3.02E+05	26	6.79E+01
10	1.83E+05	27	4.02E+01
11	1.11E+05	28	2.26E+01
12	6.74E+04	29	1.37E+01
13	4.09E+04	30	8.32E+00
14	2.48E+04	31	4.00E+00
15	1.50E+04	32	5.40E-01
16	9.12E+03	33	1.00E-01
17	5.53E+03		

Tab. 18 – ERANOS 33 energy group structure [55]

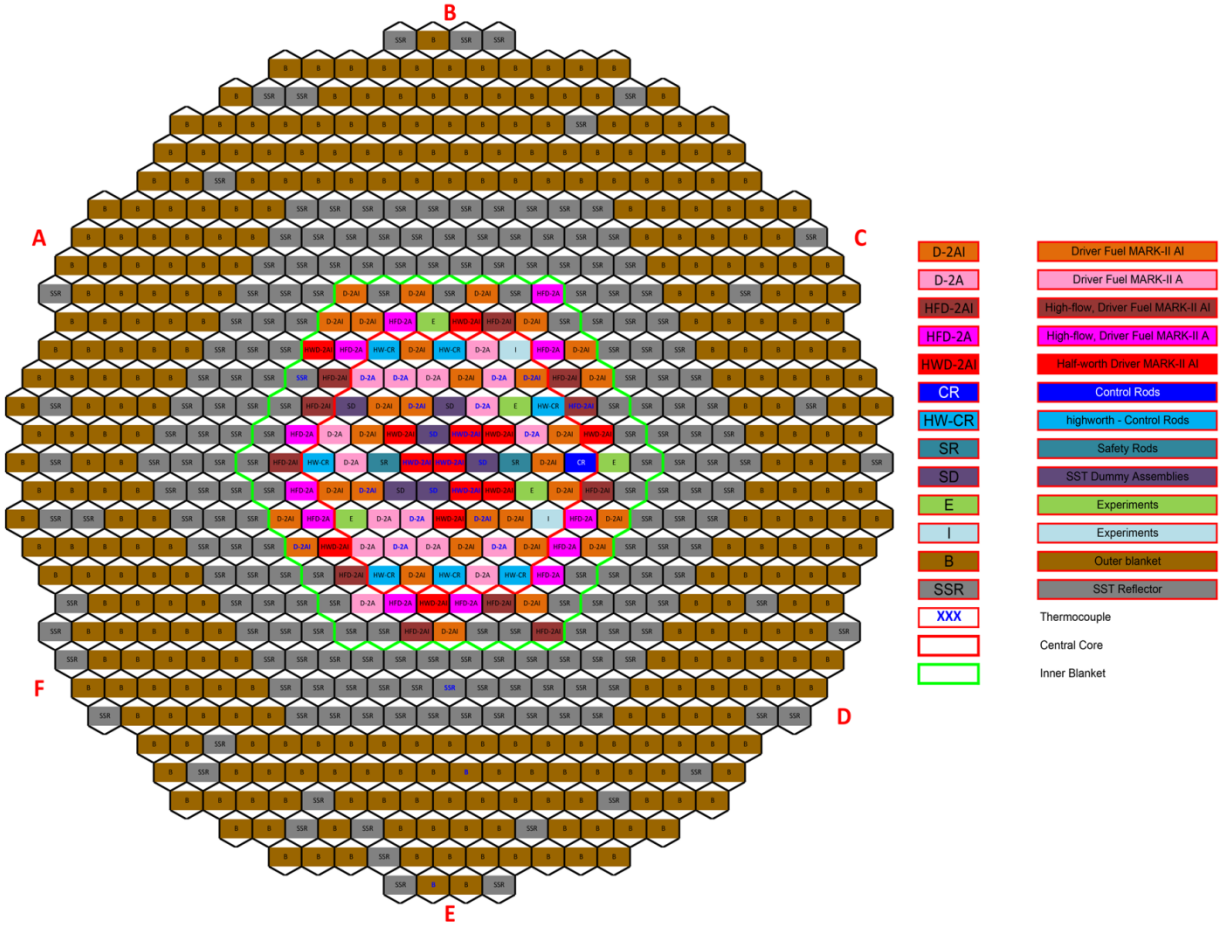

Fig. 66 – EBR-II SHRT45 full Core subassemblies map.

The core 97 fuel SA have a specific burnup, detailed at three different axial levels. Thus an overall 291 different compositions are used by the benchmark organizer for characterizing the core status. Analyzing the composition database it is possible to notice that some SA with the same geometry are almost identical, and the error produced using an average composition for both the SA is negligible. Using a specific threshold on the compositions the 97 different SA can be reduced to only 15, thus resulting in just 45 compositions. E.g., the driver and half worth driver SA MARK-IIA models are visible in Fig. 67: these two models are used to calculate 30 homogenized Xsec of the SA with such geometry.

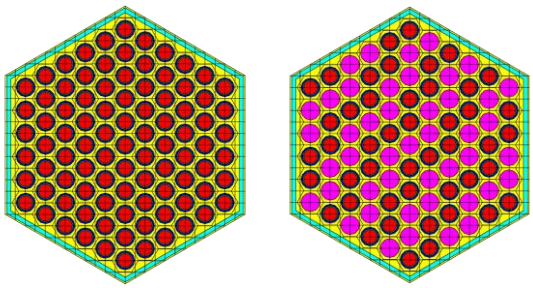

Fig. 67 – SCALE Driver Fuel SA & half worth Driver SA neutronic SCALE models

The Boundary Conditions (BC) used in the previous models are reflective BC. This is an approximation that is acceptable as first approach for modelling the MARK IIA SA. This could be not true for the MARK-IIS SA, which has less fuel pin and a thimble flow region. The Control Rods (CR) follower and one of the experimental SA, have a MARK-IIS configuration (see Fig. 68). Inside the core this fuel is never surrounded by a SA with the same geometry: the surrounding SA could be a driver or a half worth driver, therefore a super-cell model has to be used. The same model but without fuel visible (Fig. 68) is used to calculate the XSec of the part of CR without fuel and absorber. The absorber part of the CR (seven B_4C rods) was not considered because the CR are full withdrawn.

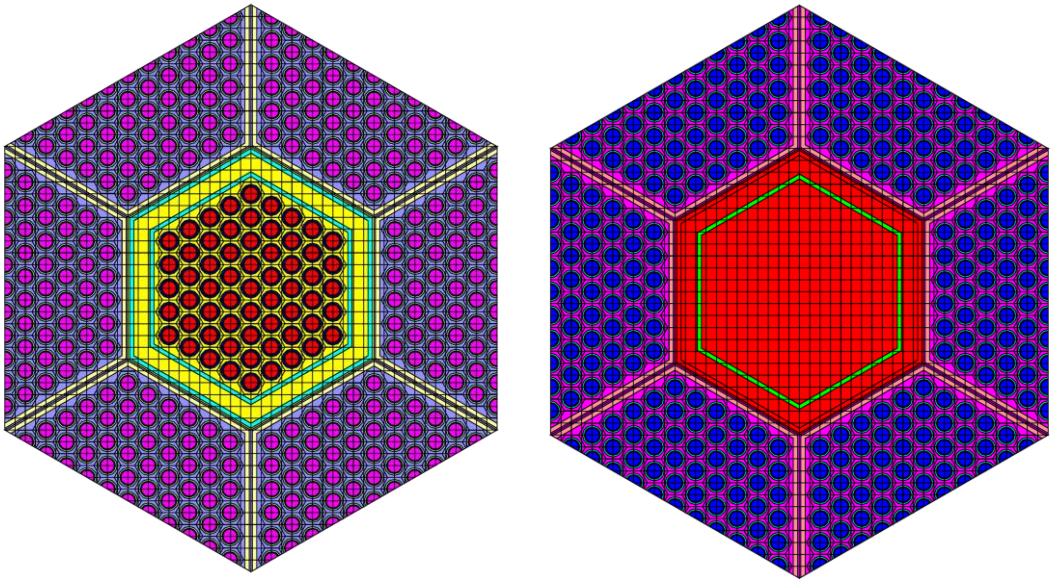

Fig. 68 – SCALE MARK-IIS and CR non-active section models

All the previous SCALE models were used to calculate the active part of a SA. However, some dummy SA are also included in the reactor. The dummy SA are made of AISI 304 steel and have a

flow thimble region as the MARK-IIS but inside there are only seven AISI 304 rods (see Fig. 69). In this assembly there is not fissile material, therefore a model similar to that of the non-active part of the CR is necessary, with some Driver SA around to generate the neutron flux.

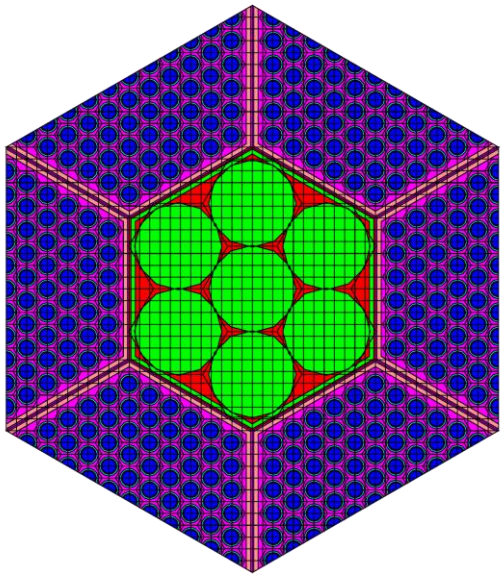

Fig. 69 – SCALE Dummy SA model.

The top and bottom reflectors models are visible in Fig. 70 (top part). They are based on steel blocks with a particular geometry which allows the flow of sodium to and from the active zone. The equivalent composition of an homogenous medium of steel and sodium was calculated and used in the model. Even if the medium is homogeneous, six different zones of homogenization were defined to produce one nodal Xsec set for each axial mesh of the reflector.

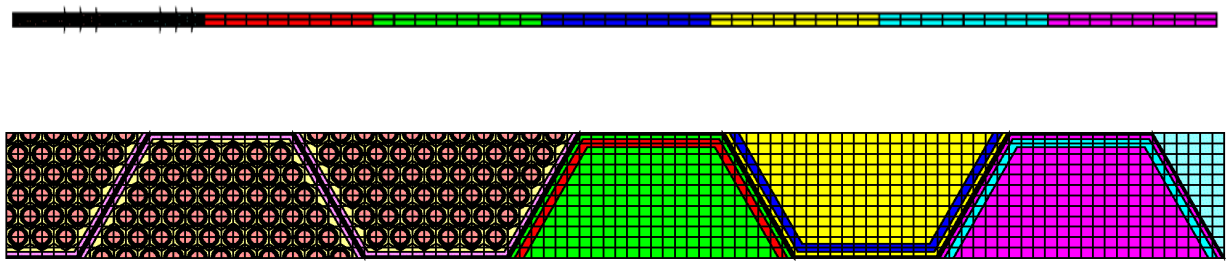

Fig. 70 – SCALE Top & Bottom (top part) and Radial Reflector (bottom part) models.

The Radial reflector is instead a SA with an hexagon of steel in the center (see Fig. 70, bottom part). There are three rings of reflector, therefore in the model, three SA of fuel plus three different SA of Reflector are included (one for each reflector ring). This macro model has reflective boundary conditions on the north, south, and west sides, while void conditions are on the left to take into account the neutron leakages. Finally, the six rings of the Uranium Blanket were not simulated in the preliminary calculations, because they are quite far from the active. Moreover, excluding the blanket from the calculations, reduces the computational load sensibly.

7.3 PHISCS model description

Once the EBR-II 33 group XSec library was generated by SCALE, the PHISICS model was set up using the reactor core geometry information. The radial view of the PHISICS model is visible in Fig. 71. There are nine rings of SA plus the central one, for a total of 271 SA. The SA pitch is almost 6 cm. Axially, the top and bottom reflector were simulated using 6 meshes of about 11 cm for the bottom reflector and 6 meshes of about 10 cm for the upper reflector. 6 meshes of about 6 cm were used for the active zone.

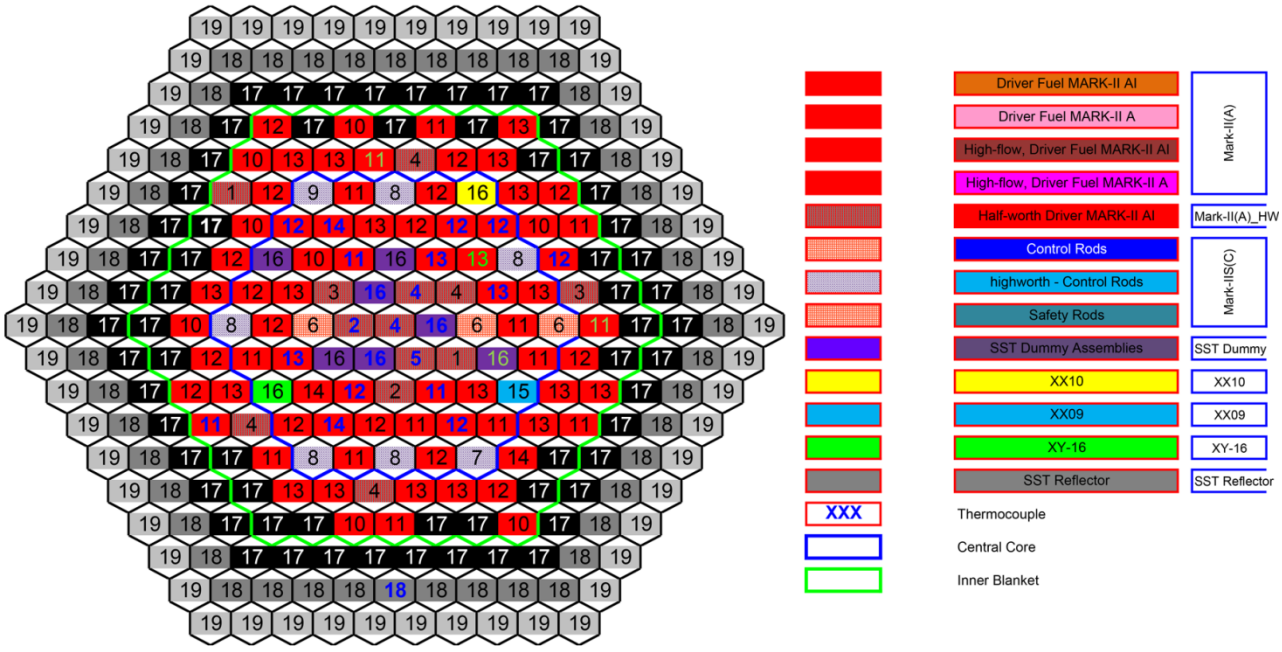

Fig. 71 – EBR- II PHISICS 3D neutronic model radial view.

The whole model uses a total of 4878 neutronic nodes. The calculations were performed in diffusion approximation (P1 approximation), using 64 CPU.

7.4 PHISICS model preliminary results

To test the model, some preliminary calculations were performed. Two configuration were studied: the first one was obtained moving the fuel follower of the CR at the same axial level of the active zone, while the second one was the real pre-SHRT-45 test configuration with the CR in the correct positions. As expected, there is a large reactivity difference (many dollars) between the two configurations. For the benchmark reference configuration, the system is subcritical (see Tab. 19). This result is consistent with the MCNP6 calculations described in the previous Paragraph.

RELAP5-3D/PHISICS	K-eff
CR fully withdrawn	1.01266
CR in (reference insertion depth)	0.98072

Tab. 19 – PHISICS 3D model preliminary calculation K-eff.

In the next figures, 3D flux data are shown to highlight the behavior of the neutron flux in the system. In Fig. 72 the neutron flux of the first energy group (10.0-19.7 MeV) is represented. In this

figure is possible to see how the fast flux is concentrated near the fissile material while it is practically absent in the reflector.

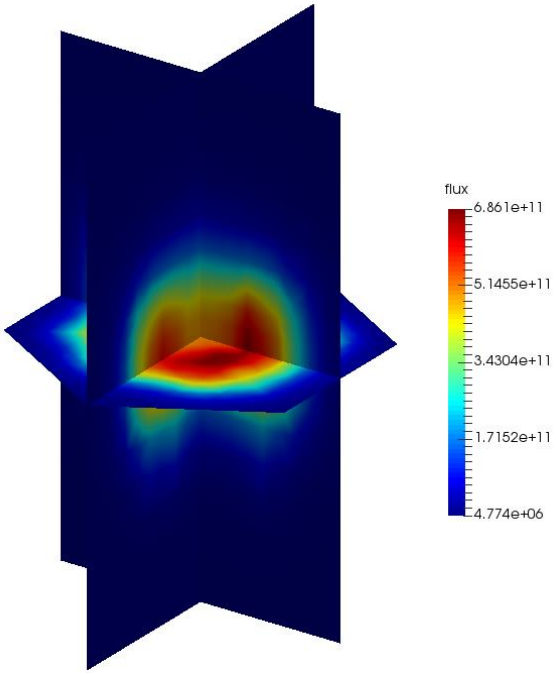

Fig. 72 – PHISICS 3D model: first (fast) group flux.

In Fig. 73 instead the neutron flux of the last energy group (below 1.00E-01 eV) is represented. In this case, the thermal flux is consistently concentrated outside the active zone.

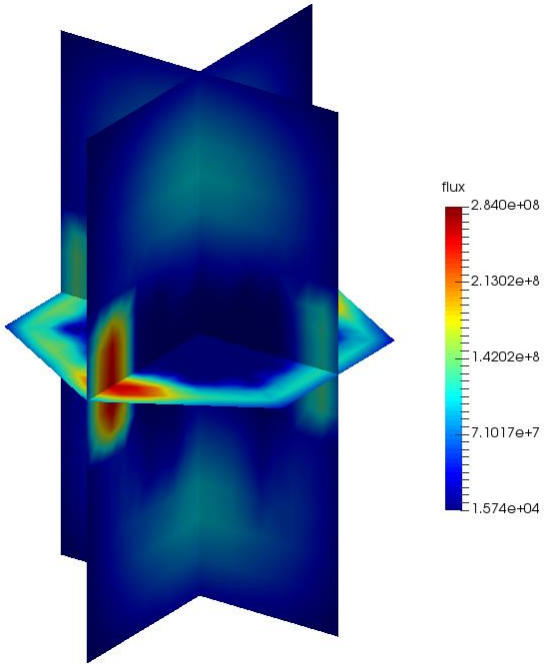

Fig. 73 – PHISICS 3D model: last (therma)l group flux.

In Fig. 74, the total Flux is represented. The Total flux maximum value is about 2.5e+15 n/cm^2*s (center of the active zone).

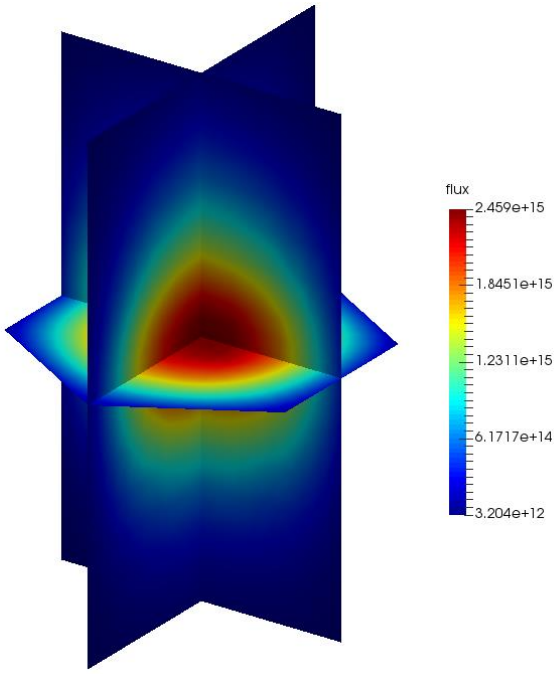

Fig. 74 – PHISICS 3D model: total flux.

Finally the radial power shape of the EBR-II is visible in Fig. 75. The maximum value is 1.48 and it is located in one of the driver SA of the second ring, instead the minimum value of 0.44 is located in one half worth driver of the peripheral ring.

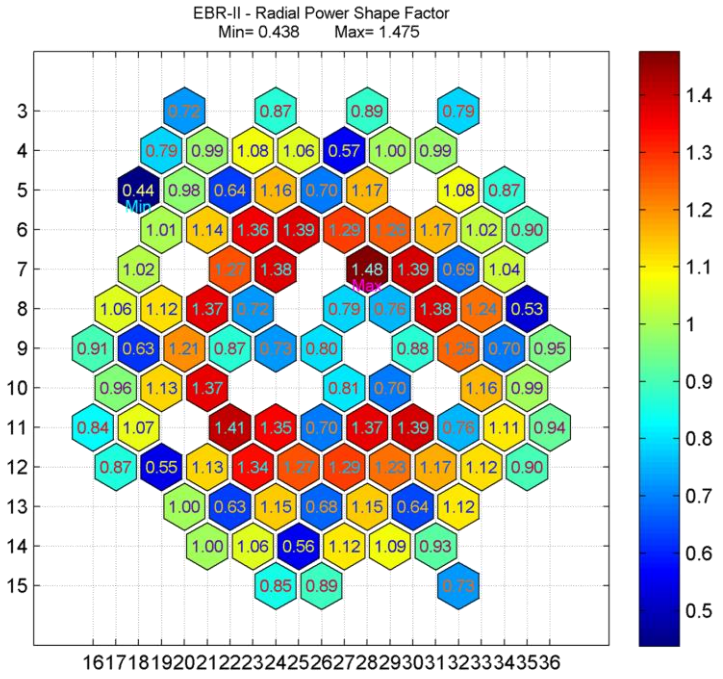

Fig. 75 – PHISICS 3D model Radial power shape factor.

7.5 Conclusive remarks and follow up

A PHISICS standalone model was developed and the preliminary results are reasonable and in accordance with the Monte Carlo MCNP6 calculations. The future steps for such activity will be:

1. include the Blanket in the 3D neutronic simulation
2. improve the results using the Super Homogenization (SPH) approach
3. coupling the PHISICS model with the RELAP5-3D© TH model

8 CONCLUSIVE REMARKS

The activity, carried out in the framework of IAEA CRP EBR-II Shutdown Heat Removal Tests, aims at improving the design and the simulation capabilities in fast reactor neutronics, thermal hydraulics, plant dynamics and safety analysis. The objective of the report is to document:

- The results of the open simulation and the analysis, comparing with experimental data of test SHRT 17;
- The ANSYS CFX model and results of the sub-assembly XX09 simulation against the experimental data from test SHRT 17;
- The preliminary assessment of neutronic model, relevant for the planned simulation of SHRT 45r.

The open simulation of EBR-II SHRT-17 has been successfully executed. The comparisons executed bring to the conclusion that RELAP5-3D code has the capability to deal with the relevant thermal-hydraulic phenomena involved in SHRT-17. The following conclusive remarks can be point-out:

- The trends of mass flow rate, of coolant and cladding temperatures in the core are well predicted (open calculation).
- Improvements might be possible if the knowledge of EBR-II features/characteristics is improved too (e.g. inlet subassemblies geometry details and characterization, better understanding and quantification of the cooling induced by the IHX structures close to the Z-pipe inlet, etc…).
- The axial conduction in the structure is challenging for the code, and the application of the code option demonstrates the need to improve the model.
- Mixing and thermal stratification, notwithstanding simulated, are beyond RELAP5-3D© capabilities and only bounding analyses are possible.
- Thermal stratification in the Z-Pipe will be further studied through sensitivity analyses.

The activity carried out by ANSYS CFX was focused on SA XX09. The following conclusions apply:

- For the stationary case at nominal mass flow rate a good agreement was obtained between CFD and experimental results in all the monitoring points.
- The SHRT-17 transient simulation (from 0 to 100s) shows that:
  - the prediction of the cladding temperature trends have a very good agreement with all monitoring points placed at MTC plane;
  - at TTC (top of the core) and 14TC (mixing region) planes, the agreement is good for t<45,70 s respectively, but there is a delay and a clad peak temperature overestimation of 50-70 K.

A neutronic activity was performed using Monte Carlo MCNP6 and PHYSICS. This is necessary to perform the simulation of the SHRT45r, which is an unprotected transient (i.e. relevance of NK feedbacks). In particular:

- Criticality calculations have been carried out by MCNP6. These results are also relevant for validation purposes of the SCALE-PHISICS-RELAP5-3D© deterministic solution.
- A PHISICS standalone model was developed and the preliminary results are reasonable and in accordance with the Monte Carlo MCNP6 calculations.

LIST OF REFERENCES

[1] *L. Briggs, C. Choin, W. Hub, L. Maas, W. Maschek, B. Merk, K. Mikityuk, H., Mochizuki, S. Monti, K. Morita, A. Del Nevo, H. Ohira, A. Petruzzi, U. Partha Sarathy, A. Shin, I. Shvetsov, M. Stempniewicz, D. Sui, B. Truong, Benchmark analyses of the Shutdown Heat Removal Tests Performed in the EBR-II Reactor.*

[2] *A. Del Nevo, I. Di Piazza, C. Parisi, P. Console Camprini, E. Martelli, P. Balestra, F. Giannetti, A. Naviglio "Development and validation of an approach and numerical models for safety analysis of FBR", ENEA, ADPFISS-LP2-055 (2014).*

[3] *J.-Y. Doriath, Et Al., "ERANOS1: The Advanced European System of Codes for Reactor Physics", International Conference on Mathematical Methods and Supercomputing in Nuclear Applications, Karlsruhe, Germany, (1993).*

[4] *T. Goorley Et Al., "Initial MCNP6 Release Overview" LA-UR-11-05198, Los Alamos National Laboratory, USA(2011).*

[5] *SCALE-4.4a: "A Modular Code System for Performing Standardized Computer Analyses for Licensing Evaluation", ORNL/NUREG-CR-0200, Rev. 6, Oak Ridge National Laboratory (2000).*

[6] *C. Rabiti, Y. Wang, G. Palmiotti, H. Hiruta, J. Cogliati e A. Alfonsi, Phisics: A New Reactor Physics Analysis Toolkit, 2525 North Fremont Avenue, Idaho Falls,, June,2011.*

[7] *INL, RELAP5-3D© Code Manual Volume II: User's Guide and Input Requirements, INEEL-EXT-98-00834, Revision 4.0, June 2012.*

[8] *ANSYS CFX Release 13 User Manual, 2011.*

[9] *K. Lassmann, A. Schubert, P. Van Uffelen, C. Gyory, and J. Van De Laar, "Transuranus Handbook" version v1m1j06, JRC, EC, ITU, (2006).*

[10] *IAEA. Status of Fast Reactor Research and Technology Development. IAEA-TECDOC-1691, Vienna, 2012.*

[11] *T. Sumner and T.Y.C. Wei, Benchmark Specifications and data Requirements for EBR-II Shutdown Heat Removal tests SHRT-17 and SHRT-45R, ANL-ARC-226 (rev 1), May 31, 2012.*

[12] *H.P. Planchon, R.M. Singer, D. Mohr, E.E. Feldman, L.K- Chang and P.R. Betten, The Experimental Breeder Reactor II inherent Shutdown Heat Removal Tests – Results and Analysis, Nuclear Engineering and Design 91(1986) 287-296, 1985.*

[13] *L.J. Koch, Experimental Breeder Reactor II (EBR-II) – An Integrated Experimental Fast Reactor Nuclear Power Station, Authorized by Argonne National Laboratory.*

[14] *W.J. Carmack, D.L. Porter, Y.I. Chang, S.L. Hayes, M.K. Meyer, D.E. Burkes, C.B. Lee, T. Mizuno, F. Delage, J. Somers, Metallic fuels for advanced reactors, ScienceDirect, Journal of Nuclear Materials 392(2009) 139-150.*

[15] *A. Del Nevo, C. Venturi, E. Martelli, D. Rozzia, Qualifica di codici di calcolo dedicati alle analisi di sistema avanzati quando applicati nella simulazione di impianti a metallo liquido, ENEA, ADPFISS-LP2-039, 24 Settembre 2013.*

[16] *I. Di Piazza, M. Scarpa, Rassegna di letteratura sulla termoidraulica dei bundle refrigerati a metallo liquido pesante fluente, ENEA, LM-F-R 001,*

[17] *E.H. Novendstern, Turbulent Flow pressure drop model for fuel rod assemblies utilizing a helical wire-wrap spacer system, Nucl. Eng. Des., 22, pp. 19-27, 1972.*

[18] *K. Rheme, Pressure drop performance of rod bundles in hexagonal arrangement, Int. J. Heat Mass Transfer, 15, pp2499-2517, 1972.*

[19] *K. Rehme, Pressure drop correlations for fuel element spacers, Nuclear Technology, 17, pp. 15-23, 1973.*

[20] *N.E. Todreas, M.S. Kazimi, Nuclear Systems I: Thermal Hydraulic Foundamentals, Washington DC: Hemisphere, 1990.*

[21] *C.F. Colebrook, "Turbulent Flow in Pipes with Particular reference to the Transition Region Between Smooth and Rough Pipe Laws", Journal of Institute of Civil Engineers, 11, pp. 133-156, 1939.*

[22] *D.J. Zigrang, N.D. Sylvester, "A Review of Explicit Friction Factor Equations" Transactions of ASME, Journal of Energy Resources Technology, 107, pp.280-283, 1985.*

[23] *R.B. Bird, W.E. Stewart, E.N. Lightfoot, Transport properties, New York: Wiley, 1960.*

[24] *R.A. Seban, T.T. Shimazaki, "Heat transfer to a Fluid Flowing Turbulently in a Smooth pipe with Walls at Constant Temperature", ASME Paper 50-A-128, 1950.*

[25] *R.A. Seban, T.T. Shimazaki, "Heat transfer to a Fluid Flowing Turbulently in a Smooth pipe with Walls at Constant Temperature", Transactions of the ASME, 73, 1951, pp. 803-809.*

[26] *M.S. Kazimi, M.D. Carelli, Clinch River Breeder Reactor Plant Heat Transfer Correlation for analysis of CRBRP Assemblies, CRBRP-ARD-0034, Westinghouse, 1976.*

[27] *ISL Inc, RELAP5/MOD3.3 Code Manual Volume I: Code Structure, System Models, and Solution Methods, Nuclear Safety Analysis Division, July 2003.*

[28] *INL, RELAP5-3D© Code Manual Volume I: Code Structure, System Models and Solution Methods, INEEL-EXT-98-00834, Revision 4.0, June 2012.*

[29] *INL, RELAP5-3D© Code Manual Volume II: Appendix A Input Requirements, INEEL-EXT-98-00834, Revision 4.0, June 2012.*

[30] *INL, RELAP5-3D© Code Manual Volume IV: Models and Correlations, INEEL-EXT-98-00834, Revision 4.0, June 2012.*

[31] *R.R. Shultz, RELAP5-3D© Code Manual Volume V: User's Guidelines, INEEL-EXT-98-00834, Revision 4.0, June 2012.*

[32] *SCDAP/RELAP5 Development Team, SCDAP/RELAP5/mod3.2 Code Manual Volume IV: MATPRO – A Library of Materials Properties For Light-Water-Reactor Accident Analysis, NUREG/CR-6150, INEL-96/0422 Revision 1 Volume IV.*

[33] *C.B. Davis, Evaluation of the Use of Existing RELAP5-3D Models to Represent the Actinide Burner Test Reactor, INL/EXT-07-12228, February 2007.*

[34] *C.B. Davis, Applicability of RELAP5-3D for Thermal-Hydraulic Analyses of a Sodium-Cooled Actinide Burner Test Reactor, INL/EXT-06-11518, July 2006.*

[35] *A. Del Nevo, E. Martelli, Validation of a Three-Dimensional Model of EBR-II and Assessment of RELAP5-3D© based on SHRT-17 Test, Nuclear Technology, accepted for publication.*

[36] *D. Mohr, L.K. Chang, E.E. Feldman, P.R. Betten, H.P. Planchon, "Loss-of-Primary-Flow Without-Scram Tests: Pretest Predictions and Preliminary Results" , Nuclear Engineering and Design, 101, pp. 45-56, 1987.*

[37] *W.M. Kays, M.E. Crowford, Convective Heat and Mass Transfer, Second Edition, McGraw Hill Book Company, New York, 1980.*

[38] *M.H. Fontana, L.F. Parsly, J.L. Wantland, 1971, Analytical Studies, ORNL*

[39] *Cheng, X., Tak, N.I., 2006. CFD analysis of thermal-hydraulic behavior of heavy liquid metals in sub-channels, Nuclear Engineering and Design 236, pp.1874-1885.*

[40] *Han, J.T., Fontana, M.H., 1977. Blockages in LMFBR Fuel Assemblies – A Review. Proc. Winter Annual ASME meeting.*

[41] *Menter, F.R., 1994. Two-equation eddy-viscosity turbulence models for engineering applications, AIAA J, 32, pp.269-289.*

[42] *Natesan, K., Sundararajan, T., Narasimhan, A., Velusamy, K., 2010. Turbulent flow simulation in a wire-wrap rod bundle of an LMFBR, Nuclear Engineering and Design 240 (5), pp. 1063–1072.*

[43] *Ranieri, M., 2014. Pre-test CFD analysis of the rod bundle experiment in the Heavy Liquid Metal facility NACIE-UP, Master Thesis University of Pisa.*

[44] *Rasu, N.G., Velusamy, K., Sundararajan, T., Chellapandi, P., 2014. Simultaneous development of flow and temperature fields in wire-wrapped fuel pin bundles of sodium cooled fast reactor, Nuclear Engineering and Design 267, pp. 44-60.*

[45] *Sobolev, V., 2011. Database of thermophysical properties of liquid metal coolants for GEN-IV. SCK CEN-BLG-1069.*

[46] *T. Goorley et al., "Initial MCNP6 Release Overview," LA-UR-11-05198, Los Alamos National Laboratory, USA*

[47] *CRESCO, "Centro Computazionale di Ricerca sui Sistemi Complessi", http://www.cresco.enea.it/*

[48] FP7, PELGRIMM—PELlets versus GRanulates: Irradiation, Manufacturing & Modelling. Grant Agreement Annex I - "Description of Work". Collaborative project No. 295664. FP7-Fission-2011.

[49] J. L. Conlin et al., "Continuous Energy Neutron Cross Section Data Tables Based upon ENDF/B-VII.1", LA-UR-13-20137, Los Alamos National Laboratory, USA

[50] F. B. Brown, "The MAKXSF Code with Doppler Broadening", LA-UR-06-7002, Los Alamos National Laboratory, USA

[51] Y. Wang, H. Zhang, R. Szilard e R. Martineau, Application of the INSTANT-HPS PN Transport Code to the C5G7 Benchmark Problem, Hollywood: presented at the American Nuclear Society (ANS) Summer meeting 2011, Idaho National Laboratory Report, June, 2011.

[52] S. M. Bowman, "SCALE 6: comprehensive nuclear safety analysis code system", NUCLEAR TECHNOLOGY, Special Issue on the SCALE Nuclear Analysis Code System / Reactor Safety, Vol. 174, dx.doi.org/10.13182/NT10-163, May 2011.

[53] S. M. Bowman, R. Q. Wright, H. Taniuchi, and M. D. DeHart, "Validation of SCALE-4 criticality sequences using ENDF/B-V Data", presented at American Nuclear Society 1993 Topical Meeting on Physics and Methods in Criticality Safety, Nashville, Tennessee, US, September 19-23, 1993.

[54] G. Rimpault, D. Plisson, J. Tommasi, and R. Jacqmin, "The ERANOS code and data system", Physor 2002 International Conference, Seoul, Korea, October 7-10, 2002.

[55] G. Bianchini, N. Burgio, M. Carta, V. Fabrizio, and L. Ricci, "Validazione del modulo di cinetica KIN3D di ERANOS.Analisi per i sistemi GODIVA e GUINEVERE", Rapporto Tecnico Accordo di programma ENEA-MSE: tema di ricerca "Nuovo nucleare da fissione", NNFISS-LP3-033, Rome, September, 2011.